STRUCTURE - PROPERTY RELATIONSHIPS IN COPOLYESTER FIBERS AND COMPOSITE FIBERS

A Dissertation

Presented to
The Academic Faculty

By
Hongming Ma

In Partial Fulfillment
Of the Requirements for the Degree
Doctor of Philosophy in School of Chemistry and Biochemistry

Georgia Institute of Technology
May, 2004

STRUCTURE - PROPERTY RELATIONSHIPS IN COPOLYESTER FIBERS AND COMPOSITE FIBERS

Approved:

Satish Kumar, Co-chair

David M. Collard, Co-chair

Marcus Weck

Mohan Srinivasarao

David A. Schiraldi

Charles Liotta

Date Approved: April 8, 2004

DEDICATION

This work is dedicated to my family.

ACKNOWLEDGMENTS

To begin, the author wishes to acknowledge and thanks thesis advisors Dr. Satish Kumar and Dr. David Collard for their great inspiration, tremendous support and valuable guidance throughout this research.

The benefits of having two research advisors, especially one expert in Polymer chemistry and the other in Polymer Science is that the insights in both fields broadened my vision and gives me a deeper understanding of the relationship between polymer structure, processing and properties. Their sustained tight cooperation during my graduate education is a key factor toward the successful accomplishment of this work.

The author would like to express his sincere thanks to the thesis committee members: Dr. Marcus Weck, Dr. Mohan Srinivasarao, Dr. David Schiraldi and Dr. Charles Liotta for their valuable comments and suggestions. The author would also like to express his appreciation to Dr. Shawn Jenkins, Dr. Michael Hibbs. Dr. Tao Liu. Dr. Sreekumar T. Veedu, Dr. Tetsuya Uchida, Dr. Jijun Zeng, Mr. Teijun Zhao and Ling Li, and many other group members from Dr. Kumar and Dr. Collard's research groups for their kind help during this research.

Finally, beyond all my words, the patience and support of my wife and my parents has been the key in the completion of this work.

TABLE OF CONTENTS

LIST OF TABLES

LIST OF FIGURES

SUMMARY

Polyethylene terephthalate is one of the most important engineering thermal plastics used for fibers, films and bottles. In the Chapter I, development and growth of the global PET solid-state resin market is reviewed. More than sixty years after its invention by British chemists, John Rex Whinfield and James Tennant Dickson in 1941, global consumption of PET resin grew at double-digit rates and reached 6.6 million metric tons by 2000. Consumption is projected to grow at an average rate of 9.6% per year through 2005, reaching a level of 10.4 million metric tons. Despite its wide applications and vast global market, PET has shortcomings, which limits it usage in many areas. PET has a glass transition temperature (T_g) of 80 ^{o}C, this temperature is too low so the PET bottles cannot be sterilized by washing it in boiling water. This is one of the reasons why PET containers are not recycled in US for food packaging again. For the same reason PET bottles and jars can not be filled with hot food. When used as tire cord, PET fiber will shrink and loose properties quickly above 100 ^{o}C, a condition frequently encountered when the car is running for long times in summer or a truck under heavy load. So the tire manufacture has to use more PET tire cords in a tire, than would be necessary If the PET fiber properties did not deteriorate as rapidly above 100 ^{o}C. PET has good barrier to carbon dioxide, which makes it into shatterproof carbonated beverage bottle, but does not have enough barrier to oxygen, so PET bottle can not be used for contain alcoholic drinks, such as beer. Also PET does not have good dyeability and biocompatibility.

Increase in glass transition temperature, high temperature mechanical properties, and dimensional stability is of great importance to further expand the applications of PET.

Significant research efforts have been made towards this goal, using a variety of approaches. In this work, we attempt to improve the properties of PET melt spun filament. Three strategies have been investigated: (i) copolymerization of rigid comonomer, 4, 4'-bibenzoate unit into the PET structure, (ii) UV crosslinking of functionalized PET fiber, and (iii) Reinforcing PET matrix with carbon nanofibers.

Chapter II to IV present the study on PET/BB fibers. In Chapter II crystal structure in random copolymers poly (ethylene terethphalate–*co*-4,4' bibenzoate) (PET/BB) were studied by using wide angle X-Ray diffraction (WAXD). Composition of PET/BB fiber in terms of comonomer distribution in crystalline and amorphous regions were studied by FTIR spectroscopy using the amorphous peaks at 1580 and 1560 cm^{-1} for terephthalate (T) and bibenzoate (B) units respectively. Further, PET/BB55 fibers were hydrolyzed to selectively etch the amorphous regions. The compositions of hydrolyzed products were determined by spectroscopy methods. Crystallites were further studied by using, DSC, wide angle x-ray diffraction, and transmission electron microscopy. Results show that PET/BB copolymers crystallize differently than described by the non-periodic model (npl), at least not by uniform copolymer incorporation. Crystal structure in low BB-content samples are "T" type and that of high BB-content copolymer are "B" type. Crystal structures are very close to that of respective homopolymer, PET and polyethylene bibenzoate, (PEBB). Crystalline region of high BB-content fibers are composed of mainly PEBB units. In PET/BB55 fiber, among the 30 wt % of the copolymer which was not etched, there is only one terephthalate unit per every 5 repeat units of bibenzoate. Crystal size of B type crystals along the c axis was found to be only

couple of repeat units long. Short chain segments rich in BB are sufficient to induce crystallization, to form PEBB crystals.

Chapter III presents the crystallinity and orientation analysis of various PET/BB fibers. Study showed that those two groups of fiber i.e. high BB content fiber and low BB content fibers have different structure and morphology. In PET/BB15 and 35, the crystal structure is similar to PET fiber crystal structure and crystallinity decreases with the increasing BB content. Also this group of fiber has similar or poorer orientation as compared to the PET fiber. On the other hand, high BB content fibers have much higher orientation and a different crystal structure. This crystal structure is similar to that of the homopolymer polyethylene bibenzoate (PEBB) as determined by WAXD study.

In the light of Chapter II and III Chapter IV presents the dynamic mechanical study of PET/BB fibers. Fibers containing more than 40 mol% bibenzoate units exhibited much higher storage modulus (E') as well as higher modulus retention at elevated temperatures than the low BB content fibers. The α-relaxation attributed to the glass transition temperature was not seen in the fully drawn and heat-treated PET/BB45, 55 and 65 fibers. The β transitions of PET/BB fibers diminished with the increasing of BB concentration. This may explain the improved gas barrier properties of PET/BB films. A new secondary transition in high BB content fibers was tentatively attributed to the motion of the BB containing units.

Chapter V presents the crosslinking study of PET/PBA fiber with UV irradiation. Crosslinking moiety phenyl bisacrylate was incorporated in the polymer backbone. Several compositionally different poly(ethylene terephthalate-*co*-1,4-phenylene bisacrylate) (PETPBA) copolymers were melt spun into fibers. The resulting fibers were

subjected to UV irradiation to induce crosslinking. Evidence of crosslinking was obtained from FTIR, solid-state ^{13}C-NMR, thermal analysis, and solubility. Irradiation of the fiber results in an increased glass-transition temperature, reduced thermal shrinkage, and enhanced modulus retention at elevated temperature.

Chapter VI presents the reinforcement of PET fiber by carbon nanofibers (CNF). Poly(ethylene terephthalate) (PET) resin has been compounded with carbon nanofibers. The amount of carbon nanofibers utilized in each case was 5 wt%. Compounding methods included ball-milling, high shear mixing in the melt, as well as extrusion using a twin-screw extruder. PET/CNF composite resins were melt-spun into fibers using the conventional PET fiber spinning conditions. The results show that CNFs can be incorporated into PET matrix with good dispersion and orientation. Compressive strength and torsional moduli of PET/CNF composite fibers were considerably higher than that for the control PET fiber. However the tensile properties of the composite fiber did not improved significantly. Lack of improvement of tensile modulus has been explained in the terms of graphite plane mis-orientation as well as carbon nanofiber aspect ratio.

Finally, Chapter VII summarizes the work done to improve the properties of PET fiber as well as recommendations for future work.

CHAPTER I

INTRODUCTION

1.1 Poly(ethylene terephthalate)

British chemists, John Rex Whinfield and James Tennant Dickson, patented poly(ethylene terephthalate) (PET or PETE) in 1941, after advancing the earlier research of Wallace Carothers. Whinfield and Dickson along with inventors W.K. Birtwhistle and C.G. Ritchiethey also created the first polyester fiber called Terylene, first manufactured by Imperial Chemical Industries or ICI.[1]

The saw that Carothers had not investigated the polyester formed from ethylene glycol and terephthalic acid. However, DuPont chose to concentrate on the more promising nylon research. By the time DuPont resumed its polyester research ICI had patented Terylene fiber and DuPont purchased the U.S. rights in 1945. In 1950, a pilot plant at Seaford, Delaware, produced PET fiber with the trade name Dacron. Dupont's polyester research led to a range of trademarked products, including Mylar (1952), an extraordinarily strong PET film that grew out of the development of Dacron.

Poly(ethylene terephthalate) is now one of the most important commercial thermoplastics. Development and growth of the global PET solid-state resin market has been quiteimpressive. More than sixty years after its introduction in the early-1940s, global consumption of PET resin reached 6.6 million metric tons in 2000. Consumption

is projected to grow at an average rate of 9.6% per year through 2005, reaching a level of 10.4 million metric tons.[2]

PET has wide applications because of its excellent combination of mechanical, optical, and gas barrier properties as well as excellent processability. PET can be processed by different methods such as melt spinning, inject molding, stretch blow molding, flat film extrusion and thermofoaming. It can be processed reliably at high speeds and in large volume. Accordingly many products can be made out of PET, such as synthetic fibers, biaxially oriented films, films for food packaging, blow molded carbonated drink bottles, photographic films, recording audio and video tapes, and electrical insulation material for capacitors.

Polyester fiber is the most important synthetic fiber produced worldwide. In 1978, polyester's share of worldwide production by fiber type was 34%. By 1998, its share had grown to 54%. PET has taken global markets by storm as the material of choice for beverage bottles. In the past ten years, a large part of the production of beverage bottles has been converted to PET, particular for water bottles. PET has excellent properties as packaging material. It is light and strong. Bottles made of PET are practically unbreakable. Even when dropped from a certain height, a PET bottle has hardly a scratch on it. PET is tasteless. As a packaging material for food and drink the material has to satisfy very strict regulations. PET is as transparent as glass. Such clarity enhances the presentation value of a product.. PET provides a protective barrier in both directions, it stops oxygen getting in from the outside and it keeps in carbon dioxide for sparkling beverages. In addition, the material is also 100% recyclable. Discarded PET products can be recycled for other applications using a variety of recycling procedures.

PET is a material with a great future. Three regions (North America, Western Europe and Asia) accounted for about 91% of world production and 82% of world consumption. Asian producers are expected to be the major suppliers of PET. Continued overcapacity and relatively lower feedstock costs compared with North America and Western Europe will be the primary drivers of Asian exports.

1.2 Limitations

Despite its wide applications and vast global market, PET has shortcomings, which limits it usage in many areas. PET has a glass transition temperature (T_g) of ~80 ^oC, which is too low to allow PET bottles to be sterilized by washing in boiling water. This is one of the reasons why PET containers are not re-used in US. For the same reason PET bottles and jars cannot be filled with hot content.

When used as tire cord, PET fiber will shrink and loose properties quickly above 100 ^oC, a condition frequently encountered when an automobile is running long for time in summer or a truck under heavy load. This requires that more PET tire cords in a tire than would be necessary if the fiber properties did not deteriorate as rapidly.

PET is a good barrier to carbon dioxide, which makes it useful for storage of carbonated beverage, but does not provide a high enough barrier to oxygen. This limits the use of PET bottles for storage of alcoholic drinks. In addition, PET does not have good dyeability or biocompatibility.

1.3. PET Modification

Increasing the glass transition temperature, high temperature mechanical properties and dimensional stability are of great importance to further expand the applications of PET. Significant research efforts have been made towards this goal, using a variety of approaches. In this work, we attempt to improve the properties of PET melt spun filament. To improve the glass transition temperature and thermomechanical properties, it is critical to restrict chain motion in the amorphous region of the fibers. Increasing chain rigidity, crosslinking of the amorphous chains and introducing interfacial barrier by adding stiff nano-structures are all expected to be effective methods to enhance selected properties of PET. Three strategies have been investigated; (i) copolymerization of more rigid linear comonomer, 4,4'-bibenzoate unit into PET, (ii) UV crosslinking of functionalized PET fiber, and (iii) Reinforcement of PET with carbon nanofibers.

1.3.1. Increasing chain rigidity by copolymerization poly(ethylene terephthalate-*co*-bibenzoate).

Increasing the rigidity of polymer backbone will limit chain motion and thereby increase the glass transition temperature. However, this often elevates the melting temperature. Copolymerization to incorporate rigid linear units night serve as a general method to increase chain rigidity while avoiding an increase in the melting temperature. Initial report in the 1970's on the incorporation of 4-hydroxybenzoic acid (HBA) into poly(ethylene terephthalate) (PET)[3] to form a thermotropic liquid crystalline polyester led to the development of Vectra, poly(hydroxybenzoate-*co*-hydroxynaphthalate), by

Celanese in 1980s.[4] The physical properties of a large number of liquid crystalline copolyesters derived from PET and a variety of dicarboxylic acids have been discussed and reviewed.[5] The 4,4'-biphenyl moiety has been incorporated as a rigid structure unit both as a diol and diacid in wholly aromatic as well as in semiflexible polyesters.[6,7] Homopolymers prepared by condensation of 4,4'-bibenzoic acid (BB) and-alkanediols, $HO(CH_2)_nOH$, in which the number of repeating methylene groups ranges from 4 to 10, are all smectic.[8,9,10,11,12,13,14,15,16,17] Modification of PET by BB resulted in an increase in T_g, strength, modulus, and gas barrier properties.[18,19,20,21,22,23]

The high cost of liquid crystalline polyesters is primarily a result of the high cost of monomers (4-hydroxybenzoic acid, 6-hydroxy-2-naphthoic acid, *trans*-stilbene-4,4'-dicarboxylic acid) coupled with commercial syntheses that require in situ acylation of phenolic groups and recovery and recycling of acetic acid byproduct. An economical process for the production of 4,4'-dimethylbiphenyl and its oxidation to BB has recently been reported.[24] This provides new impetus for the careful examination of copolymers containing BB and especially its incorporation into PET under typical PET manufacturing conditions.

In a previous paper[25] it has been shown that the fibers spun from of PET/BB copolymers with high BB content show interesting spinning behavior, which results in fibers with dramatically improved properties. Polymers with 45, 55 and 65 mole % BB (i,e. PET/BB45, 55 and 65) spin like liquid crystalline polymers in that as-spun fiber obtained at low take-up speeds (i.e. a few hundred meters per minute) exhibit maximum achievable orientation. These fibers cannot be drawn further, even above the glass transition temperature. These fibers have modulus values in the range of 35 to 45 GPa,

which is approach the value for the thermotropic liquid crystalline copolyester Vectra. For example, Vectran fiber, a 75/25 copolymer of 4-hydroxybenzoic acid and 6-hydroxy-2-naphtholic acid, HNA/HBA, has a modulus of ~60 GPa.[26] As-spun fibers of PET, PET/BB5, 15 and 35 obtained under similar conditions are amorphous and not fully oriented. A hot drawing step must be applied to this group of fibers to achieve good orientation. Even then, the modulus of this group of fibers is only about 10 GPa. The processing conditions and tensile properties of PET/BB fibers from a previous study are shown in Table 1.1. Copolymers with higher levels of BB, PET/BB45, 55 and 65 provide fibers with much better retention of modulus at elevated temperatures than fibers of PET and copolyesters with low BB content. This is apparent by dynamic mechanical analysis, in which the tan (δ) peak corresponding to the glass transition temperature completely disappears in the fully oriented PET/BB55 fiber. (Figure 1.1.)

To understand the differences in mechanical and thermomechanical properties between high BB containing fibers and that of the PET and low BB containing fibers, it is very important to understand the structure and morphology differences between them. The studies reported in Chapter II, III and IV address the crystallization of PET/BB copolymers, crystal structure, crystallinity and orientation of PET and PET/BB fibers and the effect of the fiber structure on tensile and thermomechanical properties.

1.3.2. UV crosslinking poly(ethylene terephthalate-*co*-phenylene bisacrylate)

Crosslinking offen gives polymers with improved mechanical and chemical properties such as toughness, thermo-stability and solvent resistivity. High molecular weight PET can be prepared by solid-state polycondensation, but it is slow and requires

special equipment for large scale operation. Chain extension[27] and crosslinking[28] are common methods to improve the mechanical behavior of polyesters. However this is often achieved at the expense of processability. Post-process crosslinking of polyesters is an attractive means for improving their thermal resistance without sacrificing their melt processibility.[29] Radiation-induced crosslinking are expected to be suitable means for crosslinking PET fibers.

It was reported that PET itself can be crosslinked by ultraviolet (UV) irradiation.[30] But such self-crosslinking has no practical value, since it takes a long time to achieve the crosslinking and depolymerizition upon UV-irradiation is unavoidable. Compounds containing α,β-unsaturated carbonyl functional groups, such as *trans*-cinnamic acid derivatives, 1,4-phenylene-bis(2-acrylic acid), undergo [2+2] cycloaddition in the solid state. The efficiency of photodimerization of type is determined by the face-to-face geometry of the a, b unsaturated carbonyl groups. Phenyl bisacrylate group has been found to be thermally stable at polycondensation temperature of PET. Vargas et al[31] reported that phenylene bisacrylate structural units undergo rapid photochemical reaction in the solid state to form crosslinks. This constitutes a feasible approach for a polyesters which can be photochemically thermoset after fabrication as films and fibers. It was shown, by UV and IR spectroscopy (Figures 1.2. and 1.3.), that poly(alkylene terephthalate-co-1,4-phenylene bisacrylate) (PET/PBA) spin coated thin films undergo crosslinking upon UV(300 nm) irradiation. Absorptions due to PBA disappeared in few minutes.

Based on the successful development of PET/PBA copolymers, it is interesting to investigate the psoosibility of using UV-crosslinking to improve fiber properties. The

efficiency of cycloadition between oriented chains, and the effect of crosslinking on fiber properties is discussed in Chapter V.

1.3.3. Reinforcing PET with carbon nanotube composite fibers (CNF).

Carbon fibers for composite applications were developed during the 1960s and are being used as reinforcing materials in various matrices for high strength and high temperature applications. Carbon fibera have high tensile strength and good thermal stability. When added into polymer systems, carbon fiber can improve the thermaomechanical properties of the polymer composites. While the polymer softens at high temperature, carbon fiber properties do not change significantly . Carbon fibers have typical diameters of 7 – 10 μm, which is too large to add into polymeric fiber. Carbon nanofibers developed in early 1980s[32] have typical outer diameters of 50 – 200 nm. Multi-wall and single-wall carbon nanotubes were discovered in 1990s.[33] Multi-wall tube have a diameter in the range of 20-80 nm, and single-wall nanotubes are only 0.7 to 1.5 nm in diameter. Carbon nanofibers, multi-wall carbon nanotubes, as well as single-wall carbon nanotubes (SWNT) are all being used to reinforce polymer matrices, and are suitable for reinforce polymeric fibers. However, the cost, particularly for the single wall carbon nanotubes, is high. Currently SWNTs are expensive ($500/g) and can only be produced with mixed diameter and chirality. As-produced tubes, typically contain as much as 30 wt% catalytic impurity. On the other hand, carbon nanofibers, can be produced in high volumes at low cost, using natural gas or coal as feedstock.[34,35]

While single-wall carbon nanotubes are difficult to disperse and exfoliate into polymer matrices, carbon nanofibers and multi-wall nanotubes can be successfully dispersed in polymer matrices using melt processing. Thermoplastics, such as polypropylene [36, 37, 38] polycarbonate, [39, 40] nylon,[15, 41] poly(phenylene sulfide) [42], and thermosets such as epoxy,[43] as well as thermoplastic elastomers such as butadiene-styrene diblock copolymer [44] have been reinforced with carbon nanofibers. Property enhancements include strength, stiffness, thermal stability, solvent resistance, glass transition temperature, electrical conductivity, reduced thermal shrinkage as well as optical anisotropy.

Carbon nanofibers and carbon nanotube have high aspect ratios. Their shape and anisotropic properties make them more suitable to be incorporated into fibers. Instead of making polymer bulk composites, it is interesting to spin the composites into fibers. When the nanofibers or carbon tubes are highly oriented in the polymer fiber matrix, their properties will be fully utilized. The elongational shear during fiber spinning is the most efficient way to align the nano fiber and nanotubes. CNF has been successfully added in to polypropylene fibers.[45] At 5 wt% CNF loading, the modulus and compressive strength of polypropylene increased by 50 and 100%, respectively. CNF exhibit good dispersion in the polypropylene matrix, as observed by scanning electron microscopy. (Figure 1.4.) It will be of great potential if carbon nanofibers and tubes can be successfully incorporated into PET fiber. Dispersion, alignment and interfacial strength are important factors to be addressed in this regard. Also the processability may be change with the addition of nanofibers. In Chapter VI, we describe how different types of carbon nanofibers are added in to PET. These nanofibers are different in diameter and surface

functionality. Different processing procedures, such as ball milling, melt mixing or compounding, and the effect of various nanofibers are discussed.

Table 1.1. PET/BB Fiber Processing Conditions and Tensile Properties.[25]

Polymer	IV (dL/g)	Spinning tempera-ture (°C)	Draw ratio*	Heat-Treat-ment	Tensile modulus (GPa)	Tensile strength (GPa)	Extension to break (%)
PET	0.90	280	5	Y	10 ± 1	0.6 ± 0.1	28 ± 5
PET/BB5	0.88	280	4	Y	10 ± 2	0.4 ± 0.1	22 ± 5
PET/BB15	0.94	290	3	Y	8 ± 2	0.5 ± 0.1	21 ± 3
PET/BB35	0.88	290-300	2	Y	15 ± 3	0.3 ± 0.1	9.0 ± 1
PET/BB45	1.49	305-310	ND	N	35 ± 3	1.0 ± 0.1	4.9 ± 0.4
PET/BB55	0.92	320	ND	N	32 ± 3	0.9 ± 0.1	5.1 ± 0.6
	1.2	320	ND	N	41 ± 5	1.1 ± 0.1	5.0 ± 0.7
PET/BB65	0.9	310-315	ND	N	45 ± 4	0.9 ± 0.1	4.7 ± 0.6

ND – not drawn, N – No heat treatment, Y - Heat treated at 150 ^{o}C for 10 min.
***** Fibers drawn at 120 ^{o}C.

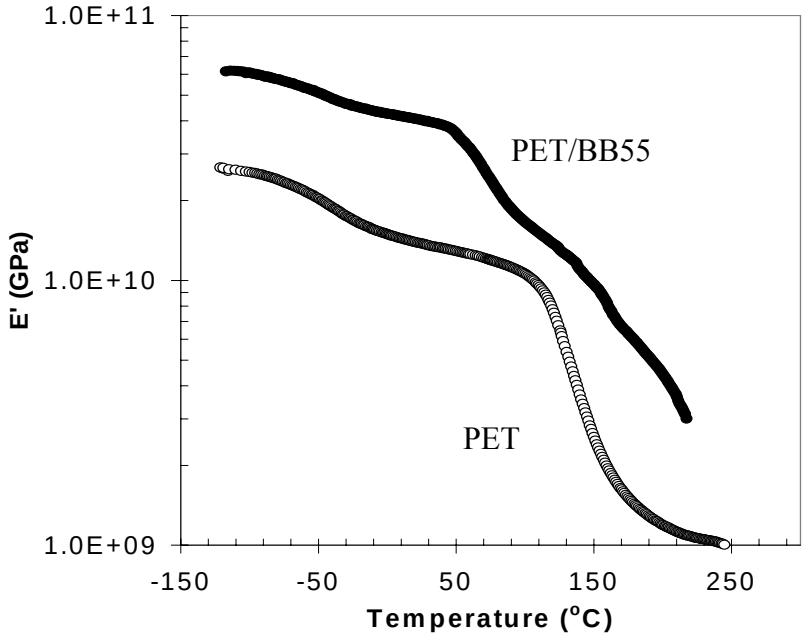

(a)

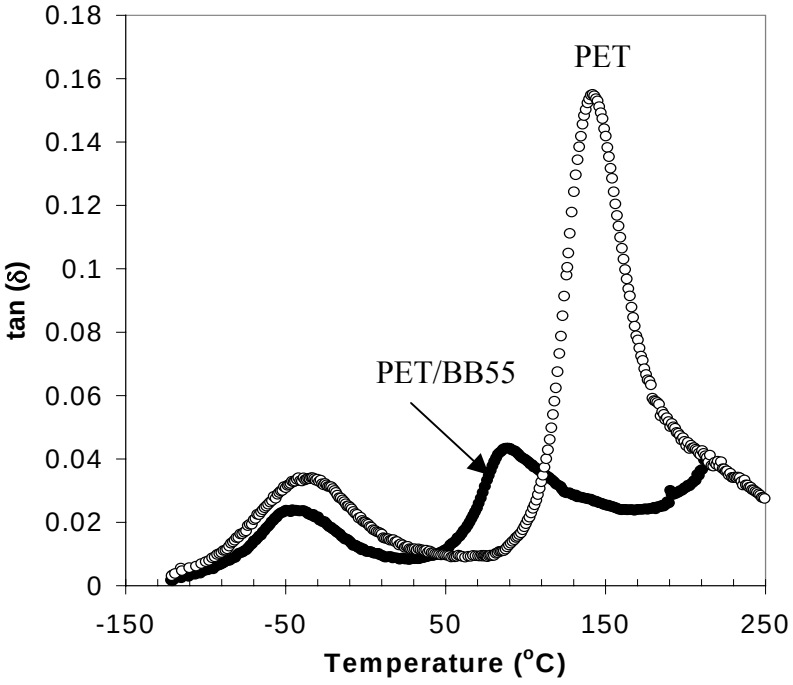

(b)

Figure 1.1. Dynamic mechanical properties of PET and PET/BB55 fibers at 1 Hz, (a) E'; (b) tanδ.

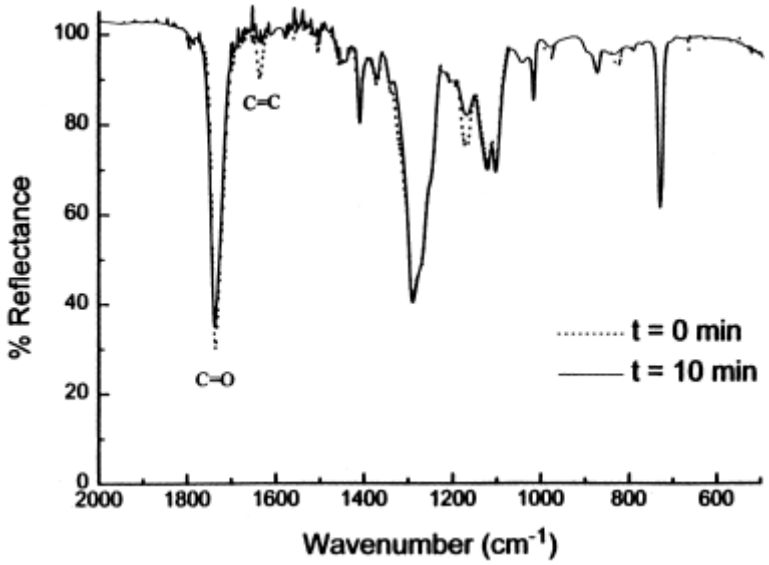

Figure 1.2. Infrared spectra of a thin film of PET containing 50% bisacrylate, before irradiation and after irradiation at 300 nm for 10 min at 25 °C.[31]

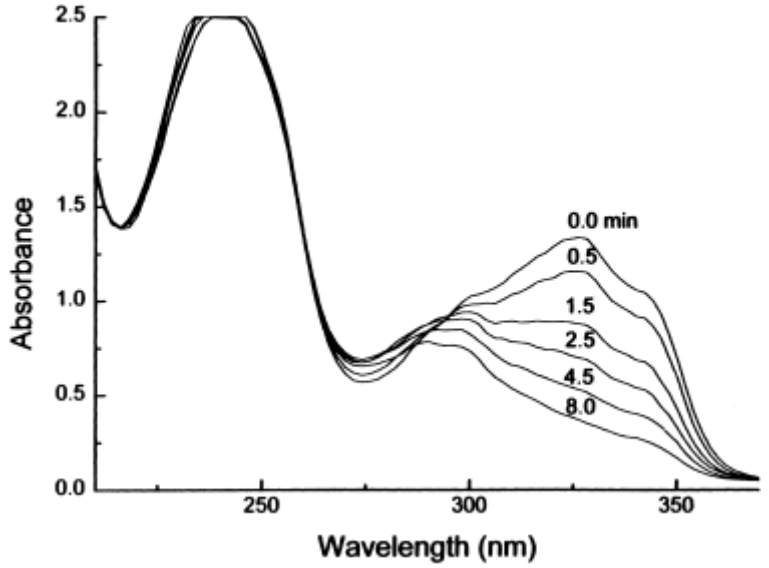

Figure 1.3. UV-vis spectra of a thin film of PET containing 20% bisacrylate irradiated at 300 nm for time *t* = 0 to 8 min at 25 °C.[31]

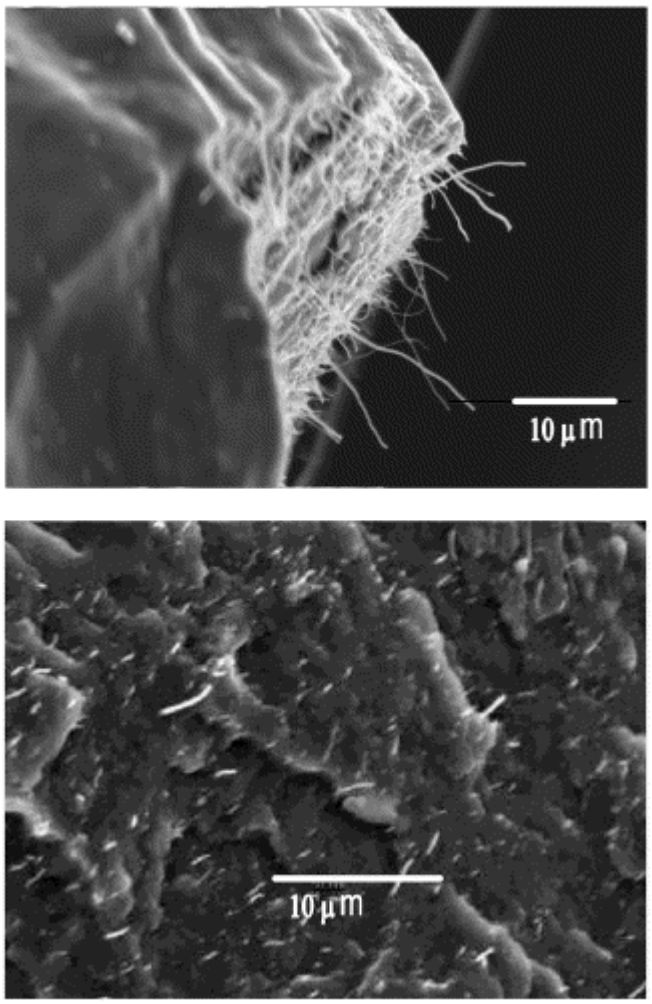

Figure 1.4. Scanning electron micrographs of fibers from PP/nano carbon fiber composite.

1.4. References

[1] Whinfield, John R.; Dickson, James T. (1946), GB 578079 19460614

[2] http://ceh.sric.sri.com/Public/Reports/541.9000/

[3] Hamb, F. L. *J. Polym. Sci.*, *Part A-1* **1972**, *10*, 3217.

[4] *Plast. World* **1985**, *43*, 65.

[5] McFarlane, F. E.; Nicely, V. A.; Davis, T. G. *Contemp. Top. Polym. Sci.* **1977**, *2*, 109.

[6] Knopka, W. N. U.S. Pat. 4,082,731, (1978).

[7] Lee, D.-K.; Tsai, H.-B. *J. Appl Polym. Sci.* **1997**, *65*, 893.

[8] Demus, D.; Richter, L. *Textures of Liquid Crystals*; Verlag Chemie: Weinheim, 1978.

[9] Watanabe, J.; Hayashi, M. *Macromolecules* **1988**, *21*, 278.

[10] Jackson, W. J., Jr.; Morrs, J. C. *Liquid Crystalline Polymers*: ACS Symposium Series 453; American Chemical Society: Washington, DC, 1990; p 16.

[11] Jackson, W. J., Jr.; Morris, J. C. U.S. Patent 4,959,450, (1988).

[12] Jackson, W. J., Jr.; Morris, J. C. U.S. Patent 5,011,878, (1990).

[13] Jackson, W. J., Jr.; Morris, J. C. U.S. Patent 5,037,946, (1990).

[14] Luyen, van D.; Strzekechi, L. *Eur. Polym. J.* **1980**, *16*, 303.

[15] Tokita, M.; Takahashi, T.; Hayashi, M.; Inomata, K.; Watanabe, J. *Macromolecules* **1996**, *29*, 1345.

[16] Tokita, M.; Osada, K.; Yamada. M.; Watanabe, J. *Macromolecules* **1998**, *31*, 8590.

[17] Osada, K.; Niwano, H.; Tokita, M.; Kawauchi, S.; Watanabe, J. *Macromolecules* **2000**, *33*, 7420.

[18] Krigbaum, W. R.; Asrar, J.; Toriumi, H.; Presston, J. *J. Polym. Sci., Polym. Lett.* **1982**,

20, 109.

[19] Asrar, J.; Krigbaum, W. R. Preston, J.; Ciferri, A.; Toriumi, H.; Watanabe, J. *Mol. Cryst. Liq. Cryst.* **1981**, *76*, 79.

[20] Cohen, S. D.; Risinger, C. A.; Poirier, J. C.; Swadesh, J. K. *Mol. Cryst. Liq. Cryst* . **1981**, *78*, 135.

[21] Asrar, J. *Speciality Polyesters '95*, *Proceedings*; Schotland Business Research: Skillman, NJ, 1995; p 155.

[22] Schiraldi, D. A.; Lee, J. J.; Gould, S. A. C.; Occelli, M. L. *J. Ind. Eng. Chem.* **2000**, *7*, 67.

[23] Polyakova, A.; Liu, R. Y. F.; Schiraldi, D. A.; Hiltner, A.; Baer, E. *J. Polym. Sci., Part B*: *Polym. Phys.* **2001**, *39*, 1889.

[24] Sherman, S. C.; Iretskii, A. V.; White, M. G.; Schiraldi, D. A. *Chem. Innovations* **2000**, *30*, 25.

[25] Ma, H.; Hibbs, M.; Collard, D. M.; Kumar, S.; Schiraldi, D. A. *Macromolecules* **2002,** *35*, 5123.

[26] Beer, D.; Ramirez, E. *J. Text. Inst*. **1990,** 4, 81.

[27] Demetris, N.; Bikiaris, G.; Karyannidis, P. *J. Appl. Polym. Sci* **1998**,797.

[28] Yu, Y. *Polym. Materi. Sci.. Engi.* **1994**, 4 125.

[29] Stephenson, C.V.; Moses, B.C.; Burks, R.E. Jr.; Coburn, W.C.; Wilcox, W.S. *J.Polym. Sci.,* **1961**, 53.465.

[30] Kobayashi, T.; . Kawase, S.; Inata, H.; Shima, T. *Janpan Kokai, Tokkyo Koho* **1974**, *132*,160.

[31] Vargas, M.; Collard, D. M.; Liotta, C. L.; Schiraldi, D. A. *J Polym Sci Part A: Polym Chem* **2000**, *38*, 2167.

[32] Tibbetts, G. G.; Devour M. G U. S. Patent 4,565,684 (1986).

[33] Ijima, S. *Nature,* **1991**, *354*, 56.

[34] Rodriquez N.M. *J Mater Res* **1993** *8*, 3233.

[35] Tarasen W.L.; Alig, R.; Glasgow, G.; Jacobsen, R. Pyrograf-III: VGCF Nano-fibers for Engineered Composites, Prograf Products Inc. report.

[36] Van Hattum, F.W.J.; Bernardo, C.A.; Finegan, J.C.; Tibbetts, G.G.; Alig, R.L.; Lake, M.L. *Polym. Comp.* **1999**; *20*, 683.

[37] Gordeyev, S.A.; Macedo, F.J.; Van Hattum, F.W.J.; Bernardo, C.A. *Physica B: Condensed Matter* **2000**, *279*, 33.

[38] Tibbetts, G.G.; McHugh, J. J. *J Mater Res* **1999**;*14*, 2871.

[39] Carneiro, O.S.; Covas, J.A.; Bernardo, C.A.; Caldiera, G. Van Hattum, F.W.J.; Ting, J.M.; Alig, R.L.; Lake, M.L. *Comp. Sci. and Tech.* **1998**, *58*, 401.

[40] Carneiro, O.S.; Maia, J.M. *Polym. Comp.* **2000**, *21*, 960.

[41] Pogue, R.T.; Ye, J. Klosterman, D.A.; Glass, A.S.; Chartoff, R.P. *Composites, A* **1998**; *29*,1273.

[42] Patton, R.D.; Pittman, C.U. Jr, Wang, L.; Hill, J.R. *Composites, A* **1999**;*30*,1081.

[43] Ciminelli, D.L.; Kearns, K.M.; Ragland, W.R. *Proc 41st Inter SAMPE Symp* 1996; 496.

[44] Chellappa, V.; Chiou, Z.W.; Jang, B.Z. *Proc 26th SAMPE Tech Conf* **1994,**12.

[45] Kumar, S.; Doshi, H.; Srinivasarao, M.; Park, J. O. *Polymer* **2002***, 43***,** 1701.

CHAPTER II

CRYSTAL STRUCTURE AND COMPOSITION OF CRYSTALLINE AND AMORPHOUS REGIONS IN RANDOM POLY(ETHYLENE TERETHPHALATE–*co*-4,4' BIBENZOATE) COPOLYMERS

2.1 Abstract

Crystal structure in random copolymers poly (ethylene terethphalate–*co*-4,4' bibenzoate) (PET/BB) were studied by using wide angle X-Ray diffraction (WAXD). Composition of PET/BB fiber in terms of comonomer distribution in crystalline and amorphous regions were studied by FTIR spectroscopy using the amorphous peaks at 1580 and 1560 cm^{-1} for terephthalate (T) and bibenzoate (B) units respectively. Further, PET/BB55 fibers were hydrolyzed to selectively etch the amorphous regions. The compositions of hydrolyzed products were determined by spectroscopy methods. Crystallites were further studied by using, DSC, wide angle x-ray diffraction, and transmission electron microscopy. Results show that PET/BB copolymers crystallize differently than described by the non-periodic model (npl), at least not by uniform copolymer incorporation. Crystal structure in low BB-content samples are "T" type and that of high BB-content copolymer are "B" type. Crystal structures are very close to that of respective homopolymer, PET and polyethylene bibenzoate, (PEBB). Crystalline region of high BB-content fibers are composed of mainly PEBB units. In PET/BB55

fiber, among the 30 wt % of the copolymer which was not etched, there is only one terephthalate unit per every 5 repeat units of bibenzoate. Crystal size of B type crystals along the c axis was found to be only couple of repeat units long. Short chain segments rich in BB are sufficient to induce crystallization, to form PEBB crystals.

2.2. Introduction

Poly(ethylene terephthalate–co–4,4'-bibenzoate) (PET/BB) copolymers crystallize across the entire composition range, especially upon orientation and annealing.[1] Theories developed by Flory,[2] Baur[3] and Wunderlich's[4] based on random copolymer crystallization by homo-sequence aggregation and comonomer exclusion do not explain the crystallization behavior of random copolymers in the intermediate composition range. Co-crystallization of aromatic and semiaromatic copolyesters has been a subject of intensive research[5,6,7,8,9,10] Hachibosh, et al.[11] have shown that 10 to 15% of the isophthalate units of poly(ethylene terephthalate-*co*-isophthalate) PET/I(with less than 15 mol% of I), enter into the crystalline phase. However, the comonomer units do not cocrystallize in the case of copolyesters with phthalate and sebacate. Differences in the length of the repeat unit and the conformational flexibility of the chain were found to be critical for isomorphous cocrystallization. Windle and coworkers proposed a non-periodic layer (NPL) model for random liquid crystalline copolymers poly(1-hydroxy-4-benzoic acid-*co*-2-hydroxy-6-naphtholic acid)[8,9,10] and extended it more generally to semi-aromatic copolyesters e.g., PET/N.[12,13] They found that these random copolymers crystallize by segregation and lateral matching of short chain sequences in the polymer backbone. The crystals therefore contain both types of monomers to form a

layered structure having periodicity perpendicular to the chain direction, but a non-periodic structure along the chains. Similarly, Wendling et al. found the poly(ethylene 4,4'-bibenzoate-*co*-2,6-naphthalate) (PEN/BB)[5] random copolymers cocrystallize uniformly by aggregation of like and segregation of unlike repeat units. Biswas and Blackwell[14,15] proposed a different explanation for crystallization of the same random copolymers: the plane start model. In this model there is no sequence matching but chains are in registry on one single plane in the crystal. It is uncertain whether these aggregates can reach the minimum size of thermodynamically stable nuclei and the plane start model can be considered as a special case where crystallization arise from aggregation of only one or two repeat units. The difference between the two models is difficult to discuss X-ray diffraction alone. The question really reduces to how many repeat units (or how long is the chain segment of same sequence) are needed to inducing crystallization.

Fibers spun from of PET/BB copolymers wit high BB-content show interesting spinning behavior which results in fibers with dramatically improved properties. Polymers with 45, 55 and 65 mole % BB (i,e. PET/BB45, 55 and 65) spin like liquid crystalline polymers in that as-spun fiber obtained at low take-up speeds (i.e. a few hundred meters per minute) exhibit maximum achievable orientation. These fibers cannot be drawn further, even above the glass transition temperature. These fibers have modulus values in the range of 35 to 45 GPa, which is approaching to the value for thermotropic liquid crystalline copolyester Vectra. For example, Vectran fiber, a 75/25 copolymer of 1-hydroxy-4-benzoic acid and 2-hydroxy-6-naphtholic acid HNA/HBA, has a modulus of ~60 GPa.[16] On the other hand, as-spun fibers of PET, PET/BB5, 15 and 35 obtained under similar conditions are amorphous and not fully oriented. A hot drawing step must

be applied to this group of fibers to achieve good orientation. Even then, the modulus of the second group of fibers is only around 10 GPa. Moreover, PET/BB45, 55 and 65 fibers have much better retention of modulus at elevated temperatures than fibers of PET and copolyesters with low BB content. This is apparent by dynamic mechanical analysis, in which the tan (δ) peak corresponding to the glass transition temperature completely disappears in the fully oriented PET/BB55 and 65 fibers.

Given the strong influence of BB units on the fiber properties of PET/BB copolymers, we set out to examine the crystal structure of these copolymers and to compare these to PET/N[12] and PEN/BB.[5] Given the random nature of this copolymer and the potential for crystallization of particular segments along the backbone it is important to determine how the crystal structure and crystallinity varies as a function of polymer composition, as well as the composition of crystalline and amorphous phase. To study the composition of the crystalline regions in PET/BB, it was desirable to separate the crystals from the amorphous polymer. PET has been selectively hydrolyzed to remove amorphous regions and to preserve the crystals. [17,18] Thus we have followed a similar procedure to selectively remove the amorphous chains from the PET/BB55 fibers. This allows the composition of the amorphous and crystalline regions to be elucidated and for correlation of physical properties with phase structure and orientation. In this contribution we used X-ray diffraction to study the crystal structure as a function of copolymer composition.

2.3. Experimental

Poly(ethylene terephthalate – *co* – 4,4' bibenzoate) copolymers were made by mixing dimethyl terephthalate and dimethyl bibenzoate during the melt condensation

with ethylene glycol.[19] Polymer randomness was confirmed by sequence analysis using ^{13}C NMR spectroscopy.[1] Fibers of PET/BB copolymer were melt-spun as reported in a pervious study.[1] Crystal structures of bulk polymers and fibers were studied by wide angle X-ray diffraction (WAXD) on a Rigaku Small/Wide Angle X-ray Scattering system with a MicroMax 002™ X-ray beam Generator (XBG), operating at 45 kV and 0.66 mA. CuK_α irradiation was obtained by using a confocal Max-Flux® optics. 2D diffraction images were collected using a Rigaku R-AXIS IV^{++} detector. Air background scattering was subtracted after making a correction for absorption by the sample. Radial, equatorial and azimuthal scans were integrated using AreaMax® software and profile fittings were carried out using MDI Jade 6.1. A linear background was fitted for all the curves. Profile fittings were repeated until the residual error of fit was less than 2%. The d-spacing and crystal thickness of PET and PET/BB fibers were obtained from either equatorial scans or meridional scans, while radial scans were used for the bulk polymer. Crystal size was calculated by using the Scherrer equation,[20] with a value of K of 0.9. Crystallinity was determined from the ratio of the peak area for crystalline peaks and the total area under the radial scan curves.[21]

The composition the crystalline and amorphous regions of PET/BB were studied by FTIR spectroscopy using the peaks at 1580 and 1560 cm^{-1} for terephthalate (T) and bibenzoate (B) units, respectively. PET/BB55 fibers were hydrolyzed to separate the amorphous regions from the crystals. A mixture of water (50 mL) and fiber (0.86 g) was heated to 160 ^oC for 60 hours in an autoclave with a Teflon liner. These conditions were chosen based on previous reports of the hydrolytic etching of semicrystalline PET in which weight loss and lamella thickness levels off after 50 hours.[18] The solid product

was removed by filtration and washed with dimethyl sulfoxide (DMSO). IR spectra of the pristine fiber and hydrolyzed materials were obtained on a Perkin Elmer Spectrum One FTIR spectrometer. ^{1}H-NMR spectra were obtained using a Varian Mercury Vx 300 spectrometer at room temperature. The fiber and the DMSO-insoluble part were dissolved in trifluoroacetic acid-d_1, while the DMSO-soluble fraction as recorded in dimethyl sulfoxide-d_6. Samples for transmission electron microscopy were prepared by depositing the aqueous suspension of the DMSO-insoluble part onto carbon grids and drying in air at room temperature. Bright field images and selected area electron diffraction (SAED) patterns were collected on a JEM 4000 EX operated at 400 kV and recorded on Kodak Microscope Film (SO163). SAED patterns were taken at a camera length of 66 cm. The TEM camera length was calibrated by using the d-spacing of evaporated gold.

2.4. Results and discussions

2.4.1. X-ray diffraction on unorientated samples

Wide angle X-ray diffraction (radial scans) of annealed bulk PET homopolymer and PET/BB copolymers are shown in Figure 1. The scans clearly indicate the crystalline nature the copolymer across the whole composition range. Crystallinity estimated from X-ray diffraction is plotted in Figure 2. The radial scan of PET/BB15 is similar to that of the PET. On the other hand, the radial scans of PET/BB45, 55 and 65 are comparable to each other and match the diffraction patterns of homopolymer poly(ethylene bibenzoate), PEBB by Li and Brisse.[22] For PET/BB35, diffraction peaks corresponding to the crystal structures of both PET and PET/BB can be seen. These observations suggest that the crystal packing changes from that of PET to PEBB with increasing bibenzoate content,

and that at intermediate levels of bibenzoate (e.g. PET/BB35) both PET and PET/BB crystals co-exist. Hereafter, we refer the PET like crystals as "T" type crystal and PEBB like crystal structure as "B" type crystal. The indexing for PET and PEBB homopolymer were used for T type unit cells and B type unit cells respectively. d-spacings observed for PET/BB copolymers (Figure 1) are listed in Table 1 for T type crystal structure and Table 2 for B type crystal structure. The presences of (101) and (110) diffraction peaks indicate that the crystal has a 3-D structure. For both crystal structures, the d-spacings change gradually with increasing bibenzoate content, which may be due to the incorporation of BB unit into T crystals or T unit incorporation into B crystals. Both PET and PEBB crystallize in the triclinic form. Using the unit cell parameters of PET obtained by Fu et al.[23] (a = 4.508, b = 5.882, c = 10.787, α=100.01, β=118.36, γ= 110.56), that of PEBB by Li and Brisse [22] (a = 5.75, b = 3.82, c = 14.62, α= 90.1, β= 90.3 γ= 78.1) and various d-spacing collected from Table 1 and 2, we calculated the unit cell parameters for PET/BB copolymer for both T type and B type crystals, which are compared in Figure 3a-c. In the lateral direction, the length of a and b in both T and B type crystals change as the composition changes, but there is a difference in lattice parameters between the two types of crystals. It is understandable that different comonomers may be able to enter the crystal of different type. Along the chain direction, length of the c-axis would change continuously, if the copolymer were to crystallized by sequence matching model (NPL), as in the case of PET/N[12] However in PET/BB copolymers, (as shown in Figure 3c) as the amount of BB increase, there is a transition for a T type lattice a B type lattice structure at 35 mol% of B. For PET/BB35 two crystal forms coexist. The length of the c axis in T type crystal increase by the addition of the B

comonomer. However that of B crystals does not change significantly with the addition of T. These results suggest that in PET/BB copolymers, the T and B units do not co-crystallize uniformly across the entire composition range of PET/BB.

2.4.2. X-ray diffraction of fibers

Radio wide angle X-ray diffraction scans of PET/BB fibers are shown in Figure 4. Flat plate diffraction photographs of PET/BB fibers are shown in Figure 5a-f. The crystals of fibers, again, can be divided into two groups. PET/BB15 and 35 have T-type crystals, PET/BB45, 55 and 65 fibers have B-type crystals. However, in the case of high BB-content fibers the (010) and (110) present in bulk annealed polymers are absent that the chain packing is not perfectly ordered in the 010 plane normal direction. Crystal size determined from this peak at ~25^{o} (3.5 Å d-spacing) is about 3 nm. Annealing at high temperature result in separation of this broad peak into two separate peaks corresponding to (010) and (110) diffractions as observed for the annealed bulk polymer. On the other hand chain packing in the (100) and (101) normal directions is efficient as can be seen from the sharp diffraction spots.

Meridian scans of PET/BB45, 55 and 65 fibers are plotted in Figure 6. (001), (002), and (005) diffraction spots are observed. (the (106) diffractions also appeared due to leaching of their intensities into the meridian direction). Two diffraction peaks at 14.71 and 7.34 Å, corresponding to the (001) and (002) diffractions of PEBB, respectively, can be seen in PET/BB55 and 65. The crystal thickness of B type crystal structure along the chain direction determined from the (001) peak using the Scherrer equation is 75 Å, which corresponds to the length of about 5 PEBB repeat units. In addition, horizontal

streaks are seen in diffraction pattern of high BB-content fibers (Figure 4d-f). These narrow and high intensity streaks are a prominent feature in the meridional direction of the high BB-content fibers. The 3.5 Å spacing of the horizontal streak in PET/BB55 fiber is less than the expected spacing of the (004) plane for PEBB, which is 3.65 Å. The width of the horizontal streaks corresponding to a domain size of about 49 Å, which is about the length of three repeat units along the PEBB chain axis. The BB average sequence length in PET/BB55 is calculated to be 2.3, based on a ideal random copolymer distribution. Similar horizontal streaks were observed in many rigid rode polymers as well as semi-aromatic polyester fibers.[12] The origin of streaks has been ascribed to diffraction from single chaind, and the position of the streak is therefore a function of copolymer composition. The aperiodic spacing of the streaks are accord with the aperiodic nature of the structure along the random chains.

To further examine the meridional streak observed in PET/BB fibers, we stretched a amorphous copolymer at room temperature (PET/BB55 has a T_g of 105 ^{o}C) to provide a noncrystalline but oriented fiber. WAXD of this fiber shows a diffuse diffraction in the equatorial direction and horizontal streaks in the meridional direction. Upon annealing, the fiber crystallizes and the meridional streaks observed in the amorphous fiber were preserved. These streaks disappeared when the fiber was heated without constraint to ~200 ^{o}C, while the diffraction pattern of the crystal survived. These observations suggest that the streaks in PET/BB45, 55 and 65, fibers originate from the oriented chains in the amorphous regions of the fiber rather than from the crystals. The fact that we observe diffraction from crystals and amorphous chains, in PET/BB55 and 65 indicates that the crystals are formed by pure PEBB units rather than a random sequence as in the case of

PET/PEN copolymer.[12,13] The crystalline regions in high BB-content fibers give sharp periodic diffractions spots, while the amorphous region gives aperiodic diffraction streaks. The streaks are dominated in intensity due to large volume fraction of the amorphous regions. A similar situation was found in a wholly aromatic copolyester fiber composed of p-hydroxybenzoic acid, 4,4'-dihydroxydiphenyl, terephthalic acid and isophthalic acid, where both diffraction spots and horizontal streaks in the meridional direction were observed.[24] The diffraction spots came from the PHB crystals and the streaks originated from the disordered chains.

From X-ray analysis, we conclude that high BB-content fiber crystallizes in the PEBB form, rather than homogeneous incorporation of the two monomer units in crystals by sequence matching. The difference in the *c*-axis length, between T (10.75Å) and B (14.62Å) crystals is significant, which may not be easily compensated for by rotation of the ethylene glycol unit. To determine the composition of the crystallites in the copolymers we carried out spectroscopic analysis and hydrolytic etching.

2.4.3. Vibration spectroscopy

FTIR can be used to estimate the composition of the crystalline and amorphous regions of PET/BB fibers. The V_{8a} vibration mode from the terephalate unit is symmetric to the inversion center of the molecule in the crystalline state so it is IR-inactive. In the amorphous regions the chains deviate from a symmetric position and the V_{8a} motion becomes IR active with absorption at 1580 cm^{-1}, thus this peak is only a characteristic of the terephthalate rings in the amorphous regions.[25,26] Due to the centrosymetric nature of the PEBB crystal structure,[22] the same situation occurs with respect to bibenzoate units in

PET/BB copolymers. FTIR spectra of PET and PET/BB fibers are shown in Figure 7. In PET there is only one peak at 1580 cm^{-1}. With the incorporation of BB a new peak appears at 1560 cm^{-1} and its intensity increases with increasing BB content. The ratio of these two peaks gives the relative concentration of the two monomers in the amorphous regions. Combined with the crystallinity data obtained from the wide angle X-ray diffraction, the distribution of repeat units in the amorphous and crystalline regions can be calculated, Table 5. This result shows that in low BB-content fibers the BB units are mainly in the amorphous region. However, in high BB-content fibers the crystalline region is rich in BB units and the amorphous region has both BB and T units.

2.4.4. Hydrolysis

Under our hydrolysis conditions, it is expected that only the amorphous regions are hydrolyzed and that the crystalline regions remain intact. After hydrolysis the residual solid was washed several times with DMSO at room temperature to give DMSO-soluble and insoluble fractions. Hydrolysis of 860 mg of PET/BB55 fiber gave 250 mg of DMSO-insoluble solid. Both the DMSO-soluble and insoluble parts were subjected to FTIR and NMR analysis.

The FTIR spectra of PET/BB55 fiber together with the DMSO-insoluble and soluble fractions are shown in Figure 8. For the fiber, there are no observable acid or ethylene glycol end group absorptions (i.e., O-H stretch). The absorption at 1750-1720 cm^{-1} (carbonyl stretching), 1200-1150 cm^{-1} (CO-O stretching) and 1100-1050 cm^{-1}, (O-CH_2 stretch) are characteristic of main chain polyesters. The absorptions at 1370 and 1340 cm^{-1} arise from the ethylene glycol wagging in gauche and trans conformations,

respectively. After hydrolysis, the IR spectrum of the DMSO-insoluble part resembles that of the polymer, except the prominence of –OH stretching at 3600 cm^{-1}, broadening of the carbonyl stretching vibration to lower frequency, and the decreased absorbance at 1100 cm^{-1}, which are all indications of a decrease in the length of the polymer chain. The ratio of the absorbances at 1370 and 1340 cm^{-1} indicates that the trans/gauche ratio increases upon hydrolysis. This is consistent with selective etching away the amorphous regions since the gauche contribution of the original polymer only comes from the amorphous regions. The IR spectrum of the DMSO-soluble part is dramatically different from that of the fiber and the DMSO-insoluble part. The bands at 2850 cm^{-1} and 1650 are characteristic of an aromatic carboxylic acid rather than an ester. The ethylene glycol CH_2 wagging mode 1370 and 1340 cm^{-1} and the ester O-CH_2 stretch at 1018 cm^{-1} are all absent, suggesting that the hydrolysis byproducts are mainly low molecular weight acids rather than polyester and the ethylene glycol formed by the hydrolysis reaction would be removed during evaporation of the DMSO.

More quantitative results can be obtained from ^1H NMR. The spectrum of the pristine polymer, and the DMSO-insoluble and soluble parts are shown in Figure 9. The spectrum of the fiber shows a ratio of aromatic to aliphatic units of 1:1, consistent with the structure of the polymer. The ratio of the phenyl and biphenyl rings is 45:55, consistent with the ratio of comonomers used in the polymerization. The spectrum of the DMSO-soluble part indicates a ratio of 1,4-phenyl and 4,4'-biphenyl units of 52 to 48. On the other hand, in the DMSO-insoluble part the ratio between aromatic units to ethylene glycol units is close to 50:50. The ratio between phenyl and biphenyl unit is 17:83. This result suggests that the DMSO-insoluble part, i.e. crystalline regions, consists

mainly of bibenzoate units. There are some terephthalate units in this fraction, which might be incorporated inside the crystal or lie between the lamella planes. In the case of PET, Calleja et al.[17] have shown that hydrolytic etching is inefficient towards removal of the chain segments within the intralamellar regions.

X-ray diffraction radio scan of the DMSO insoluble part is shown in Figure 10, which indicates a degree of crystallinity of 87%. The d-spacings listed in Table 6 match those of the PEBB crystal.[5,22] Thus, the DMSO-insoluble portion consists of crystal lamellae of B. The mass-balance and crystallinity of the DMSO-insoluble fraction corresponds to a weight percent crystallinity in the pristine fiber of 29%. This is in good agreement with the X-ray crystallinity index of the pristine fiber prior to hydrolysis (30%). PET/BB55 polymer annealed at 210 ^{o}C for 10 hours shows crystallinity of 32%. Assuming there was no significant increase in crystallinity took place during the hydrolysis, these results suggest that the hydrolysis is selective for ester linkages in the amorphous regions. Crystal thickness normal to (100), (101) and (001) diffraction planes for PET/BB55 fiber and that of the DMSO-insoluble part are compared in Table 6. The crystal thickness normal to the (100) plane increased significantly upon hydrolysis, which may be due to lateral aggregation of crystallite. However, crystal thickness in the (101) and (001) normal directions did not change. This is expected as chains are being cut and the crystal size cannot increase along the chain direction. Thus, we obtained thin lamellar crystal plates of BB rich polymer by hydrolysis.

The DMSO-insoluble part was dispersed in water and deposited on a carbon grid and observed by transmission electron microscopy. Typically, lamellar crystal aggregate were observed. (Figure 11) Electron diffraction pattern (Figure 12a) can be assigned by

using the unit cell of the PEBB crystal (Table 7). The pattern suggests that the view direction of this image is corresponds to the $(\bar{1}11)$ direction of the PEBB crystal and that the lamella is composed of 100 twinned crystallites. This, coupled with the chain packing in the unit cell suggests that the polymer chains in the each twinned crystal are anti-parallel. Diffraction pattern from other different lamella (Figure 12b) can also be assigned by PEBB unit cell viewed from (101) direction. These results further confirm that the crystal structure of BB rich PET/BB copolymers is dominated by PEBB units. The terephthalate units, which observed by FTIR, must lie between the lamellar crystals.

2.5. Discussion

From the X-ray diffraction analysis above we conclude that PET/BB random copolymers crystallize into either T or B type crystals depending on the copolymer composition. The difference of the length of the *c* axis between T type and B type crystals suggests that crystals are not formed by sequence matching, but rather by relatively pure segments of T or B units. In copolymer with intermediate levels of BB, random BB rich chain segments of five repeat units, e.g. "BBTBBB" aggregate and crystallize to form B crystals. The probability to find this type of chain segments in random PET/BB45 to 65 is significant.

Homopolymers of 4,4'-bibenzoate and various diols have been shown to be liquid crystalline.[22,27,28,29,30,31] Mesophase and transient liquid crystallinity have been reported in PET,[32,33,34,35] and PET/N copolymers.[36] Although, no direct evidence of liquid crystallinity from thermal and rheological analysis was obtained, we did observe a highly

birefringent and mobile phase for PET/BB45 at 210 ^{o}C, under shear upon cooling from the isotropic melt.[1] Spinning behavior and mechanical properties of PET/BB45, 55 and 65 suggests the formation of a liquid crystalline phase. With the increased chain rigidity, as a result of bibenzoate unit providing sequences rich in high BB units, it is possible that the few homo-sequences of B unit segments aggregate in the melt and form a transient liquid crystalline regions of limited size, which than crystallize into thin plate-like crystals. Thus, a structured melt formed during melt spinning could provide for better fiber orientation. We will show in a separate paper that the amorphous chains in high BB-content PET/BB fiber indeed have much better orientation than that of PET and low BB-content fibers.[37] The resulting structure imparts superior physical properties to fibers than the conventional two phases (i.e. crystalline and amorphous) of the same composition.

2.6. Conclusions.

The results of this study show that PET/BB random copolymer can develop significant crystallinity over the entire composition range, but in two different forms. There is not a continuous change between these two forms, but rather there is a discontinuity at 35 mol% of BB. This is inconsistent with the NPL model for cocrystallization. PET crystals are formed in low BB-content copolymer. Thin PEBB crystals are formed by lateral registry of only a few repeat units in copolymers containing 45 to 65 mol% of BB.

Table 2.1. d-spacings (in Å).for T type crystals in PET/BB unoriented samples

Polymer	**$(0\bar{1}1)$**	**(010)**	**$(\bar{1}10)$**	**(100)**
PET	5.447(3)	5.028(6)	3.898(5)	3.392(8)
PET/BB15	5.454(1)	5.013(7)	3.898(6)	3.471(3)
PET/BB35	5.432(4)	4.983(4)	3.886(4)	3.473(2)

Table 2.2. d-spacings (in Å) for B type crystals in PET/BB unoriented samples For comparison PEBB d-spacings from literatures are also given.

Polymer	**(100)**	**(101)**	**(010)**	**(110)**
PET/BB35	5.490(2)	5.149(1)	3.634(1)	3.356(1)
PET/BB45	5.523(1)	5.159(1)	3.648(1)	3.365(1)
PET/BB55	5.563(1)	5.193(2)	3.665(1)	3.378(2)
PET/BB65	5.549(1)	5.208(2)	3.667(1)	3.386(1)
PEBB[22]	5.628	5.252	3.699	3.404
PEBB[5]	5.545	5.206	3.651	3.377

Table 2.3. d-spacings (in Å) of the T type crystals in PET, PET/BB15 and PET/BB35 fibers.

Fiber	**(010)**	**$(\bar{1}10)$**	**(100)**
PET	5.036(6)	3.892(4)	3.453(8)
PET/BB15	5.082(7))	3.901(6))	3.464(3)
PET/BB35	5.260(6)	3.791(4)	3.471(2)

Table 2.4. d-spacings (in Å) of B type crystals in PET/BB45, PET/BB55 and PET/BB65 fibers.

Fiber	**(100)**	**(101)**	**-**	**(001)**
PET/BB45	5.610 (2))	5.230(1)	3.560(4)	14.30(8)
PET/BB55	5.607(3)	5.22(3)	3.583(3)	14.87(5)
PET/BB65	5.629(3)	5.24(1)	3.580(1)	14.75(1)

Table 2.5. Monomer distribution in the amorphous and crystalline regions as estimated by FTIR for PET/BB fibers

Fiber	**Crystallinity (wt%)**	**A^a_{1560}/ $A_{(1560+1579)}$**	**Amorphous region**		**Crystalline region**	
			B	**T**	**B**	**T**
PET	40	0	0	60	0	40
PET/BB15	30	0.12	10	65	5	20
PET/BB35	21	0.30	30	60	5	15
PET/BB45	23	0.40	30	50	15	5
PET/BB55	30	0.43	30	40	25	5
PET/BB65	43	0.52	30	30	35	5

a: area under the peak.

Table 2.6. Comparison of crystal thickness (in Å) before and after hydrolysis

hkl	**(100)**	**(101)**	**(001)**
PET/BB55 fiber	96	73	75
DMSO-insoluble part	150	78	71

Table 2.7. d-spacings (in Å) of DMSO insoluble part obtained from X-ray and electron diffraction. For comparison literature values are also given.

hkl	$d_{obs,\ X\text{-}ray}$	$d_{obs,\ ED}$	**Li, Brisse [22]**	**Lu, Windling [5]**
100	5.58	5.2	5.62	5.54
010	3.65	3.7	3.69	3.65
110	3.37	-	3.44	3.37
101, $\bar{1}01$	5.21	-	5.26	5.2
111		3.3	3.32	-
$1\bar{1}1$		2.7	2.80	-
$\bar{1}02$	4.44	-	4.43	4.53
002	8.89, 7.53	-	7.36	8.71
201	2.75	-	2.78	-
202		2.6	0.263	-
212	2.33		2.34	-
007	2.06		2.06	-
300	1.85		-	-

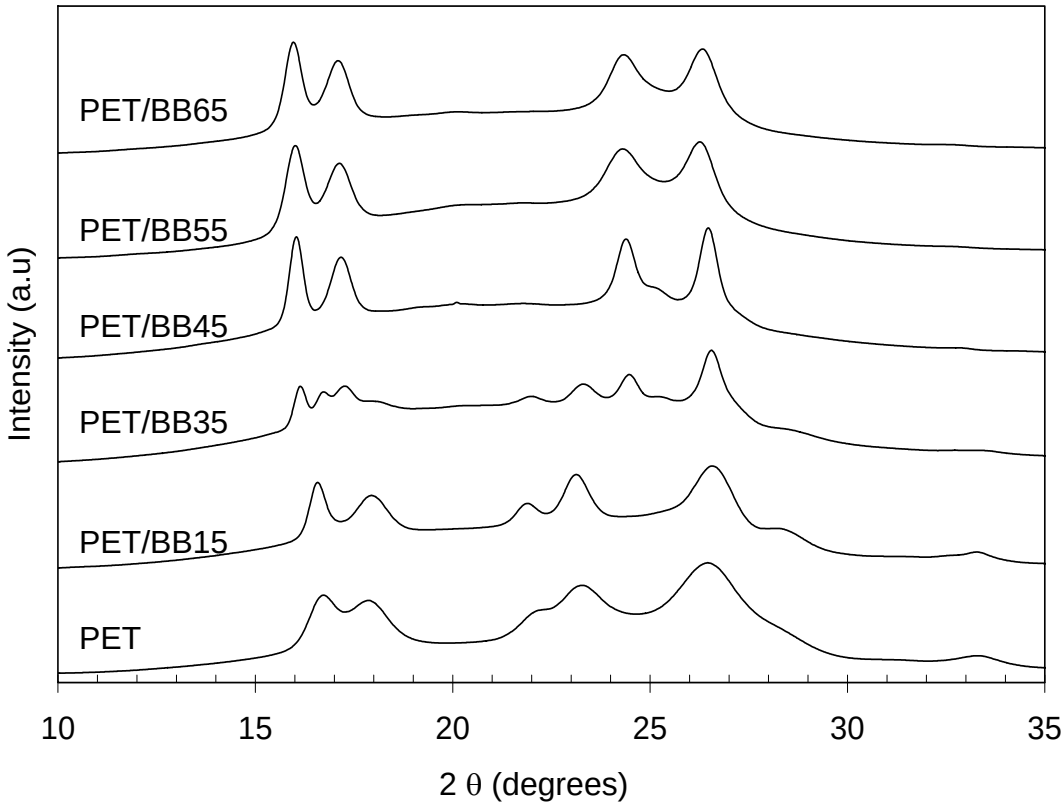

Figure 2.1. WAXD (radial scans) of PET and PET/BB bulk copolymers

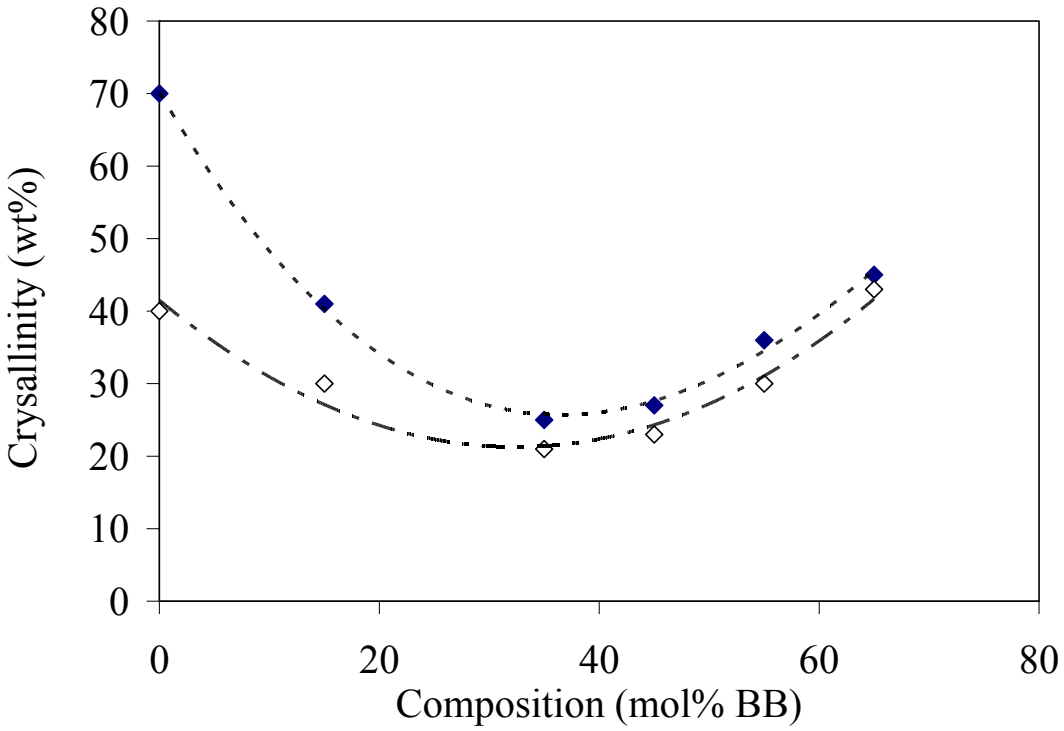

Figure 2.2. Crystallinity in PET/BB copolymers as measured by X-ray method. Solid symbol: annealed bulk polymer, Open symbol: heat-treated fibers**.**

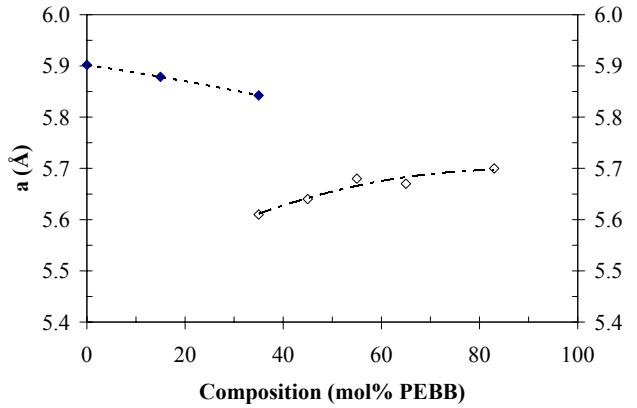

(a)

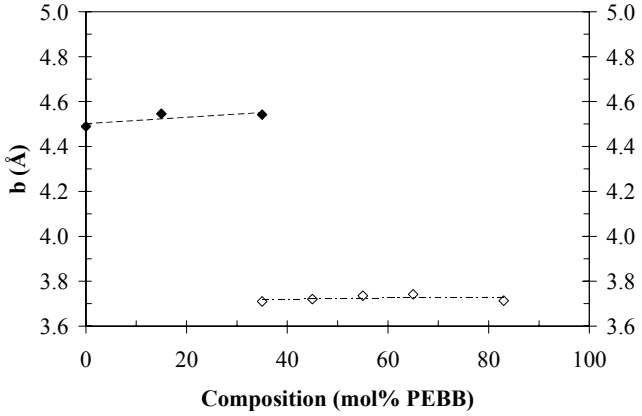

(b)

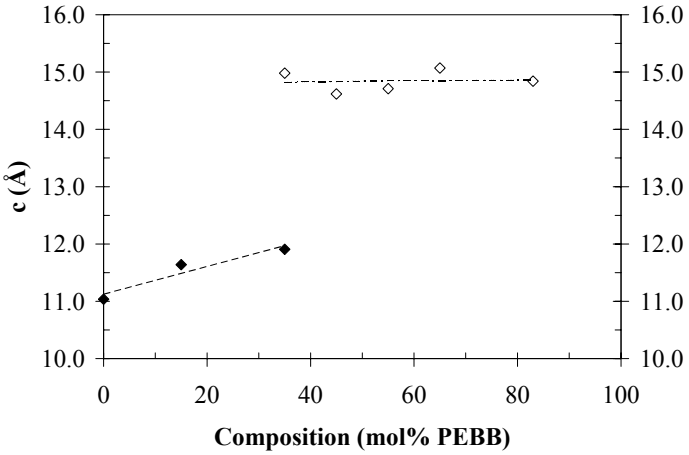

(c)

Figure 2.3. PET/BB unit cell parameters as a function of copolymer composition

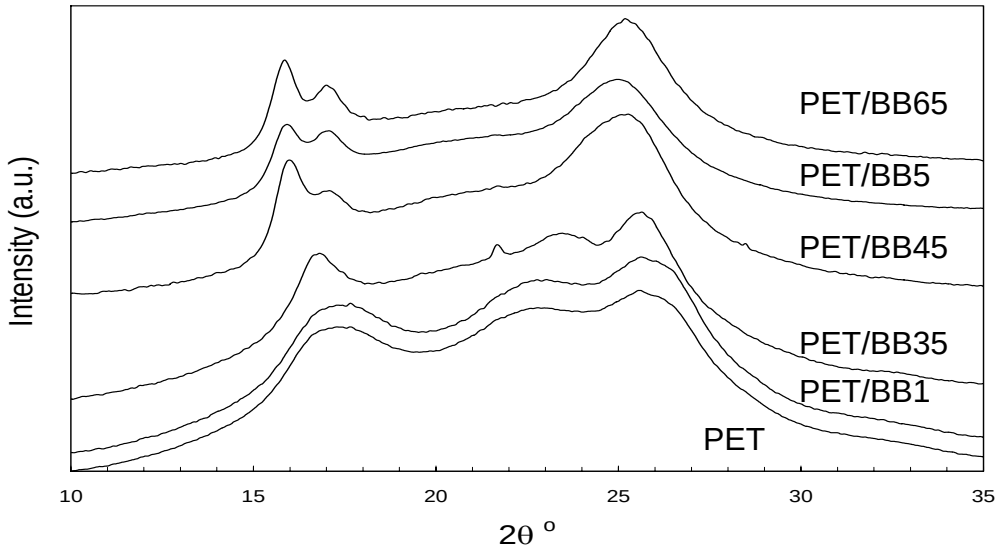

Figure 2.4. WAXD (radial scans) of PET and PET/BB fibers.

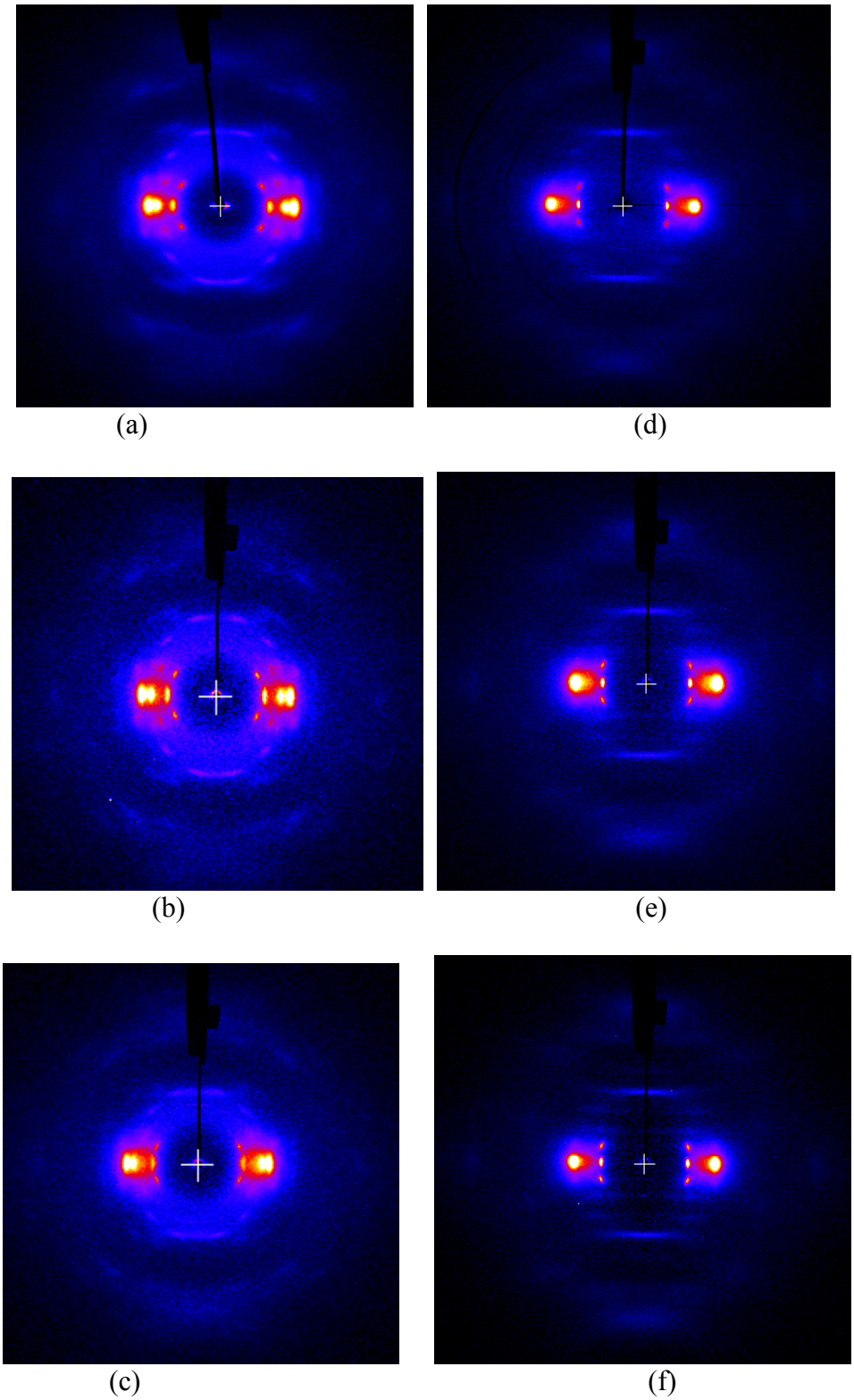

Figure 2.5. WAXD of PET and PET/BB fibers. (a) PET, (b) PET/BB15, (c) PET/BB35, (d) PET/BB45, (e) PET/BB55, (f) PET/BB65.

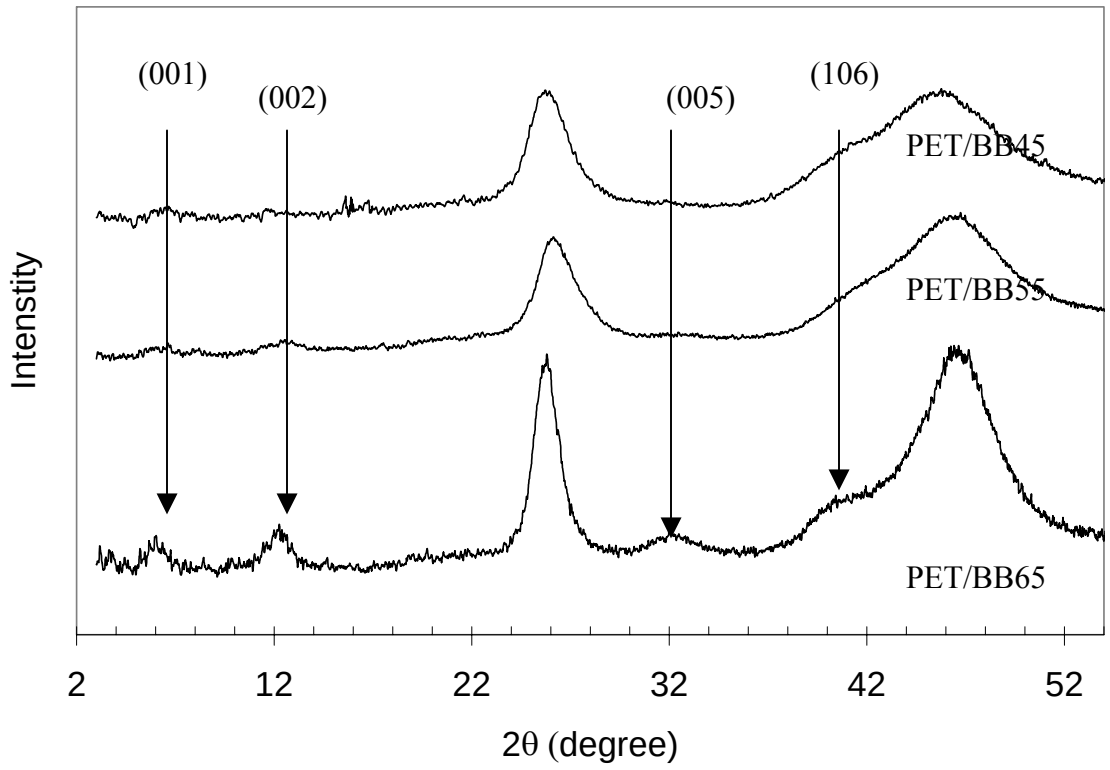

Figure 2.6. WAXD meridional scans of PET/BB fiber.

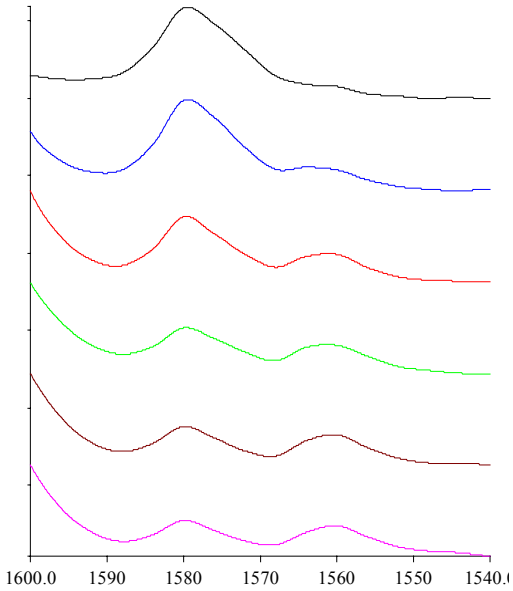

Figure 2.7. FTIR of PET and PET/BB fibers in the vicinity of V_{8a} absorption region.

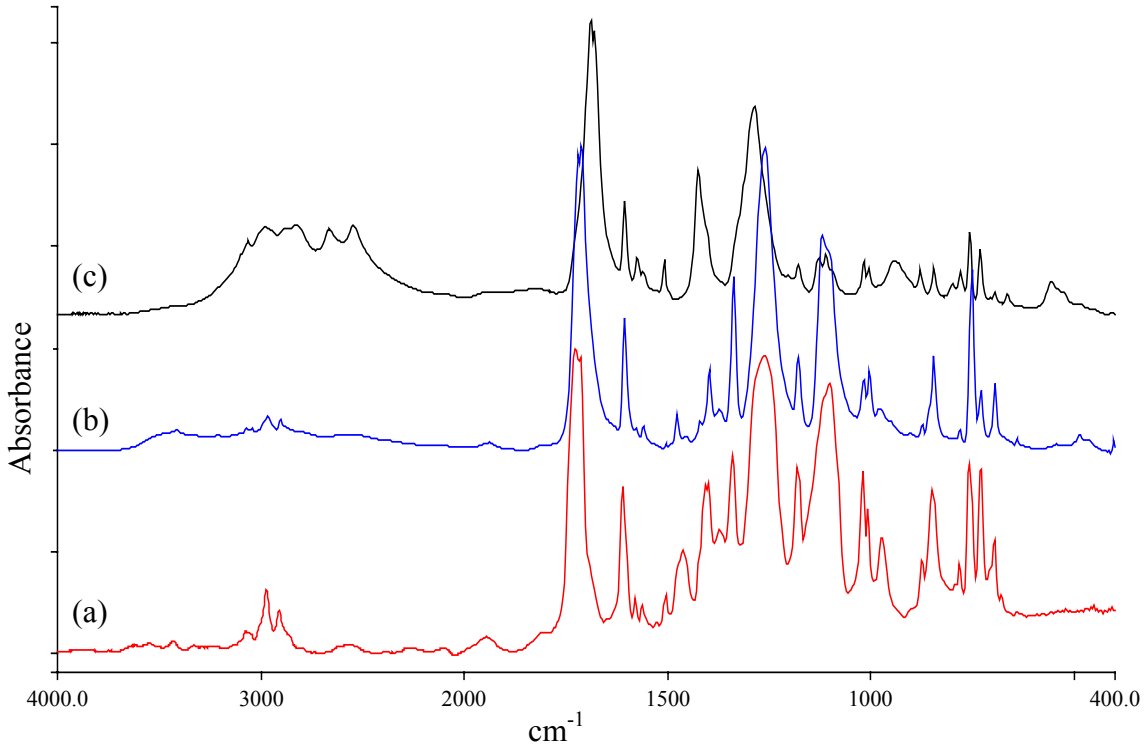

Figure 2.8. FTIR of (a) PET/BB55 fiber; (b) DMSO insoluble part (c) DMSO soluble part.

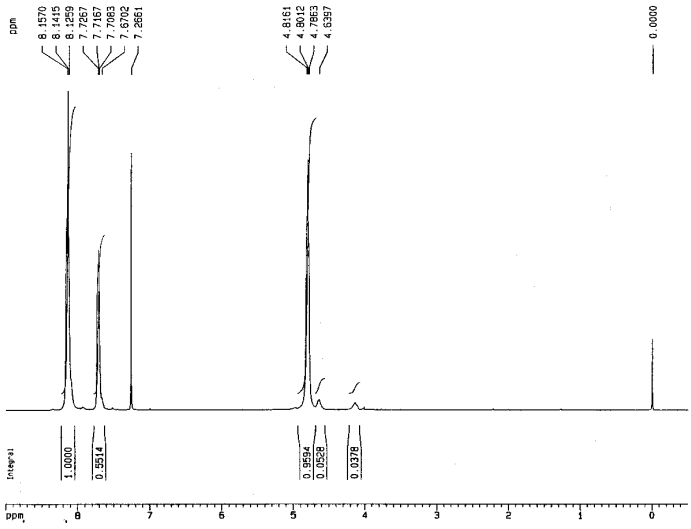

(a) PET/BB55 polymer

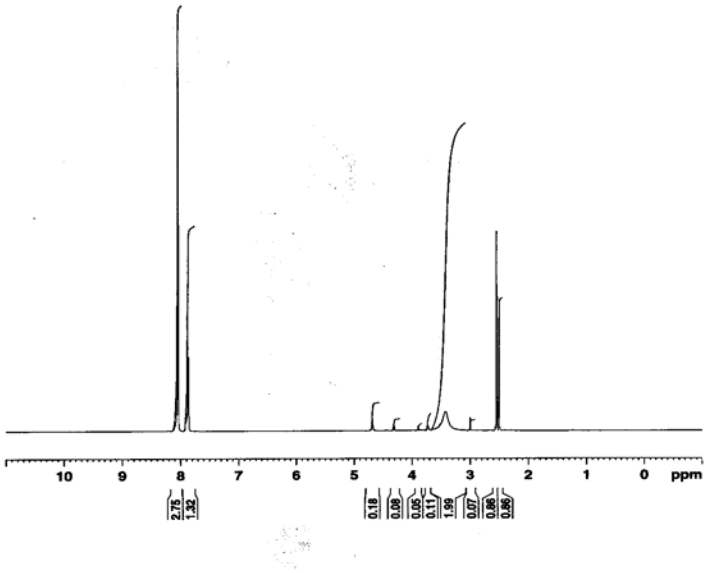

(b) DMSO soluble part

Figure 2.9. ^{1}H-NMR of (a) PET/BB55, (b) DMSO soluble part and (c) DMSO insoluble part.

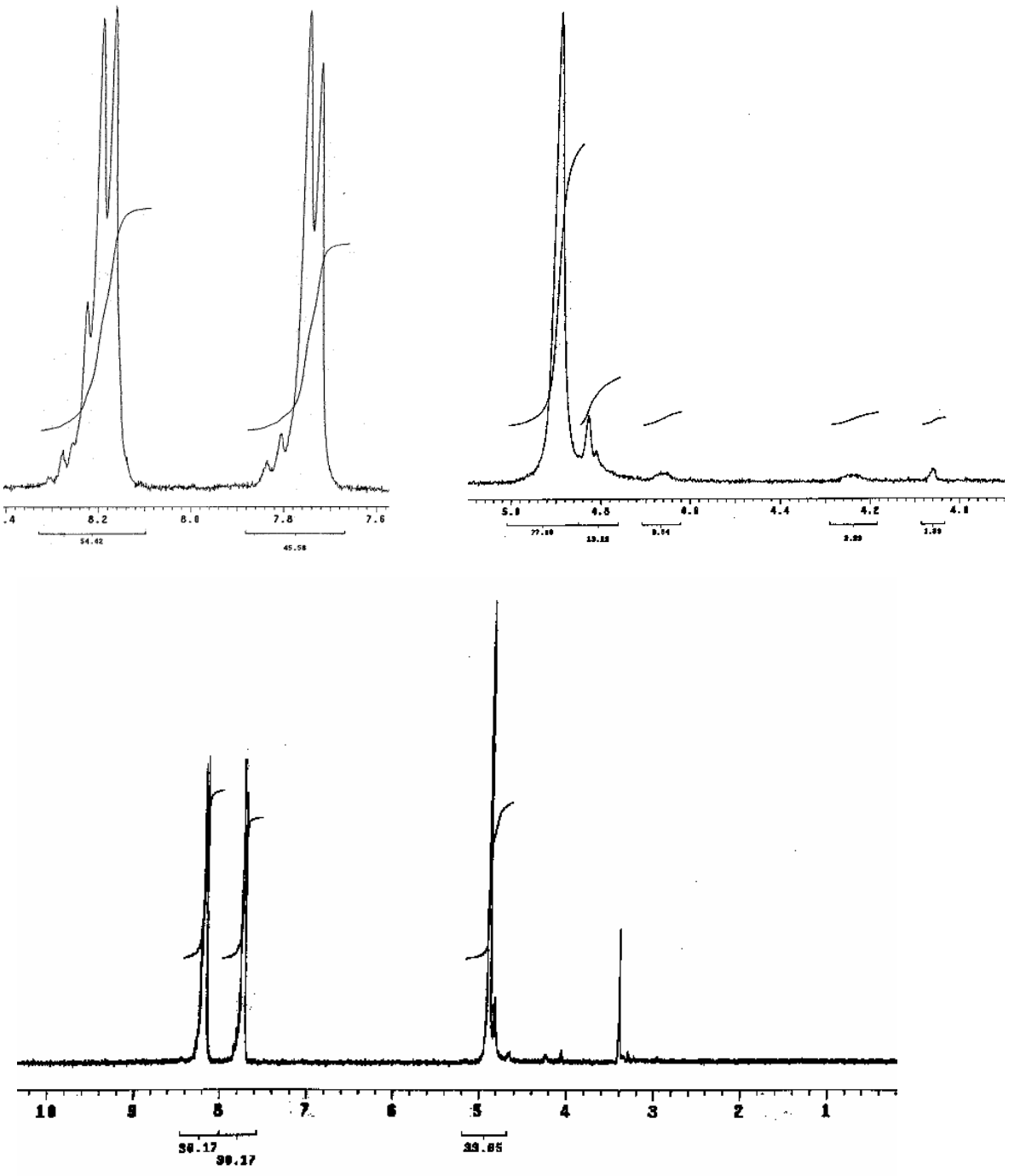

(C) DMSO insoluble part

Figure 2.9. ^{1}H-NMR of (a) PET/BB55, (b) DMSO soluble part and (c) DMSO insoluble part.(continued from previous page)

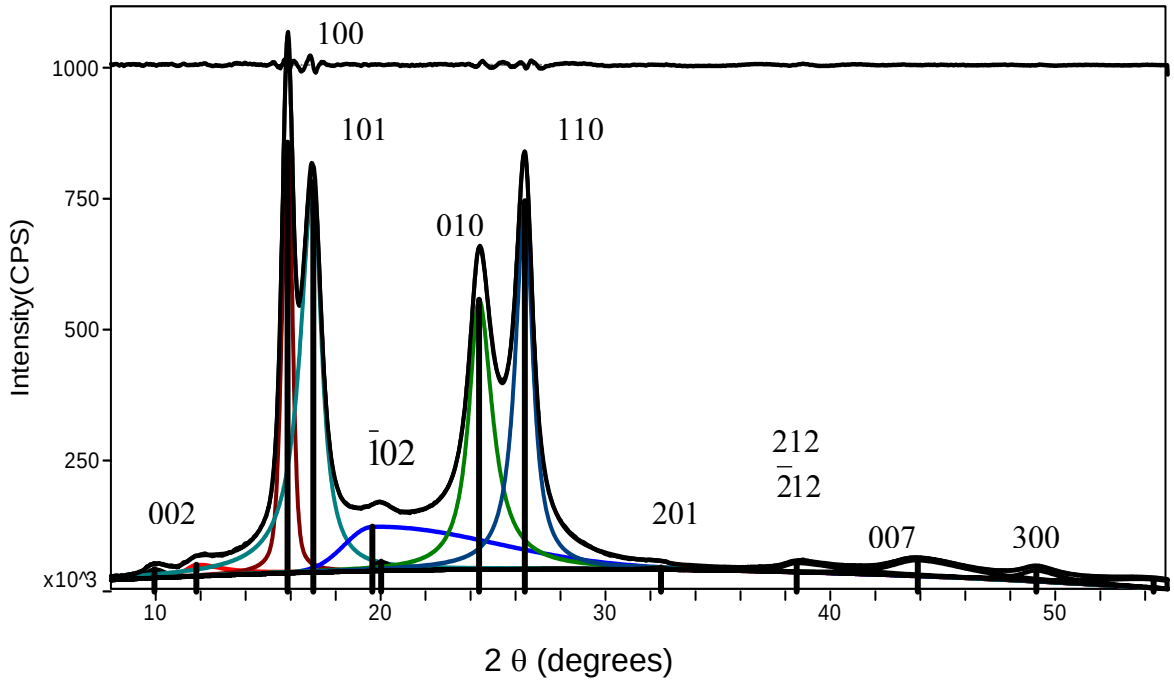

Figure 2.10. WAXD radial scan of the DMSO insoluble part

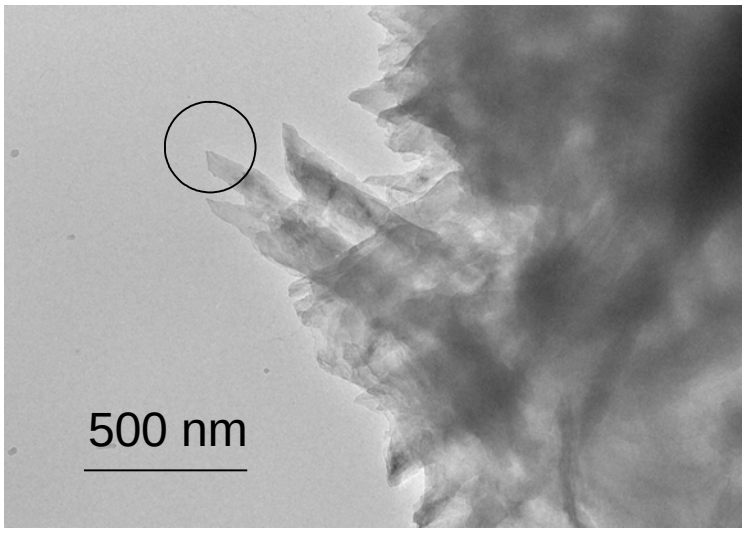

Figure 2.11. Transmission electron micrograph of the DMSO insoluble part from hydrolyzed PET/BB55 fiber.

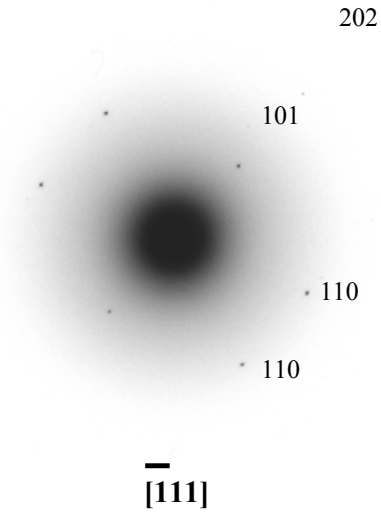

(a)

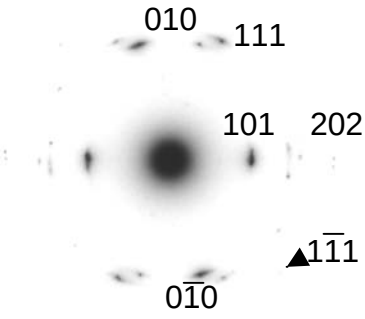

(b)

Figure 2.12. Selected area electron diffraction from isolated lamellar crystals obtained by hydrolytic etching of PET/BB55 fiber. (a) $\bar{1}11$ diffraction and (b) 101 diffraction.

2.7. References

[1] Ma, H.; Hibbs, M.; Collard, D. M.; Kumar, S.; Schiraldi, D. A.; *Macromolecules* **2002,** *35*; 5123.

[2] Flory, P.J. *J. Chem. Phys.* **1947**, *15*, 684.

[3] Baur, V. H. *Makromol. Chem*. **1966,** *98*, 297.

[4] Wunderlich B. *J. Chem. Phys.* **1958,** *29*, 1395.

[5] Wendling, J.; Gusev, A.A.; Suter, U.W.; Braam, A.; Leemans, L.; Meier, J.R.; Aerts, J.; Heuvel, J. v. d.; Hottenhuis, M. *Macromolecules* **1999,** *32*, 7866.

[6] Wendling, , J.; Suter, U.W. *Macromolecules* **1998**, *31*, 2509.

[7] Wendling, , J.; Suter, U.W. *Macromolecules* **1998**, *31*, 2516.

[8] Hanna, S. ans Winle, A. H. *Polymer* **1988**, *29*, 207.

[9] Golombok, R., Hanna, S. and Windle, A. H. *Mol. Cryst. Liq. Cryst*. **1988**, *155*, 281.

[10] Hanna, S., Romo-Uribe, A. and Windle, A.H. *Nature* **1993**, *366*, 546.

[11] Hachiboshi, M.; Fukuda, T.; Kobayashi, S. *J. Macromol. Sci. Phys.* **1969**, *B(3)3*, 525.

[12] Lu, X.; Windle, A.H. *Polymer* **1995**, *36*, 451.

[13] Lu, X.; Windle, A.H. *Polymer* **1996**, *37*, 2027.

[14] Biswas, A. and Blackwell, J. *Macromolecules* **1998**, *21*, 3152

[15] Biswas, A. Blackwell, J. *Macromolecules*, **1988**, *21*, 3146.

[16] Beer, D.; Ramirez, E. *J. Text. Inst*. **1990,** *4*, 81.

[17] Baltà Calleja F. J. : Cagiao, M.E. *J. Mcromol. Sci. Phys.* **1994**, *B33*, 333.

[18] Miyagi, A.; Wunderlich, B., *J. Poly.Sci., Phys.* **1972,** *10*, 2073.

[19] Schiraldi, D. A.; Lee, J. J.; Gould, S. A. C.; Occelli, M. L. *J.Ind. Eng. Chem.* **2000**, *7*, 67.

[20] H. P. Klug and L.E. Alexander, *X-Ray Diffraction Procedures*, Wiley, New York, 1954, Chapter 3.

[21] L.E. Alexander, *X-Ray Diffraction Methods in Polymer Science*, John Wiley & Sons, New York, 1969, Chapter 9.

[22] Li, X; Brisse, F. *Macromolecules* **1994**, *27*, 2276.

[23] Fu, Y.; Busing, W.R.; Jin, Y.; Affholter, K.A. Winderlich, *Macromolecules* **1993**, *26*, 2187.

[24] Uchida, T.; Shimamura, K. *Polym. Adv. Technol*. **2000**, *11*, 198.

[25] Liang, C.Y.; Krimm, S., Infrared Spectra of High Polymers: Part IX, Polyethylene Terephthalate, *J. Molec. Spectr.* **1959**, *3*, 554.

[26] K.C. Cole, J.Gu'evremont, A. Ajji, and M.M. Dumoulin, *Appl. Spectr.* **1994**, *48*, 1513.

[27] Watanabe, J.; Hayashi, M. *Macromolecules* **1988**, *21*, 278.

[28] Tokita, M.; Osada, K.; Watanabe, J. *Liq. Cryst.* **1998**, *24*, 477.

[29] Watanabe, J.; Kinoshita, S. *J. Phys. II* **1992**, *2*, 1273.

[30] Tokita, M.; Takahashi, T.; Hayashi, M.; Watanabe, J. *Macromolecules* **1996**, *29*, 1345

[31] Watanabe, J.; Hayashi, M.; Morita, A.; Tokita, M. *Macromolecules* **1995**, *28*, 8073.

[32] Gutiérrez, M.C.G.; Karger-Kocsis, J., Riekel, C. *Macromolecules* **2002**, *35*, 7320.

[33] Ran, S.; Wang, Z.; Burger, C.; Chu, B.; Hsiao, B.S. *Macromolecules* **2002**, *35*, 10102.

[34] Carr, P.L.; Nicholson, T. M.; Ward, I.M. *Polym. Adv. Tech*. **1997**, *8*, 592.

[35] Auriemmam, F.; Corradini, P.; Rosa, De C. Gureera, G. Petraccone, V.; Biachi, Riccardo, Dino, Di. G. *Macromolecules* **1992**, *25*, 2490.

[36] Welsh, G. E; Blundell, D.J.; Windle, A. H., *Macromolecules* **1998**, *31*, 7562.

[37] Orientation analysis of PET/BB fibers will be published in a separate paper

CHAPTER III

STRUCTURE AND MORPHOLOGY OF POLY(ETHYLENE TEREPHTHALATE–*co* -4,4'-BIBENZOATE) PET/BB FIBERS

3.1. Abstract

Crystallinity and orientation in poly(ethylene terephthalate–*co*-4,4'-bibenzoate) PET/BB fibers were studied by wide angle X-ray diffraction and FTIR spectroscopy. When drawn to their respective maximum draw ratios, the morphology of high bibenzoate (BB) containing fibers, PET/BB45, 55 and 65, PET/BB fibers is dramatically different than that of low BB-content, PET/BB35, PET/BB15 and PET fibers. (PET/BBx represents PET/BB copolymer containing x mol % of 4,4'-bibenzoate). High BB-content fibers are more extended and better oriented. Approximately 90% of the ethylene glycol units in high BB-content fibers are in the *trans* conformation whereas only 80% are in *trans* conformer in low BB-content and PET fibers. High BB-content fibers have higher overall orientation ($f > 0.85$) than that of low BB-content fibers ($f \sim 0.6$). While orientation of the crystalline regions are all very high, f_c = (~0.95), in both groups of fibers, the amorphous regions of the high BB-content fibers has significantly higher orientation ($f_a \sim 0.8$) than the low BB-content fibers and PET fibers ($f_a \sim 0.4$).

3.2. Introduction

Poly(ethylene terephthalate – *co* - 4,4'-bibenzoate) (PET/BB) copolymers have received significant attention in recent years on account of their considerable commercial potential in high performance fibers and films.[1,2] Recent innovation in terms of making bibenzoate monomers[3]which has the potential to lower the cost of PET/BB copolymers to a competitive price, provided us with the impetus to investigate the structures of these materials. In a previous paper[1] it was shown that PET/BB copolymers with various compositions show interesting spinning behavior which results in fibers with dramatically improved properties. Polymers with 45, 55 and 65 mole % BB (i,e. PET/BB45, 55 and 65) spin like liquid crystalline polymers in that as-spun fiber obtained at low take-up speeds (i.e. a few hundred meters per minute) exhibit maximum achievable orientation. These fibers cannot be drawn further, even above the glass transition temperature. These fibers have modulus values in the range of 35 to 45 GPa, which is approaching to the value for thermotropic liquid crystalline copolyester Vectra. For example, Vectran fiber, a 75/25 copolymer of 1-hydroxy-4-benzoic acid and 2-hydroxy-6-naphtholic acid HNA/HBA, has a modulus of ~60 GPa.[4] On the other hand, as-spun fibers of PET, PET/BB5, 15 and 35 obtained under similar conditions are amorphous and not fully oriented. A hot drawing step must be applied to this group of fibers to achieve good orientation. Even then, the modulus of the second group of fibers is only around 10 GPa. Moreover, PET/BB45, 55 and 65 fibers have much better retention of modulus at elevated temperatures than fibers of PET and copolyesters with low BB content. This is apparent by dynamic mechanical analysis, in which the tan (δ) peak corresponding to the glass transition temperature

completely disappears in the fully oriented PET/BB55 and 65 fibers. To understand the differences in mechanical and thermomechanical properties between high BB-content fibers and in PET and low BB-content fibers, it is very important to understand the structure and morphology differences between them. In this paper we describe the crystallinity and orientation of PET/BB fibers. Wide angle X-ray diffraction and infrared dichroism has been used to study crystallinity and orientation in these fibers. FTIR dichroism has proven to be a powerful tool to study the orientation of the individual copolymer unit. With the use of IR microscope, exactly the same location of the sample can be probed in parallel and perpendicular directions, thus eliminating the needs for thickness correction (why this is relevant).

3.3. Experimental

Poly(ethylene terephthalate-*co*-bibenzoate) (PET/BB) copolymers containing various amounts of bibenzoate (BB) were produced from dimethyl terephthalate, dimethyl 4,4'-bibenzoate, and ethylene glycol according to the literature method.[5] Specific polymers used in this study are listed (along with their intrinsic viscosities) in Table 1. Intrinsic viscosity was measured in dichloroacetic acid solution at 25 ^{o}C. The Mark-Houwink-Sakurada (MHS) parameters for PET/BB copolymers have not been determined. The relationship between intrinsic viscosity, and viscosity average molecular weight, M_v, was assumed using the MHS parameters for PET (Table 1).

$$[\eta] = 1.7 \times 10^{-4} (M_v)^{0.83} \qquad (1)$$

The issues of polymer randomness, crystal structure and the composition of the crystalline and amorphous regions have also been addressed in previous studies.[1] Fibers

were spun at 270 – 310 ^{o}C and drawn to their maximum draw ratios either by on-line drawing, in the case of PET/BB45, 55 and 65, or by a separate drawing step on a hot plate at 120 ^{o}C (for PET/BB15, 35 and PET fibers). All fibers were further heat-treated at constant length at 150 ^{o}C for 10 minutes. Fiber spinning and processing conditions are listed in Table 2. Tensile modulus, birefringence and densities of various fibers are also given. X-ray diffraction was carried out on a Rigaku Small/Wide Angle X-ray Scattering system with a MicroMax 002™ X-ray beam Generator (XBG), operating at 45 kV and 0.66 mA. CuK_{α} irradiation was obtained using confocal Max-Flux® optics. A small bundle of fibers were placed vertically in the beam path. 2D diffraction images were collected using a Rigaku R-AXIS IV^{++} detector. Air background scattering was subtracted after making a correction absorption due to the sample. Radial, equatorial and azimuthal scans were integrated using AreaMax® software and profile fittings were carried out using MDI Jade 6.1. A linear background was fitted for all of the curves. Profile fittings were repeated until the residual error of fit was less than 2%. Percent crystallinity was obtained from the ratio of the area of the crystalline peaks and that over the entire range. FTIR spectra of the fibers were obtained on a Perkin Elmer Spectrum One FTIR spectrometer. IR spectra were collected in transmission mode at 4 cm^{-1} resolution with the unpolarized beam, as well as with beam polarized parallel and perpendicular to the fiber axis. The molecular orientation is defined as the probability distribution function of the angle θ between the polymer chain axis and the fiber direction.[6] IR dichroism allows the determination of an orientation function (*f*) equal to the averaged second-order Legendre polynomial of the orientation distribution function:

$$f = < P_2(\cos\theta) > = \frac{(3 < \cos^2\theta > -1)}{2} \qquad (2)$$

For a given transition moment, the orientation function is related to the experimentally observed dichroic ratio D (= $A_{//}/A_{\perp}$) by:

$$f = \frac{D-1}{D+2} \times \frac{D_0+2}{D_0-1} \qquad (3)$$

where, $A_{//}$, $A_{\perp}$ are the peak areas in parallel and perpendicular directions. The intrinsic dichoric ratio (D_0) of a perfectly oriented sample is given by

$$D_0 = 2\cot^2\alpha \qquad (4)$$

where α is the transition moment angle, which is the angle between the polymer chain axis and the transition moment direction of the vibrational mode under discussion. The birefringence of the fibers was measured using the Leitz Ortholux polarizing microscope and a Zeiss 122 order compensator. Three fibers were measured for each sample.

3.4. Results and discussion

3.4.1. X-ray diffraction: Crystallinity

Wide angle X-ray diffraction radial scans of copolymer fibers are shown in Figure 1. The structure of crystals in PET/BB fibers can be divided into two groups. PET/BB15 and 35 have a crystal structure reassembleing that of PET. PET/BB 45, 55 and 65 have crystal structures similar to that of the crystal structure of the poly(ethylene bibenzoate) (PEBB) homopolymer.[7] Peaks can be indexed to PET-like and PEBB-like structures, Table 3 and 4. Crystal thickness normal to various reflection planes are also given. A detailed study on crystal structure on PET/BB copolymers has been presented in Chapter

II. One significant difference between the two crystal forms is that the PEBB-like crystal structures in high BB-content fibers have crystal thickness of 100 Å along (100) normal direction, which is more than twice that of the PET-like crystals in fibers of PET and low BB-content fibers. The other crystal dimensions are comparable in the two groups of fibers. Thus, the crystals in high BB-content fibers are larger than those in PET and low BB-content fibers. Crystallinity indices of various fibers (Table 5) were obtained from the ratio between the sum of area under the crystalline peaks versus the total area under radial scans. Examples of peak fittings are shown in Figure 2. Crystallinity of the PET fiber is about 40%, which is typical for fiber obtained under the processing condition used. Addition of the bibenzoate unit lowers the crystallinity significantly. At 35% BB, the crystallinity is only about 20%. However the crystallinity increases again with incorporation of more bibenzoate and reaches 43% in PET/BB65 fibers.

3.4.2. X-ray diffraction: Crystallite orientation

The degree of uniaxial orientation of a polymer chain axis is described by the Herman-Stein orientation function:

$$f = \frac{3 < \cos^2 \phi_{c,z} > -1}{2} \qquad (5)$$

where $< \cos^2 \phi_{c,z} >$ is the average cosine square angle of the chain axis of the polymer makes with the draw direction, Z. For an isotropic material, $f = 0$. For a fully oriented chain, $f = 1$; $f = -0.5$ when the chain is oriented perpendicular to the draw direction. Orientation of crystallites in polymer samples is commonly determined by X-ray

diffraction. Wilchinsky's treatment [8, 9] is the most generally used method to measure $< \cos^2 \phi_{c,z} >$.

According to this method, the average square cosine angle, $<\cos^2 \phi_{c,Z}>$, is given by: (e, f, g are director consines of N with respect to the axes X, Y and c, respectively)

$$\begin{aligned} < \cos^2 \phi_{hkl,z} >= e^2 < \cos^2 \phi_{x,z} > + f^2 < \cos^2 \phi_{y,z} > + g^2 < \cos^2 \phi_{c,z} > \\ + 2ef < \cos\phi_{x,z} \cos\phi_{y,z} > \\ + 2fg < \cos\phi_{y,z} \cos\phi_{c,z} > \\ + 2eg < \cos\phi_{c,z} \cos\phi_{x,z} > \end{aligned} \quad (6)$$

The following conditions were applied to simplify Wilchinsky's equation: (1) for the (hk0) reflection, the director cosine g is 0, so that $e^2+f^2 = 1$; (2) in uniaxial orientation, $<\cos^2\phi_{x,z}> = <\cos^2\phi_{y,z}>$ since the transition moments are equally distributed around the c-axis (3) using the orthogonal relationships between the two sets of director cosines e, f, and g, and $<\cos\phi_{x,z}>$, $<\cos\phi_{y,z}>$ and $<\cos\phi_{c,z}>$. this reduces equation (6) to:

$$\begin{aligned} < \cos^2 \phi_{hkl,z} >= 1 - 2 < \cos^2 \phi_{c,z} > \\ + 2ef < \cos\phi_{x,z} \cos\phi_{y,z} > \end{aligned} \quad (7)$$

For PEBB, the unit cell parameters, a = 5.75, b = 3.82, c = 14.62, $\alpha = 90.1^o$, $\beta = 90.3^o$ $\gamma = 78.1^o$ reported by Li and Brisse[7], this suggests that the unit cell is almost monoclinic, i.e. $\alpha \approx \beta \approx 90^o$. Therefore the normal of (100), **N**(100), is perpendicular to both the b and c axes, Thus, $<\cos\phi_{x,z}> = 0$, and equation (7) is further reduced to:

$$< \cos^2 \phi_{c,z} >= 1 - 2 < \cos^2 \phi_{100,z} > \quad (8)$$

The Herman-Stein orientation function is thus obtained by measuring $<\cos^2\phi_{(100),z}>$ from the azimuthal scan of the (100) reflection, and is given by:

$$f_c = 1 - 3 < \cos^2 \phi_{100}, z > \quad (9)$$

However, in the case of PET the unit cell is triclinic; three (*hk0*) reflections are needed to determine the orientation of the crystallites accurately. In this study, we adopt equation (10) developed by Gupta and Kumar[10] to calculate the f_c based on (010), (110) and (100) reflections.

$$<\sin^2\theta>=0.356<\cos^2\phi_{(010),Z}>+0.767<\cos^2\phi_{(1\bar{1}0),Z}>+0.877<\cos^2\phi_{(100,Z)}>$$

$$f_c=1-\frac{3}{2}<\sin^2\theta> \tag{10}$$

The average cosine square angle $<\cos^2\phi_{hkl,Z}>$ the normal of (*hkl*) plane **N**(*hkl*) made with the fiber direction, *Z*, can be calculated from the azimuthal intensities, $I(\phi)$, as follows:

$$<\cos^2\phi_{hkl},z>=\frac{\int_0^{\pi/2} I(\phi)\sin(\phi)\cos^2(\phi)d\phi}{\int_0^{\pi/2} I(\phi)\sin(\phi)d\phi} \tag{11}$$

Azimuthal intensities were scanned at the tail ends of the (010), $(1\bar{1}0)$ and (100) peaks for PET, PET/BB15, PET/BB35 fibers, and along the (100) for higher BB-content fiber. The calculated orientation factors, f_c, of the crystallites in various fibers are shown in Table 5. Orientations of the crystalline regions are all above 0.95, indicating the crystals are highly aligned along the fiber direction. The two phase approximation for the overall orientation factor *f* includes contributions from the of orientation of crystalline phase f_c and amorphous phase f_a, equation (9), where V_c is the volume fraction of the crystalline phase.

$$f = f_c V_c + f_a(1-V_c) \tag{12}$$

While the crystalline regions are all highly oriented, the birefringence of the fibers increase upon increasing the amount of BB incorporated. (Table 2). Increasing the

amount of BB units results in an increase in orientation. Considering the significant change in tensile modulus, we expect a major increase in the orientation of the chains in the amorphous regions of these fibers.

3.4.3. Vibrational Spectroscopy

FT infrared spectra of drawn and heat-treated PET and PET/BB fibers are shown in Figure 3. The peaks corresponding to carbonyl carbon oxygen (C=O) stretching at 1730 cm^{-1}, COO stretch at around 1260 cm^{-1} and COC stretch at 1120 cm^{-1} in the spectra of PET/BB are all very similar to those of PET fibers. In PET/BB new peaks appear at 1560, 1401, 1008, 845, 780 and 760 cm^{-1} due to addition of the bibenzoate units.

We will discuss the orientation of the aromatic rings first and then the ethylene glycol units. The orientation of the aromatic ring can be determined from various aromatic C-H bending or stretching vibrations, in Table 6. The in-plane-bending peak from the phenyl ring at 1018 $cm^{-1}$and from the biphenyl ring at 1008 cm^{-1} give the overall orientation of each unit. On the basis of the reported transition moment angle of 20^{o} for this vibration,[11] the calculated orientation factor for phenyl rings in PET fiber is 0.6. The orientation factor of the phenyl rings in PET/BB15 and 35 are lower ascribable in part to a of lower achievable maximum draw ratio. However, in PET/BB45, 55 and 65 the phenyl ring orientation factor is much higher (0.79-0.84). For the biphenyl ring, if we use the same transition moment angle of 20^{o}, similar trends are observed (Table 6). However, the orientation factor for the biphenyl rings is significantly higher than that of the phenyl ring in high BB-content fibers. It is reasonable that the biphenyl ring will have higher orientation due to its larger aspect ratio, which makes it easier to orient during the fiber

spinning and drawing processes. A strong peak at 730 cm^{-1} in PET arises from benzene ring out-of–plane C-H bending and has a strong perpendicular dichroism with a transition moment angle close to 90^{o}.[14~~15~~] This peak is too strong to be used for orientation analysis OF PET fiber. However in higher BB-content copolymers this peak has moderate intensity due to the reduced concentration of terephthalate units. The C-H out-of-plane bending from the BB unit appears at 756 cm^{-1}. Again, the overall orientation of BB and T units are significantly higher in high BB-content fibers and the BB has better overall orientation than the T units.

FTIR dichroism allows for the determination the orientation of terephthalate units in the amorphous region by analysis of a peak at 1579 cm^{-1}, characteristic of 1,4 para-para ring stretching mode V_{8A}.[12] When we treat the vibration of ethylene glycol links and the terephthalate units separately this vibration should only be Raman-active in the pure crystalline form of PET, due to the centrosymmetric nature of the configuration of the terephthalate units in the crystal.[13] However it is IR-active in the amorphous region of the PET: As the C=O adjacent to the ring rotates out the plane of the ring, the OC-Ph-CO segment deviates from coplanarity, thereby breaking the centrosymmetry. Thus this peak is characteristic of the amorphous regions.[14,15] In the 4,4'-bibenzoate unit this vibration appears at 1560 cm^{-1}. FTIR spectra of various fibers in the range of 1600 – 1540 cm^{-1} are shown in Figure 3. In PET/BB copolymers there two peaks in this region, the 1579 cm^{-1} and 1560 cm^{-1} peaks. The 1579 cm^{-1} peak arise from the terephthalate unit and the 1560 cm^{-1} peak corresponds to the bibenzoate unit, as deduced from analysis of dimethyl terephthalate and dimethyl 4,4'-bibenzoate as model compounds. Table 7 lists the dichoric ratio (D) of the peaks at 1579 and 1560 cm^{-1}. It can be seen that the amorphous

region of the low BB-content fiber and PET fiber has low orientation, but the amorphous region of the high BB-content fiber are highly oriented. It can also be seen that in the whole composition range, BB units in the amorphous region has higher orientation than the T units.

The ethylene glycol unit in PET/BB can adopt either *trans*- or *gauche* conformation and will give rise to different absorption peaks corresponds to CH_2 wagging: *trans*, 1340 cm^{-1}; *gauche* 1370 cm^{-1}. In the crystalline region the EG units are purely *trans*. In the amorphous region they can be in either form.[16] Spectra of various fibers in the range of 1300-1400 cm^{-1} are shown in Figure 5. The amount of *gauche* and *trans* configurations can be obtained from the spectra, Table 6. In low BB-content fibers, 80% of the EG units are in a *trans* conformation, which is typical of oriented PET fiber. However in PET/BB45, 55 and 65 fibers, there is significantly more *trans* conformer. After taking into account the crystallinity, we can calculate the percentage of *trans* conformers in the amorphous regions of fibers as show in Table 8. Approximately 85% of the ethylene glycol units in the amorphous regions of PET/BB45, 55 and 65 fibers are in the *trans* conformation. *Trans*-Conformers accounts for only 65% in the amorphous regions of PET fiber. This result suggests that the chains are more extended in PET/BB45, 55, and 65 than in the case of PET and low BB-content fibers.

Orientation of the *trans* conformer can be obtained from the dichorism of the peaks at 1340 cm^{-1} ($\alpha = 21^o$) and 973 cm^{-1} peaks (*rans* glycol C-O stretching, $\alpha = 4^o$.[17]) as shown in Table 8. The *trans* conformers in the high BB-content fibers are highly oriented along the fiber direction, much more so than in the case of low BB-content and PET fibers. This suggests that the chains in high BB-content fibers are more extended

and oriented. WAXD of all the fibers shows high orientation ($f_c \sim 0.95$) of the crystalline regions. This further suggests that for PET and low BB-content fibers the amorphous chains are not very well aligned, but for high BB-content fibers the amorphous regions are highly aligned. By using the overall orientation factor calculated from 1018 and 1008 cm^{-1} for T and B (Table 6) one can calculate the orientation factor of the fibers, f_{fiber} by using the following relationship:

$$f_{fiber} = f_T \times X_T + f_B \times X_B \qquad (13)$$

where f_T, f_B and X_T, X_B are the orientation factor and mole fraction of T and B units respectively. Then the orientation factor of the amorphous regions of the fibers can be obtained by using the equation (12) and the orientation factor of the crystalline region f_c obtained from X-ray (Table 5). The calculated orientation factor for the fibers and their amorphous regions are given in Table 9. As can be seen from Table 9, the orientation of high BB-content fiber is much higher than the orientation of the PET and low BB-content fibers. In the amorphous regions the orientation factor, f_a, for PET and low BB-content fibers are bellow 0.4 while that of the high BB-content fibers are all above 0.8, which is the most prominent difference between these two groups of fibers.

3.5. Discussion

From this analysis we see that fibers of high BB content PET/BB copolymers processed using a spinning process analogous to the process of making liquid crystalline polymeric fibers posses highly extended and oriented chains. The orientation is much greater than for polymers processed by conventional two step (spin and draw) processing of PET and low BB-content copolymers. Higher chain extension and orientation

contributes to the improved tensile modulus of high BB-content fibers. In the amorphous regions of high BB-content fibers, 90% of the ethylene glycol units are in their *trans* conformation and the amorphous chains are highly aligned (f_a ~ 0.85).

Onset of macroscopic chain motions at the glass transition temperature results in chain relaxation and loss of mechanical properties. In PET the scope of cooperative motion at T_g is on the order of seven repeat units. The amorphous region of PET and low BB-content fibers are poorly oriented (f_a~0.4) and contain a large portion of ethylene glycol units in a *gauche* conformation (Table 8). This accounts for the presents of a strong glass transition. The amorphous region of high BB content fibers has a lower fraction of ethylene glycol units in the *gauche* conformation, and the amorphous regions are highly aligned (fa ~ 0.85). The macroscopic motion of the chains is retarded and dynamic mechanical analysis reveals the absence of a tan(δ) peak associated with a glass transition.[1] Homopolymers of 4,4'-bibenzoate and various diols have been shown to be liquid crystalline.[18,19,20,21,22,23] Transient liquid crystallinity has been discovered in PET[24,25,26,27] and PET/PEN copolymers.[28] The spinning behavior of PET/BB45, 55 and 65, the highly extended and orientated structure of the resulting fibers and their tensile properties, as well as thermomechanical properties suggest the formation of a liquid crystalline phase in the spinning process. Thus, the structured melt formed during melt spinning provides for better orientation which imparts superior physical properties to the fibers compared to those prepared by a conventional spin and draw process.

3.6. Conclusions

The most important finding of this study is that high BB-content fibers are much more extended (90% ethylene glycol conformer are in trans) and have significantly higher orientation (f = 0.85) than PET and low BB-content fibers (f = 0.6). These differences are more evident in the amorphous regions. f_a for high BB-content fibers is ~0.8, while that of PET and low BB-content fibers is ~0.4.

Table 3.1. Intrinsic viscosity and molecular weight for various copolymers.

Polymer [a]	IV (dL/g)	M_v (g/mol)
PET	0.90	30,700
PET/BB15	0.94	32,300
PET/BB35	0.88	29,800
PET/BB45	0.92	31,400
PET/BB55	0.92	31,400
PET/BB65	0.90	30,700

[a] PET/BBx represents poly(ethylene terephthalate-*co*-4,4'-bibenzoate) copolymer containing x mol % of 4,4'-bibenzoate.

Table 3.2. Fiber processing conditions and physical properties. [a]

Polymer	T_m (°C)	Spinning temperature (°C)	Draw ratio[b]	Tensile modulus (GPa)	Birefringence
PET	260	280	6	12 ± 2	0.18 ± 0.02
PET/BB15	245	270	4	10 ± 2	0.21 ± 0.02
PET/BB35	230	270	3	9 ± 3	0.26± 0.02
PET/BB45	245	290	ND	38 ± 3	0.36 ± 0.04
PET/BB55	275	300	ND	40 ± 5	0.451 ± 0.006
PET/BB65	290	310	ND	45 ± 4	0.40 ± 0.06

[a]: all fibers were heat-treated at constant length at 150°C for 10 min.
[b]: fibers were drawn on a hot plate set at 120 °C; ND, not drawn was performed.

Table 3.3. d-spacings (Å) and crystal thickness (in parentheses, Å) for PET-like structures in PET, PET/BB15 and PET/BB35 fiber from the equatorial WAXD-scan.

Fiber	**(010)**	**($\bar{1}$10)**	**(100)**
PET	5.028 (56)	3.828 (45)	3.372 (38)
PET/BB15	5.073 (60)	3.898 (45)	3.471 (40)
PET/BB35	5.260 (48)	3.786 (34)	3.473 (45)

Table 3.4. d-spacings (Å) and crystal thickness (in parentheses, Å) for PEBB-like crystal structures in PET/BB45, PET/BB55 and PET/BB65 fiber from equatorial WADX-scans.

Fiber	**(100)**	**010**	**(110)**
PET/BB45	5.546 (92)	3.614 (42)	3.492 (44)
PET/BB55	5.607 (96)	3.657(4) (38)	3.543 (41)
PET/BB65	5.629 (100)	3.651 (41)	3.541 (44)
PEBB[7]	5.628	3.699	3.404

Table 3.5. Crystallinity, crystal orientation and birefringence of PET and PET/BB fibers.

Fiber	Crystallinity (wt%)	f_c
PET	41	0.95
PET/BB15	37	0.94
PET/BB35	21	0.95
PET/BB45	23	0.98
PET/BB55	32	0.97
PET/BB65	43	0.98

Table 3.6. Orientation of phenyl and biphenyl rings in PET/BB and PET fibers.

Fiber	1018 C-H in-plane bending of T	1008 C-H in-plane bending of BB	730 C-H out of plane bending of T	756 C-H out of plane bending of BB
PET	0.60	-	-	-
PET/BB15	0.56	0.33	-	0.55
PET/BB35	0.54	0.48	0.46	0.67
PET/BB45	0.79	0.93	0.68	0.88
PET/BB55	0.82	0.92	0.69	0.90
PET/BB65	0.84	0.94	0.67	0.92

Table 3.7. Dichroic ratio (DR) of the 1579 and 1560 cm^{-1} peaks in various fibers

Fiber	DR_{1579}	DR_{1560}
PET	2.2	-
PET/BB15	2.4	4.48
PET/BB35	2.3	4.43
PET/BB45	7.1	16.1
PET/BB55	7.3	15.2
PET/BB65	7.7	16.6

Table 3.8. Ethylene glycol *gauche*, *trans* conformer index and orientation of the *trans* conformer.

Fiber	$I_{1340}/(I_{1340} + I_{1370})$	X-ray Crystallinity	% *trans* in amorphous region	f_{1340}	f_{972}
PET	0.80	41	64	0.65	0.64
PET/BB15	0.81	37	65	0.47	0.58
PET/BB35	0.78	21	65	0.47	0.58
PET/BB45	0.90	23	85	0.86	0.89
PET/BB55	0.90	32	84	0.85	0.91
PET/BB65	0.92	43	86	0.85	0.90

Table 3.9. Orientation factor of the fibers and orientation factor of the amorphous regions of the fibers.

Fiber	f_{all}	f_a
PET	0.60	0.39
PET/BB15	0.54	0.33
PET/BB35	0.48	0.343
PET/BB45	0.86	0.84
PET/BB55	0.88	0.83
PET/BB65	0.91	0.86

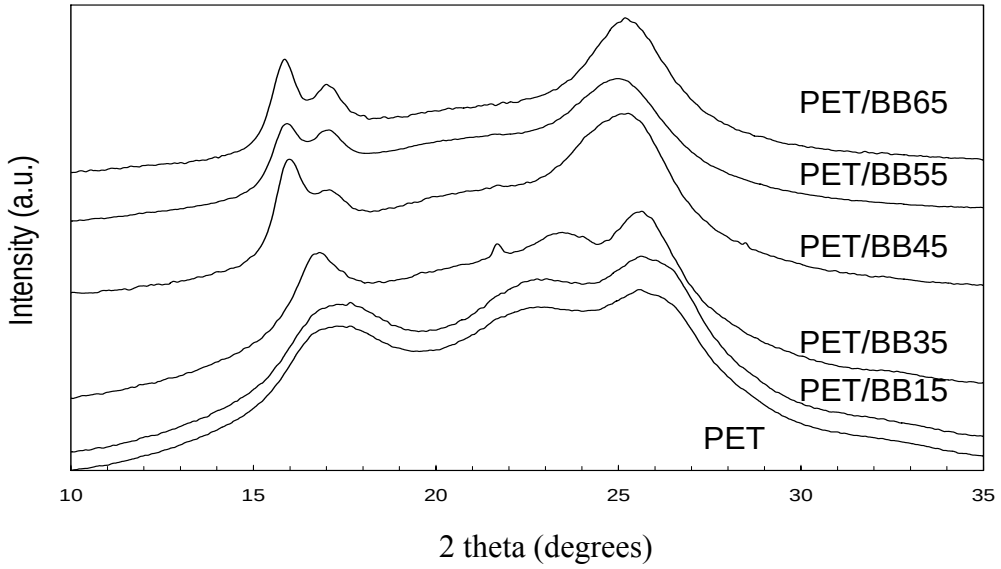

Figure 3.1. WAXD (radial scans) of PET and PET/BB fibers.

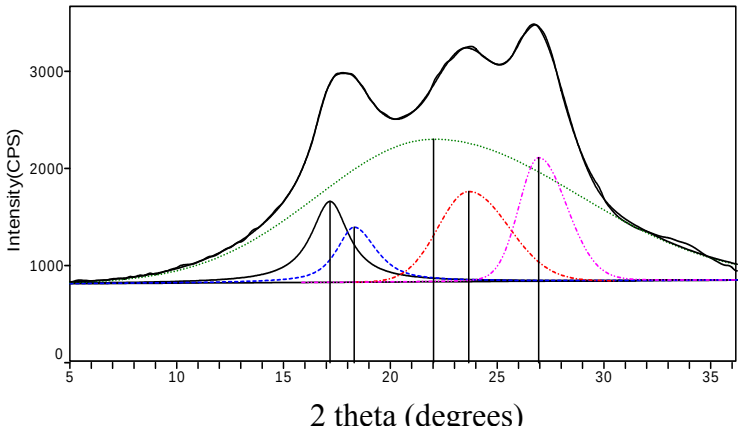

(a)

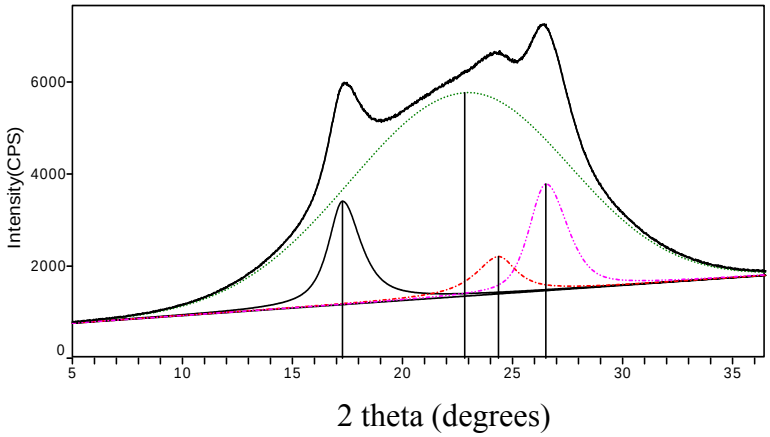

(b)

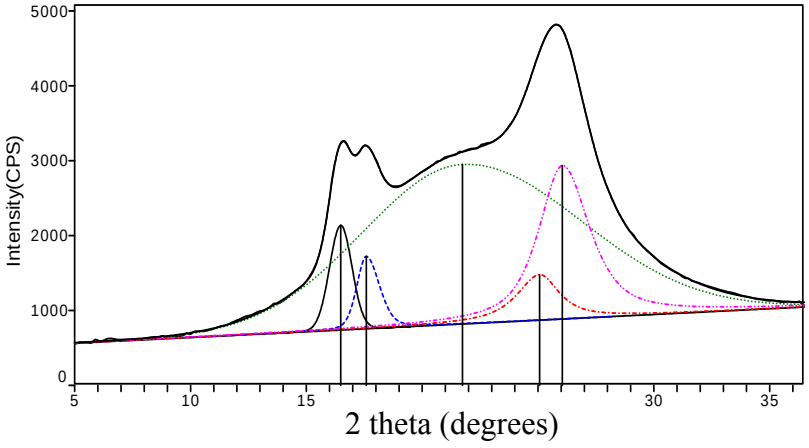

(c)

Figure 3.2. Curve fittings for selected fibers (a) PET, (b) PET/BB35, (c) PET/BB55.

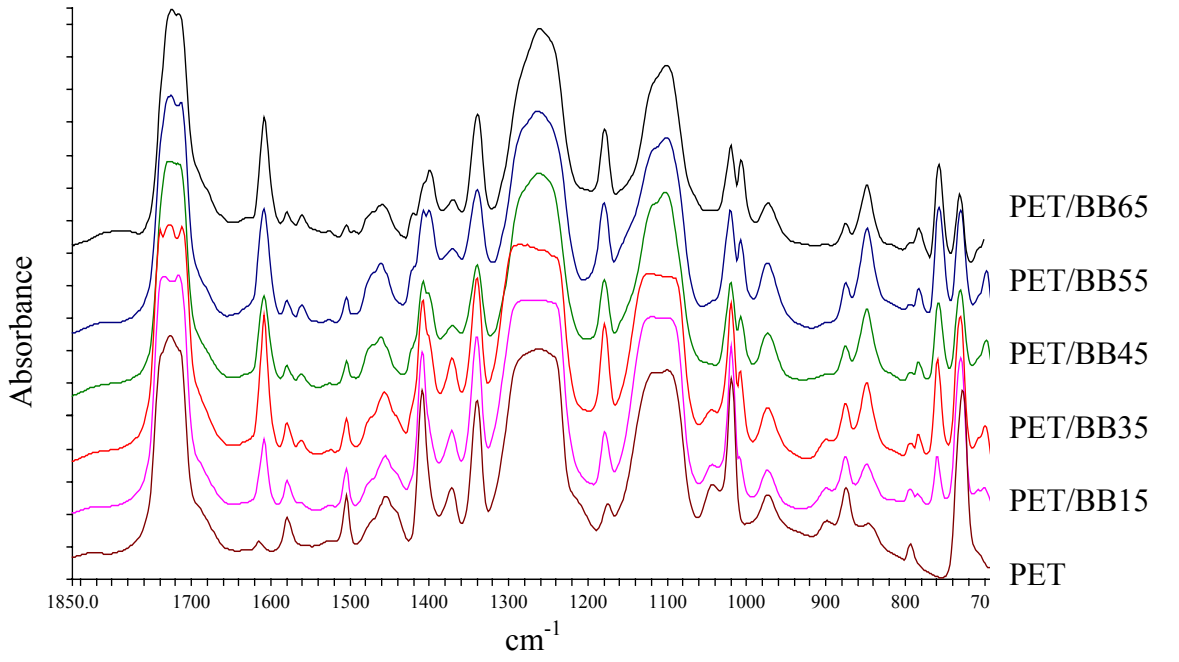
Absorbance
PET/BB65
PET/BB55
PET/BB45
PET/BB35
PET/BB15
PET
1850.0
1700
1600
1500
1400
1300
1200
1100
1000
900
800
70
cm-1

(a)

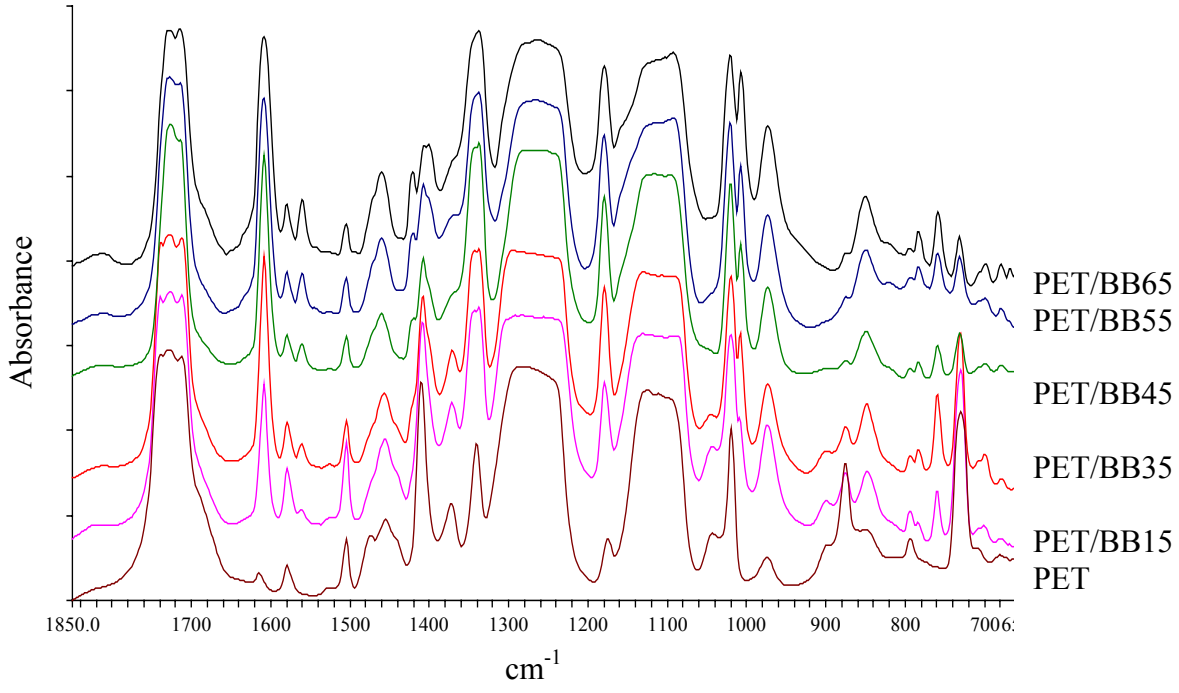
Absorbance
PET/BB65
PET/BB55
PET/BB45
PET/BB35
PET/BB15
PET
1850.0
1700
1600
1500
1400
1300
1200
1100
1000
900
800
cm-1

(b)

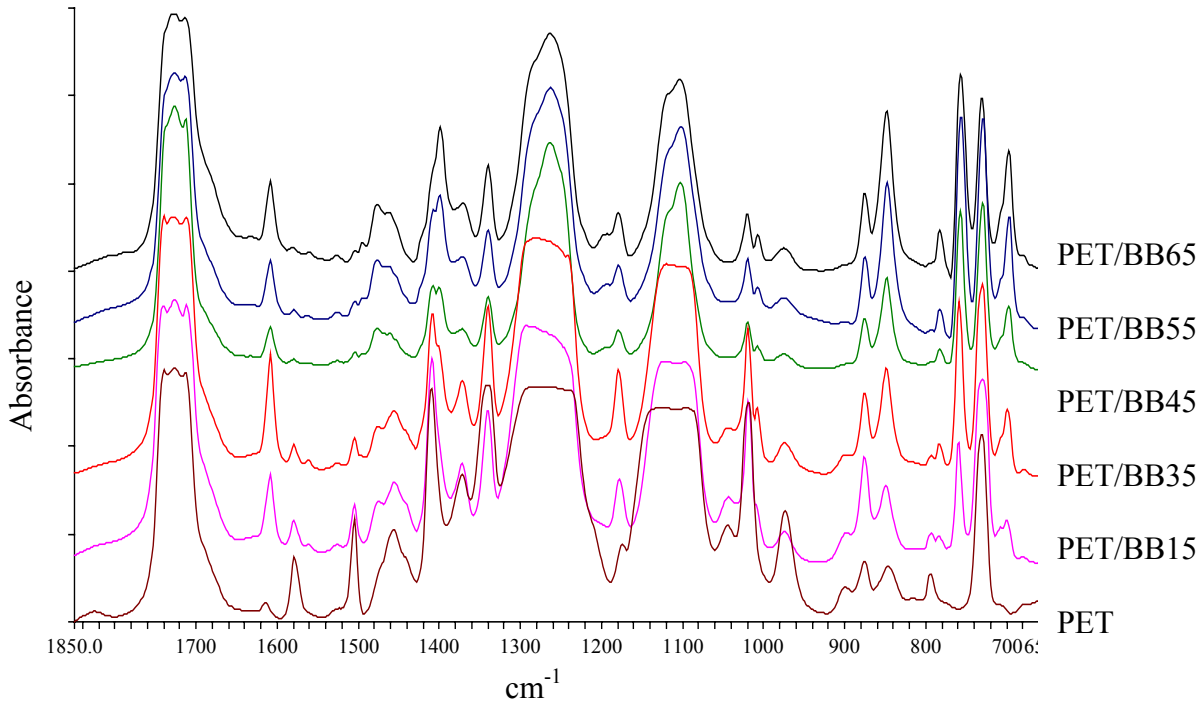

(c)

Figure 3.3. FTIR spectra of drawn and heat-treated PET and PET/BB fibers. From top to bottom are PET/BB65, 55, 45, 35, 15 and PET fibers respectively. (a) non-polarized, (b) polarization direction parallel to fiber axis. (c) polarization direction perpendicular to fiber axis.

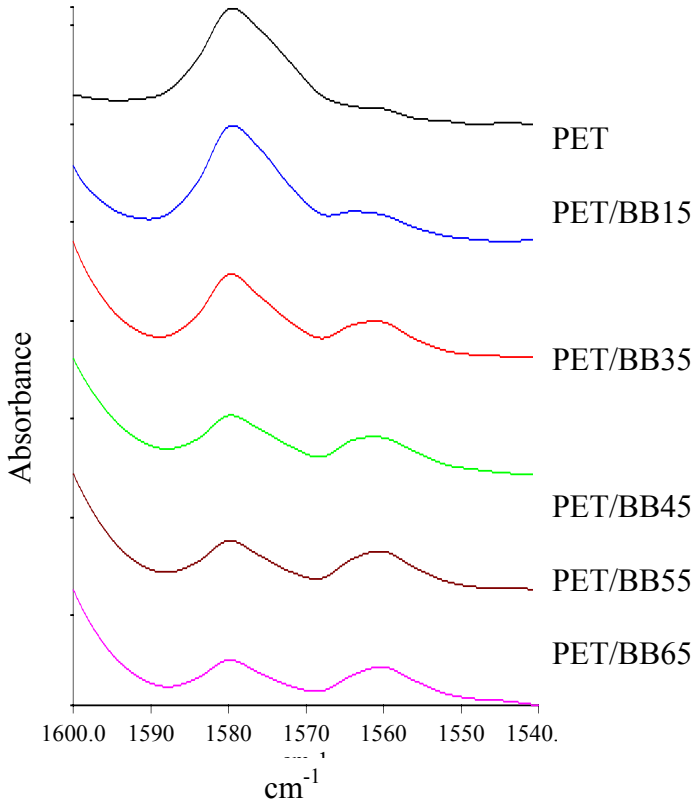

Figure 3.4. FTIR spectrum of various fibers in the range of 1600 – 1540 cm^{-1}.

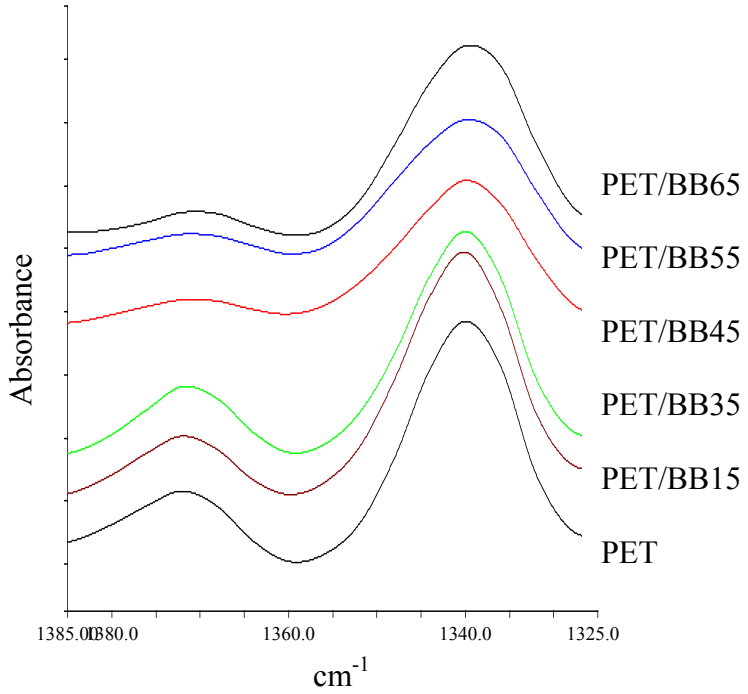

Figure 3.5. FTIR spectrum of various fibers in the range of 1400 – 1300 cm^{-1}.

3.7. References

1. Ma, H.; Hibbs, M.; Collard, D. M.; Kumar, S.; Schiraldi, D. A.; *Macromolecules* **2002**, *35,* 5123.

2. Liu, R.Y.F.; Schiraldi, D.A.; Hiltner, A. Baer, E., *J. Polym. Sci.: Part B: Polym. Phys.* **2002**, *40*, 862.

3. Sherman, S.C.; Iretskii, A.V.; White, M.G.; Schiraldi, D.A. *Chem. Innovations* **2000**, *30*,25.

4. Beer, D.; Ramirez, E. *J. Text. Inst*. **1990,** *4*, 81.

5. Schiraldi, D. A.; Lee, J. J.; Gould, S. A. C.; Occelli, M. L. *J. Ind. Eng. Chem.* **2000**,*7*, 67.

6. Siesler, H.W. *Adv. Polym. Sci*. **1984**, *65*, 1.

7. Li, X.; Brisse, F. *Macromolecules* **1994**, *27*, 2276.

8. Alexander, L.E. "X-Ray Diffraction Methods in Polymer Science," John Wiley,New Yord, 1969, 246.

9. Wilchinsky, Z. W. *Adv. In X-Ray Anal*. **1963**, *6*, 231.

10. Gupta, V.B.; Kumar, S. *Textile Res. J.* **1979**, *7*, 405.

11. Hutchinson, I.J.; Ward, I.M.; Willis, H.A.; Zchy, V. *Polymer* **1980**, *21*, 55.

12. Liang, C.Y.; Krimm, S. *J. Molec. Spectr.* **1959**, *3*, 554.

13. Daubeny, R. D. E.; Bunn, C. W.; Brown, C. J. *Proc. Roy. Soc.* **1954**, *A226*, 531.

14. Cole, K.C.; Gu'evremont, J.; Ajji, A.; Dumoulin, M.M. *Appl. Spectr*. **1994**, *48*, 1513.

15. Krimm, S. *Adv. Polym. Sci.* **1960**, *2*, 51.

16. Daubeny, R. de P.; Bunn, C.W.; Brown, C.J. *Proc. Royal Soc. (A)* **1954**, *226*, 531.

17. Spiby, P.; O'Neill, M.A.; Duckett, R.A.; Ward, I.M. *Polymer* **1992**, *33*, 4479.

18. Watanabe, J.; Hayashi, M. *Macromolecules* **1988**, *21*, 278.

19. Watanabe, J.; Hayashi, M. *Macromolecules* **1989**, *22*, 4083.

20. Tokita, M.; Osada, K.; Watanabe, J. *Liq. Cryst.* **1998**, *24*, 477.

[21] Watanabe, J.; Kinoshita, S. *J. Phys. II* **1992**, *2*, 1273.

[22] Tokita, M.; Takahashi, T.; Hayashi, M.; Watanabe, J. *Macromolecules* **1996**, *29*, 1345.

[23] Watanabe, J.; Hayashi, M.; Morita, A.; Tokita, M. *Macromolecules* **1995**, *28*, 8073.

[24] Gutiérrez, M.C.G.; Karger-Kocsis, J., Riekel, C. *Macromolecules* **2002**, 35, 7320.

[25] Ran, S.; Wang, Z.; Burger, C.; Chu, B.; Hsiao, B.S. *Macromolecules* **2002**, 35, 10102.

[26] Carr, P.L.; Nicholson, T. M.; Ward, I.M. *Polym. Adv. Tech*. **1997**, 8, 592.

[27] Auriemmam, F.; Corradini, P.; Rosa, De C.; Gureera, G.; Petraccone, V.; Biachi, Riccardo, Dino, Di. G. *Macromolecules* **1992**, 25, 2490.

[28] Welsh, G. E; Blundell, D.J.; Windle, A.H. *Macromolecules* **1998**, *31*, 7562.

CHAPTER IV

DYNAMIC MECHANICAL PROPERTIES OF POLY(ETHYLENE TEREPHTHALATE-*co*-4,4' BIBENZOATE) FIBERS

4.1. Abstract

Dynamic mechanical properties of poly(ethylene terephthalate-*co*-4,4'-bibenzoate) random copolyester fibers have been investigated. Fibers containing more than 40 mol% of bibenzoate units exhibited much higher storage modulus (E') as well as higher modulus retention at elevated temperatures than the low BB content fibers. The α-relaxation attributed to the glass transition temperature was not seen in the fully drawn and heat-treated PET/BB45, 55 and 65 fibers. The β transition at about -50 ^{o}C in PET/BB fibers diminished with the increasing of BB concentration. This may explain the improved gas barrier properties of PET/BB films. Anthor transition at about 70 ^{o}C in of high BB content was observed and attributed to the motion of the BB containing units.

4.2. Introduction

Poly(ethylene terephthalate -*co*- 4,4' bibenzoate) PET/BB has been proven to be random. Fiber spinning, structure and mechanical properties of different compositions of PET/BB have been reported in previous chapters. Incorporation of BB into copolymers of PET results in an increase in glass transition temperature from 80 °C to 110 °C for

PET/BB65. However, the α-relaxation (corresponding to glass transition) is fully suppressed in highly oriented and crystalline PETBB55 fibers. In this chapter we are interested in the dynamic mechanical relaxation of various fibers as a function of commoner composition, fiber orientation, and cystallinity. Relaxation processes in polymers are a subject of intensive research.[1,2,3]

Asrar[4] reported two transitions in PET/BB58 film at about 75 and 125 °C with peak tan(δ) values of about 0.05 and 0.3, respectively. The 125 °C transition can be attributed to the main chain motion in the PET/BB58 film. The 75 ^{o}C transition in PET/BB58 film was interpreted as due to possible of two phases resulting from compositional inhomogeneity.

4.3. Experimental

Dynamic mechanical analysis was carried out on a Seiko DMS (Model 220). A static stress of ~10 MPa and dynamic strain of 0.1% was applied for these tests. 20 mm gage length and 20 filaments were used for each test. Activation energy of various transitions were calculated using Arrhenius equation.[5]

4.4. Results and Discussion

Storage modulus (E') of PET/BB fibers as a function of temperature are compared in Figure 4.1. E' of low BB content fibers, PET/BB5, 15 and 35 resemble that of PET fiber. However, high BB content fibers have significantly higher E' than that of PET fiber and low BB content fibers. These results are in agreement with the tensile test. High BB content fibers also have better modulus retention at elevated temperatures. E' of the

PET/BB65 fiber at 150 ^{o}C is as high as that of the PET fiber at room temperature. High modulus retention at elevated temperatures is of significant importance in industrial applications such as tire cord reinforcement.

Tan (δ) curves reveal different relaxation processes between these two groups of fibers. As shown in Figure 4.2a, PET and low BB content fibers have distinct tan (δ) peaks in the temperature range of 120 to 140 ^{o}C, which arises from the glass transition. The glass transition temperature of the bulk polymers measured by DSC increases with the increasing BB mole fraction, indicating increase in polymer chains rigidity. In dynamic mechanical tests, the tan(δ) peak arising from glass transition occurs at progressively lower temperature when the BB content increases up to 35 mol%. Whereas, in high BB content fibers the peaks corresponding to the glass transition are not observed. In attempt to explain these differences fiber structure and morphology has to be considered. Crystallinity, amorphous orientation and percent *trans* conformer in the amorphous regions of PET/BB fibers obtained from previous chapters are shown in Table 4.1. Density of amorphous PETBB55[6] has been reported to be 1.307 g/cm^3, which is lower than the density of the amorphous PET (1.335 g/cm^3) and amorphous PEBB (1.32 g/cm^3).[7] This indicates incorporation of the bibenzoate moiety disrupts the chain packing, hence increases the free volume of the amorphous region and lowers the glass transition temperature of low BB content fibers.

On the other hand, the glass transitions are not seen in the high BB content fibers (Figure 4.2 b). Rather a new tan (δ) peak appeared at about 80 ^{o}C with the tan (δ) magnitude of ~0.05. This transition temperature is lower than the glass transition temperature measured on the bulk polymer by DSC. It has been demonstrated that this

transition dose not arise due to the main chain motion (glass transitions) of the high BB content fibers[8]. We termed this transition as a sub T_g transition β_2. Origin of this peak may come from the motion of the bibenzoate units similar to that of the terephthalate units in PET at ~-50 ^oC, which we termed as β_1 transition.

In Chapter III, it was reported that amorphous regions of the high BB content fibers are highly extended and oriented (also see Table 4.1) so the macroscopic main chain motion associated with T_g do not occur in these fibers. De-densification of the amorphous region also occurs in the high BB content fibers (Table 4.1). PETBB45 shows two tan (δ) peaks, the one at 106 ^oC is due to the glass transition, which has not been totally eliminated by the fiber morphology, perhaps due to the low degree of crystallinity. The other peak at 80 ^oC is the secondary transition β_2. The loss of main chain motion is responsible for much improved mechanical property retention at elevated temperatures for high BB content fibers. .

Various transition temperatures and their activation energies in PET and PET/BB fibers are listed in Tables 4.2 and 4.3 respectively. The β_1 relaxation is presented in all the fibers and has about the same activation energy. The β_2 relaxation in the high BB content fibers has much higher activation energy. As the amorphous chains in high BB content fibers have more BB units in them and they are almost extended, it is easy to see the motion of these chains will require more energy. The activation energy of the α relaxation in the low BB content fibers have values typical of PET fiber.

Although both low and high BB content copolymer fibers as well as PET fiber have sub-T_g transition occurring at about –50 ^oC (Figure 4), the intensity of this peak decrease with increasing BB content. In discussing this peak, Ward[1] wrote, “In PET the

effect of crystallinity on the β-relaxation is very small and has led to a very complex interpretation in terms of this loss peak being composed of several relaxation processes." While this peak has been studied for over half a century, recent publications[9,10,11,12,13] on this topic clearly suggest that the origins of this peak are not yet well understood and investigations on this topic remain an active area of research. As the β relaxation in PET is not significantly effected with crystallinity, it appears that this relaxation (β_1) in PET/BB fibers is also not effected by degree of crystallinity and orientation. Tan(δ) peak areas of the low temperature transition (-50 ^{o}C) for various drawn and heat-treated PET/BB samples are integrated, and the peak area ratios of PET/BB to PET (A/A_o) is plotted against BB mole fractions in the amorphous region of the fibers (data obtained from chapter II) in Figure 4.4. From this figure we can see that the peak area decreases linearly with increasing bibenzoate content. This would suggest that the motion contributing to this transition is only involves the terephthalate not the bibenzoate containing repeat units, or the corresponding motion for the bibenzoate unit occurs at higher temperature. The fact that the β_1 relaxation in PET/BB is reduced and β_2 relaxation is observed at much higher temperature than the corresponding relaxation in PET may explain the superior gas transport barrier properties of PET/BB over PET.[14] The understanding of sub-T_g transition in copolyesters will open a methodology for designing new and improved gas barrier polymeric materials.

4.5. Conclusions

PET/BB45, 55 and 65 fibers have much higher storage modulus and modulus retention at elevated temperatures than PET and low BB content fibers. The glass

transition of high BB content fibers is fully depressed by their orientation and crystallinity. β_1 relaxation is observed to decrease with increase of BB content. A new sub-T_g transition β_2 is observed in the high BB content fiber, which is proposed to related to the motion of bibenzoate units.

Table 4.1 Physical properties of PET/BB fibers.

Fiber	**Crystallinity (wt%)**	f_a[1]	**% trans$_a$**[2]
PET	40	0.39	64
PET/BB15	30	0.33	65
PET/BB35	21	0.34	65
PET/BB45	23	0.84	85
PET/BB55	30	0.83	84
PET/BB65	43	0.86	86

1. f_a: orientation factor of the amorphous regions
2. Percentage of trans EG conformation in the amorphous regions

Table 4.2. Transition temperatures (^{o}C) of PET/BB fibers at different frequencies**.**

Fiber	**Transitions temperatures (^{o}C) at 0.1, 1 and 10 Hz**		
	β_1	β_2	α
PET	-62, -51, -38		133, 138, 144
PET/BB5	-59, -49, -39		118, 123, 129
PET/BB15	-60, -49, -39		109, 114, 119
PET/BB35	-60, -51, -41		108, 114, 119
PET/BB45	-60, -52, -42	75, 78, 82	96, 101, 106
PET/BB55	-62, -53, -43	78, 84, 89	-
PET/BB65	-63, -55, -45	78, 82, 88	-

Table 4.3. Activation energy of transitions in PET/BB fibers.

Fiber	**Activation energy (kcal/mole)**		
	β_1	β_2	α
PET	18	-	140
PET/BB5	20		140
PET/BB15	20		140
PET/BB35	21		141
PET/BB45	22	102	123
PET/BB55	23	104	-
PET/BB65	23	103	-

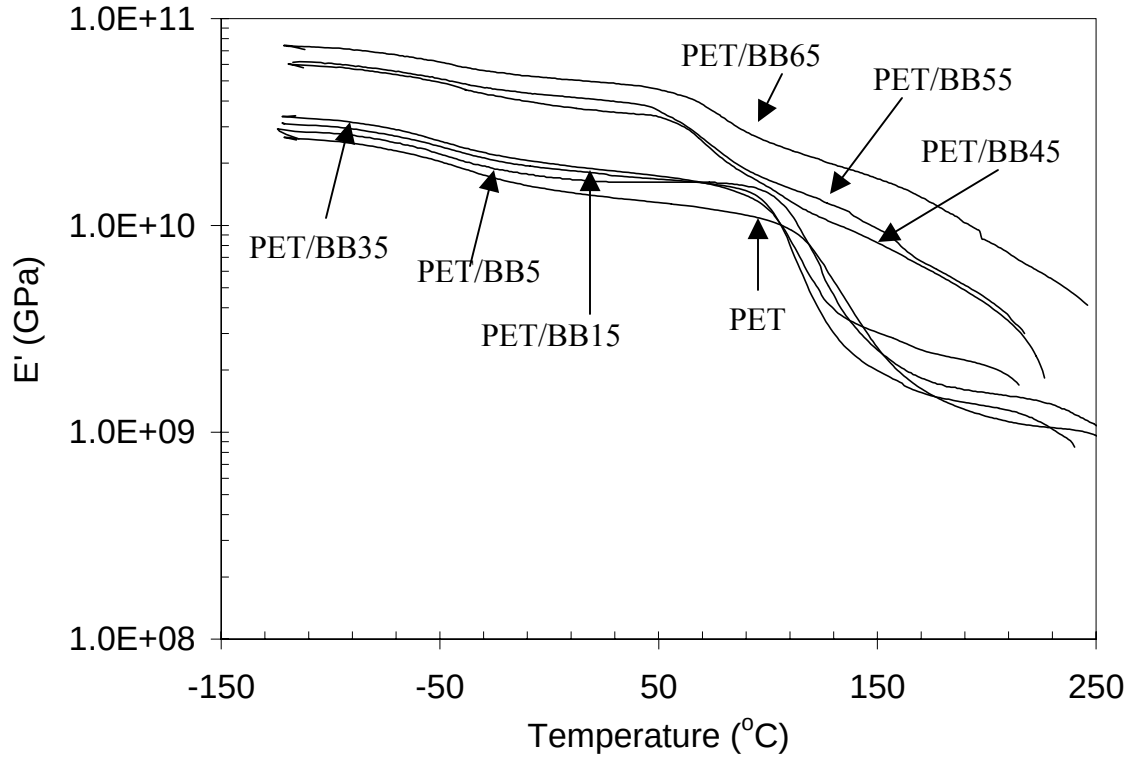

Figure 4.1. PET/BB fiber storage modulus (E') at 10 Hz

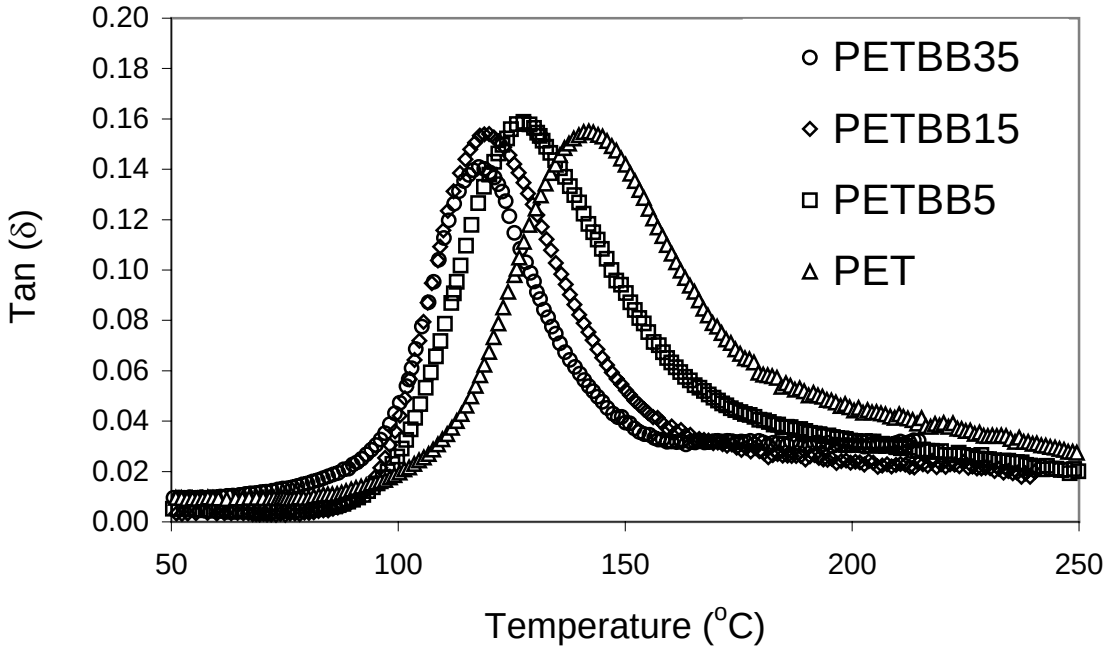

(a)

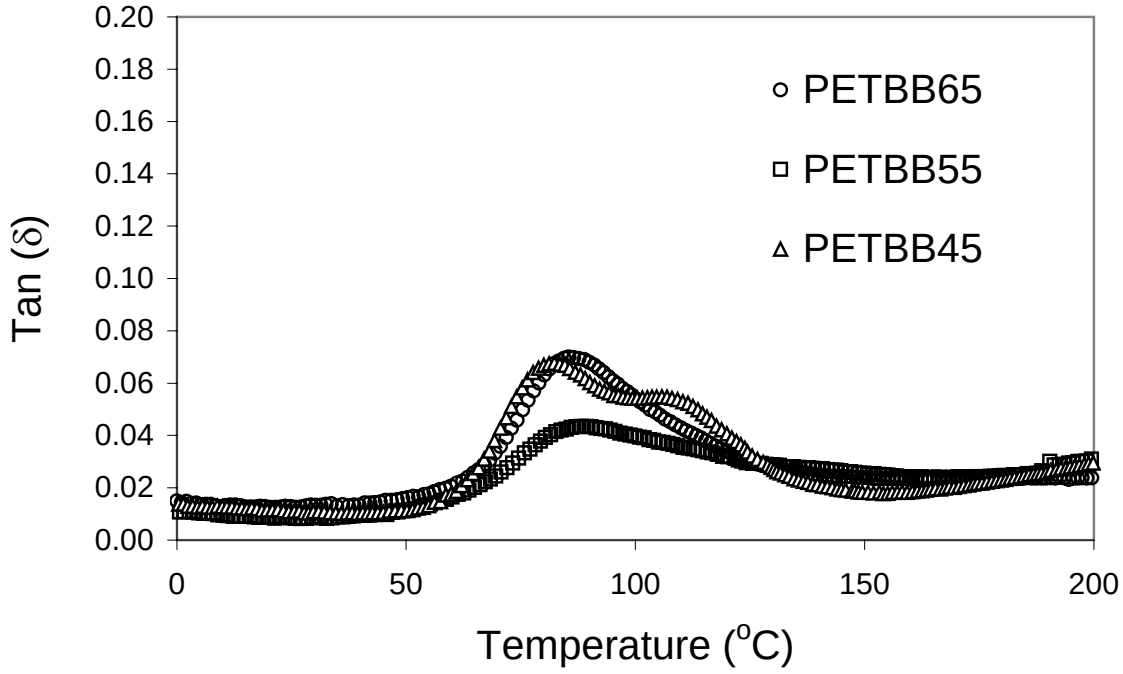

(b)

Figure 4.2. Tan(δ) at 10 Hz (a) low BB content fibers. (b) High BB content fibers.

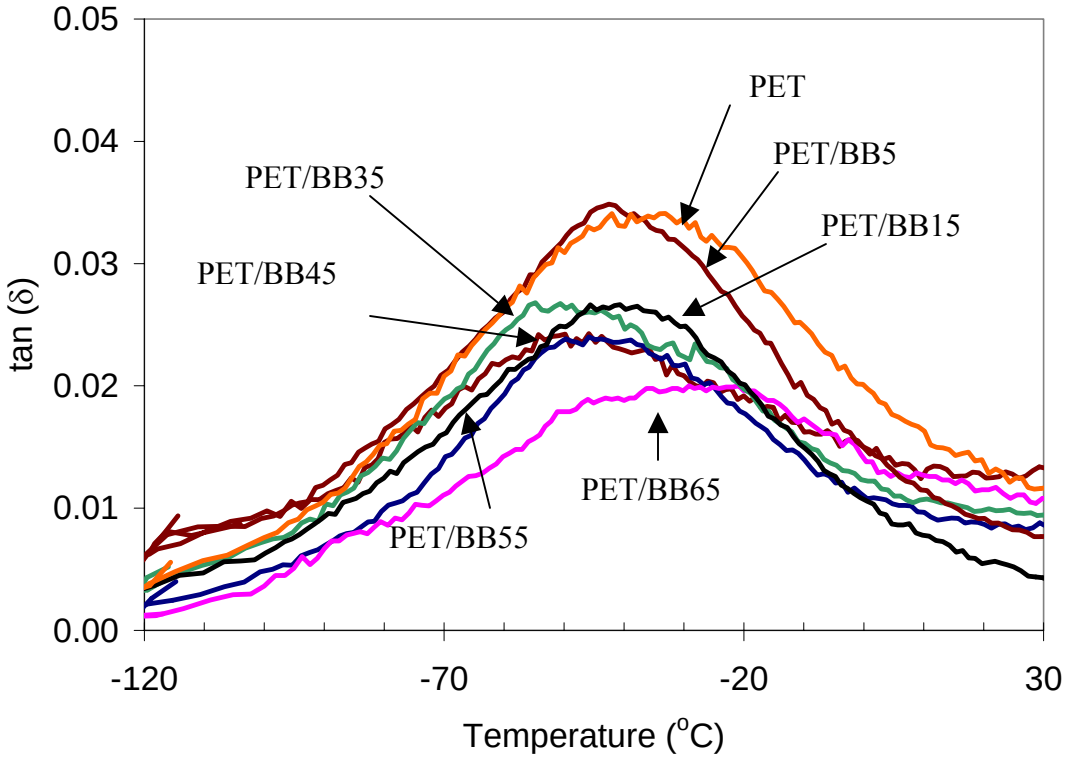

Figure 4.3. β_1 relaxation of PET/BB fibers (at 10 Hz).

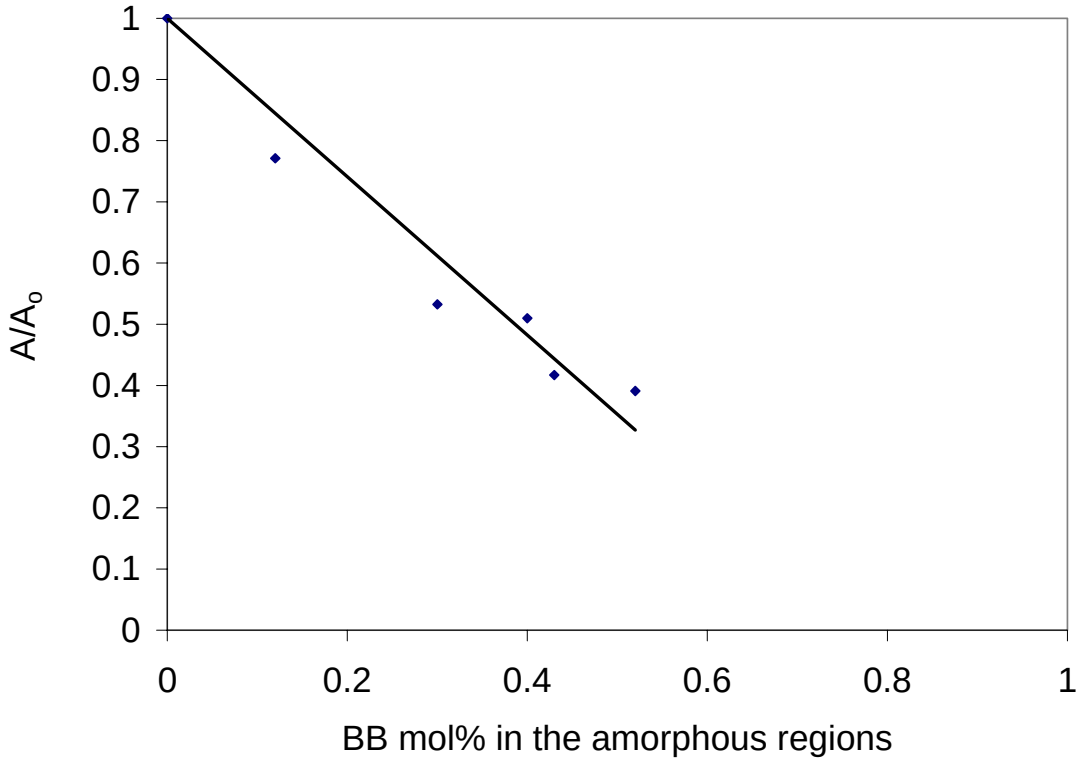

Figure 4.4. β_1 peak area ratio between PET/BB and PET (A/A_o) as a function of BB mole fraction in the amorphous region.

4.6. References

[1] Ward, I. M "*Mechanical Properties of Solid Polymers*" John Wiley and Sons, New York, 1979.

[2] Boyd, R.H. *Polymer*, **1985**, *26*, 323.

[3] Boyd, R.H. *Polymer*, **1985**, *26*, 1123.

[4] Asrar, J., Speciality Polyesters '95, Proceedings. Publisher: Schotland Business Research, Skillman, N. J., **1995**, p. 155.

[5] Troughton, M.J.; Davies G.R.; Ward, I.M. *Polymer*, **1989** *30*, 58.

[6] Liu, R.Y.F.; Schiraldi, D.A.; Hiltner, A. Baer, E., *J. Polym. Sci.: Part B: Polym. Phys.* **2002**, *40*, 862.

[7] Li, X.; Brisse, F. *Macromolecules* **1994**, *27*, 2276.

[8] Ma, H.; Hibbs, M.; Collard, D. M.; Kumar, S.; Schiraldi, D. A.; *Macromolecules* **2002**, *35,* 5123.

[9] Boyd, I.S.U.; Boyd, R.H. *Macromolecules* **2001,** *34***,** 7219.

[10] Chen, L.P.; Yee, A.F.; Goetz, J.M. Schaefer, J. *Macromolecules* **1998**, *31*, 5371.

[11] Maxwell, A. S.; Ward, I. M.; Laupretre, F.; Monnerie L. *Polymer* **1998**, *39*, 6835.

[12] Wilhelm, M., Spiess, H. W. *Macromolecules* **1996**, *29,* 1088.

[13] Gabrielse, W.; Gaur, H. A.; Feyen, F. C.; Veeman, W. S. *Macromolecule,* **1994**, *27,* 5811.

[14] Liu, R. Y. F.; Schiraldi, D.A.; Hiltner, A.; Baer, E. *J. Polym. Sci. Part B: Polym. Phys.* **2002***, 40*, 862.

CHAPTER V

CROSSLINKING STUDIES ON POLY(ETHYLENE TEREPHTHALATE-*co*-1,4 PHENYLENE BISACRYLATE)

5.1. Abstract

Several compositionally different poly(ethylene terephthalate-*co*-1,4-phenylene bisacrylate) copolymers, PETPBA, were melt spun into fibers. The resulting fibers were subjected to UV irradiation to induce crosslinking. Evidence of crosslinking was obtained from FTIR, solid state ^{13}C NMR, thermal analysis and solubility. Irradiation of the fiber results in an increased glass transition temperature, reduced thermal shrinkage, and enhanced modulus retention at elevated temperature.

5.2. Introduction

Compounds containing α,β - unsaturated carbonyl functional groups possess well-characterized photochemistry. t*rans*-cinnamic acid derivatives undergo [2+2] cycloaddition in the solid state and isomerize to the *cis* compound in solution. Since the discovery of the dimerization of trans-cinnamic acid upon UV irradiation in 1895, photocrosslinkable polymers containing cinnamic acid derivatives have been developed mainly for printing, lithographic, and resist applications.[1] It is of interest to investigate the effect of photo-crosslinking on thermal and mechanical properties of a thermoplastic

polymer, where the reactive chromophores form part of the maim chain. Poly(ethylene terephthalate) (PET) is a commercially important polymer which finds applications in textiles, and as reinforcement fiber in tires, as well as in food and beverage packaging[2,3]. Opportunities for extending the range of PET applications include enhancing its gas barrier properties, as well as maintaining its mechanical properties at elevated temperatures. Crosslinking is one of the most effective ways to improve these properties.[4] In the case of thermoplastics, where melt processing of the polymer is an important consideration, a post-processing UV crosslinking step is an attractive approach by which to improve thermo-mechanical properties without sacrificing melt processability. Random copolymers of PET and the photochemically active comonomer, *p*-phenylene bisacrylate (PBA), have been synthesized by melt polymerization[5]. PBA was chosen because it is difunctional and thermally stable under PET polymerization conditions; the resulting copolyesters undergo photochemical [2+2]-cycloadditions upon UV irradiation. The photochemistry of PBA has been thoroughly elucidated.[6,7,8,9,10,11] The steric requirement of the reaction was thought to be too stringent for cycloaddition to occur between cinnamoyl units in an amorphous polymer.[1,10] While this view was supported by early research, subsequent research has shown that compounds containing cinnamoyl units do react in the amorphous regions. Effect of solid matrix on the efficiency of the cycloaddition process has been demonstrated by Egerton et al.[11] Ethyl cinnamate undergoes cyclodimerization in high yields in the glassy state.[12] Evidence for cyclodimmer in irradiated polymer films has been reported for poly(vinyl cinnamate) and copolymers,[13,14,15] poly[1,4-bis(2-hydroxyethoxy) cyclohexane-(phenylene-bisacrylate)], poly[1,4-bis(2-hydroxyethoxy) cyclohexane-(cinnamate)],[11] liquid crystalline main chain

copolyesters[16,17] and poly(ester imide).[18,19] Gas chromatographic analysis of some these films after hydrolysis show that photocycloaddition is the principal method of crosslinking. In this paper we show the evidence of PBA crosslinking in PET matrix and the effects of resulting crosslinking on the thermal and mechanical properties of PETPBA fibers.

5.3. Experimental

5.3.1. Sample preparation

Monomeric PBA, and PET-*co*-PBA copolyesters were prepared using the published methods.[5] Polymers were produced from the dimethyl 1,4-phenylenebisacrylate, dimethyl terephthalate, and ethylene glycol, using a manganese acetate/antimony oxide catalysts system, polymerizing in the melt at 285 °C. Polymer samples used in this study are listed in Table 1. The designation PETPBAx indicates the copolyester in which x mole % of aromatic diester structure units are 1,4-phenylene bisacrylates (PBA). Intrinsic viscosity (IV) measurements were made using 1% (w/w) solutions of polymer in dichloroacetic acid at 25 ^{o}C.

5.3.2. Fiber processing

Before spinning, polymer samples were dried under vacuum at 80 °C for 48 hours. The spinning was carried out on a small-scale fiber extrusion unit manufactured by Bradford University Research Ltd. After spinning, the fibers were drawn on a hot plate at 105 ^{o}C to a draw ratio of between 3 and 4; and then heat-treated at 150 ^{o}C at constant

length in an oven. Fibers were irradiated using a Rayonet photochemical reactor equipped with medium pressure Hg bulbs producing a maximum intensity at 300 nm.

5.3.3. Characterization

Infrared spectroscopy of fibers was carried out on a Perkin Elmer Spectrum™ One FTIR spectrometer equipped with an Auto-IMAGE microscope. Solid–state NMR measurements were carried out on a Bruker DSX-300 spectrometer in a Bruker double-resonance MAS probe head. A standard cross-polarization (CP) pulse was used with ^{1}H and ^{13}C 90^{o} pulses of 4.5 μs. Recycle delays of 5 s and sample spinning speeds of 5 kHz were employed. 2k scans were accumulated for signal averaging. Differential scanning calorimetry (DSC) was performed on a TA instruments Q100 DSC. Melting temperature (T_m) and enthalpy of melting (ΔH_m) were measured from the first heating cycle. Crystallization temperature (T_c), and enthalpy of crystallization (ΔH_c) were measured from the first cooling cycle. Heating and cooling rates were 20 ^{o}C/min.

Fiber tensile properties were tested on an Instron tensile tester (model 5567) at a gage length of 2.54 cm and cross-head speed of 5 mm/min. Dynamic mechanical analysis (DMA) was carried out on Rheometric Scientific™ RSAIII; a static stress of ~10 MPa and dynamic strain of 0.1% was applied on 10 mm gage length samples containing 20 filaments. Fiber shrinkage was measured on a TA instruments Thermo-mechanical analyzer (TMA-2940) at a stress of 50 KPa. Fiber solubility was tested in trifluoroacetic acid (TFA).

5.4. Results and Discussion

PBA can be successfully incorporated into PET using the typical melt polymerization process.[5] There are few examples[5,19,20] in the literature of successful incorporation of such reactive comonomers in condensation polymers where polymerization is carried out at high temperatures. The thermal properties and intrinsic viscosities of the polymers used in this study are given in Table 1.

The fiber spinnability and post-spinning drawability of the PETPBA copolymers are similar to those of PET for all copolymer compositions used in this study. Evidence of crosslinking upon irradiation was collected from changes in the FTIR and solid-state NMR spectra as well as from changes in solubility, thermal behavior and mechanical properties of the fibers. Figure 1 shows the FTIR spectrum of the fibers irradiated at 300 nm for different times. Peaks are normalized with respect to the benzene stretching vibration at 1580 cm^{-1}. The absorption due to the bisacrylate double bound stretching mode at 1635 cm^{-1} is reduced with time. After 16 hours of irradiation, a considerable number of the double bonds remain unreacted. With UV irradiation, as crosslinking occurs at the fiber surface, the resultant bleaching allows further radiation penetration, and hence crosslinking occurs at greater depth with increased irradiation time.[21]

Structure of the irradiated fiber was studied using ^{13}C solid state NMR (Figure 2). Upon UV irradiation, intensities of the 142 and 118 ppm peaks, corresponding to the olefinic carbon atoms of the PBA unit, decreased. Consistent with formation of the cyclobutane carbons of the photodimer, low intensity new peaks appeared between 30 and 50 ppm.[21,22] The development of a shoulder on the carbonyl peak at 170 ppm indicates the generation of unconjugated carbonyl groups.

Before irradiation, the fibers dissolve completely in trifluoroacetic acid (TFA). After irradiation for 1 hour, PETPBAx fibers become insoluble, except for the PETPBA1, which is still soluble. By comparison, PET fibers dissolve rapidly even after 5 hours of irradiation. Irradiation also affects thermal properties of PETPBA fibers, especially at higher PBA mole fractions. As shown in Table 2, the melting temperature of PETPBA15 decreases by 8 ^{o}C after 1 hour of irradiation, and decreased by more than 40 ^{o}C after 5 hours of irradiation. The heat of melting did not change significantly as a result of UV irradiation. After 1 hour of irradiation, copolymers containing low mole fraction biscarylate, exhibited lower crystallization temperatures and decreased enthalpy of crystallization, while PETPBA15 did not crystallize under the experimental conditions employed herein. This is attributed to crosslinking preventing/retarding crystallization.

Photocrosslinking also results in change in mechanical properties of PETPBA15 fibers. Tensile tests show that after 5 hours of irradiation, fiber tensile strength (0.16 ± 0.02 before irradiation to 0.21 ± 0.03 GPa after irradiation) and modulus were moderately affected (6.3 ± 0.6 GPa before irradiation to 7.0 ± 1.0 GPa after irradiation), and extension to break decreased from 30% to 17% as a result of the photochemical treatment. By comparison, 5 hours of UV irradiation had no significant effect on the mechanical properties of the PET fiber. Dynamic mechanical properties of irradiated and unirradiated fibers are given in Figure 3. Irradiated fibers exhibit increased modulus retention above T_g. At 120 ^{o}C, storage modulus of the irradiated fiber is about two times that of the unirradiated fiber. However, at higher temperatures (above 170 ^{o}C), irradiated fibers show sharper drop in storage modulus. This is because irradiated fibers have relatively low melting temperature. With irradiation, Tan(δ) peak temperature increased by more

than 25 ºC and the magnitude of the tan(δ) peak decreased significantly and peak broadens towards higher temperature. Fiber shrinkage as a function of temperature is given in Figure 4. Fiber irradiated for over five hours exhibit significantly reduced shrinkage up to about 150 °C. While, above this temperature these fibers show higher shrinkage, as irradiated fibers exhibit significantly lower melting temperature. Upon melting, irradiated fibers do not break until they reach degradation temperature, while uncrosslinked (e. g. PET, Figure 5a) fiber breaks immediately. These observations are consistent with crosslinking in the amorphous regions.

5.5. Conclusions

Fibers from PETPBA copolymer can be spun by conventional melt spinning and crosslinked by UV irradiation as shown by IR and NMR spectroscopic techniques as well as solubility test. As expected, crosslinked fibers show increased T_g and reduced thermal shrinkage.

Table 5.1. Thermal properties of fibers (Data in brackets are for fibers irradiated for one hour, and the data in brackets with † are for fibers irradiated for five hours)

Sample	**IV** **(g/dL)**	**T_m** **(°C)**	**ΔH_m** **(J/g)**	**T_c** **(°C)**	**ΔH_c** **(J/g)**
PET	0.64	253 (253) †	44 (45) †	199 (199) †	37 (36) †
PETPBA 3.4	0.60	246 (245)	46 (46)	197 (170)	35 (19)
PETPBA 4.4	0.61	247 (247)	39 (37)	195 (159)	32 (7)
PETPBA 15	0.57	228 (220) (185) †	37 (39) (34) †	172 (-) (-)	27 (-) (-)

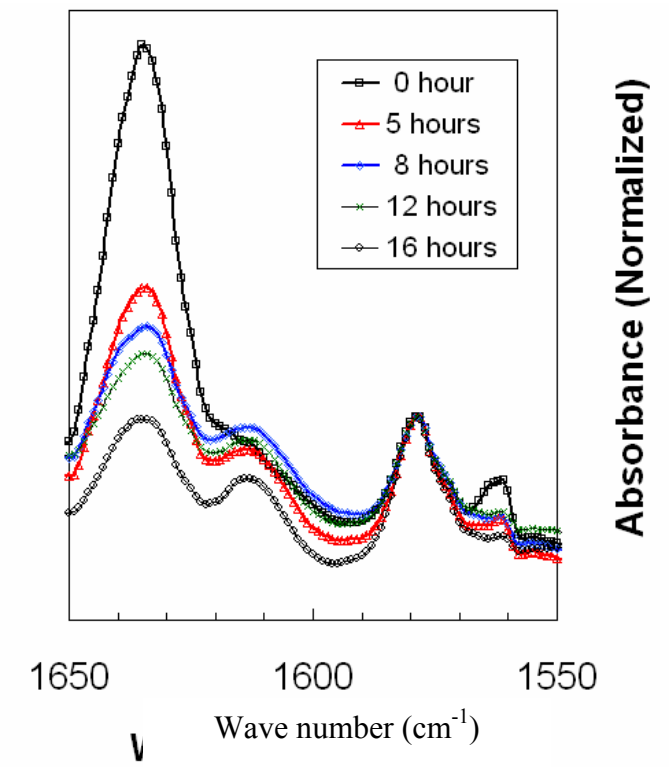

Figure 5.1. FTIR of PETPBA15 irradiated for different times.

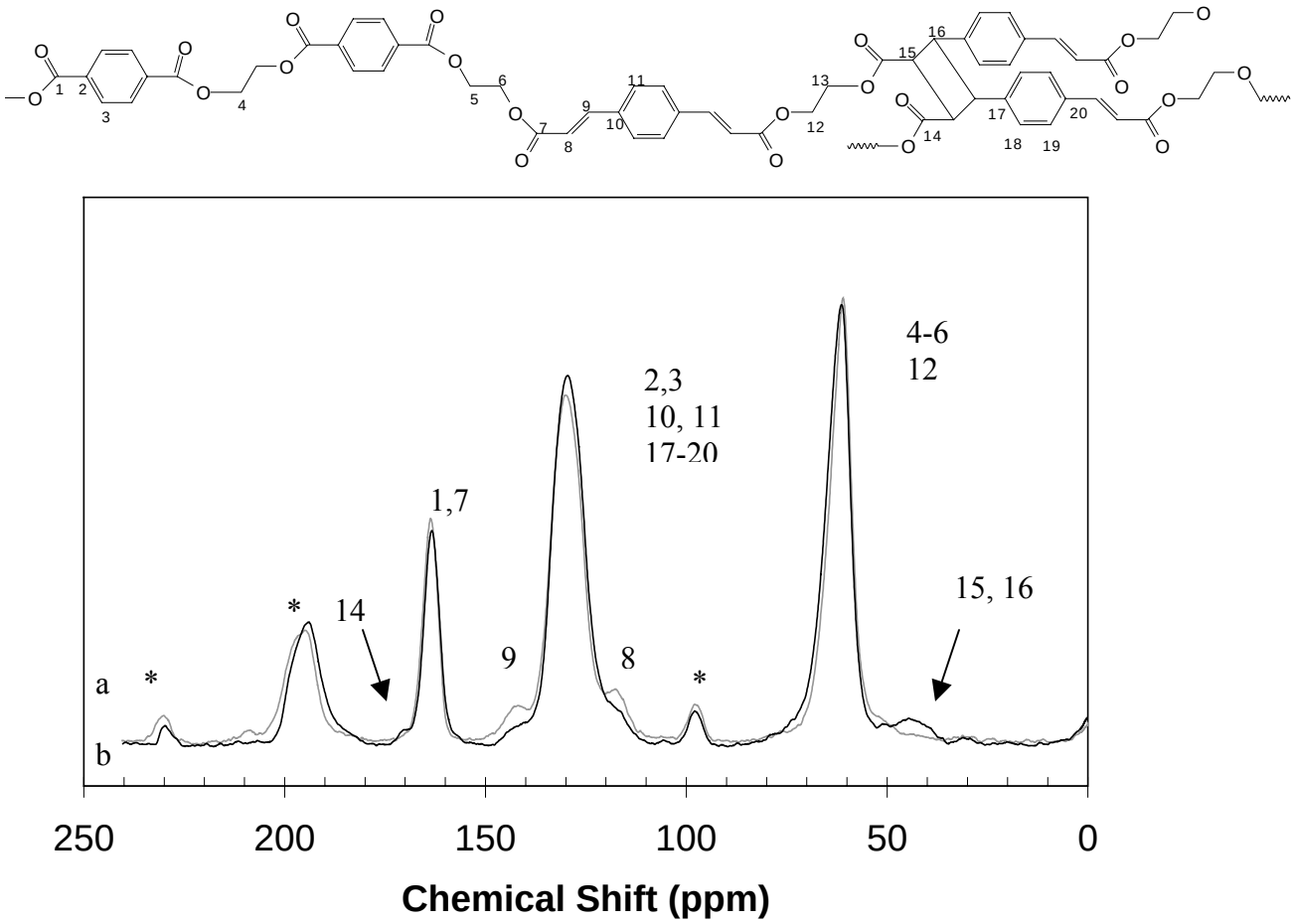

Figure 5.2. Solid state ^{13C}NMR of PETPBA 15 fibers. (a) Unirradiated, and (b) irradiated for 15 hours.

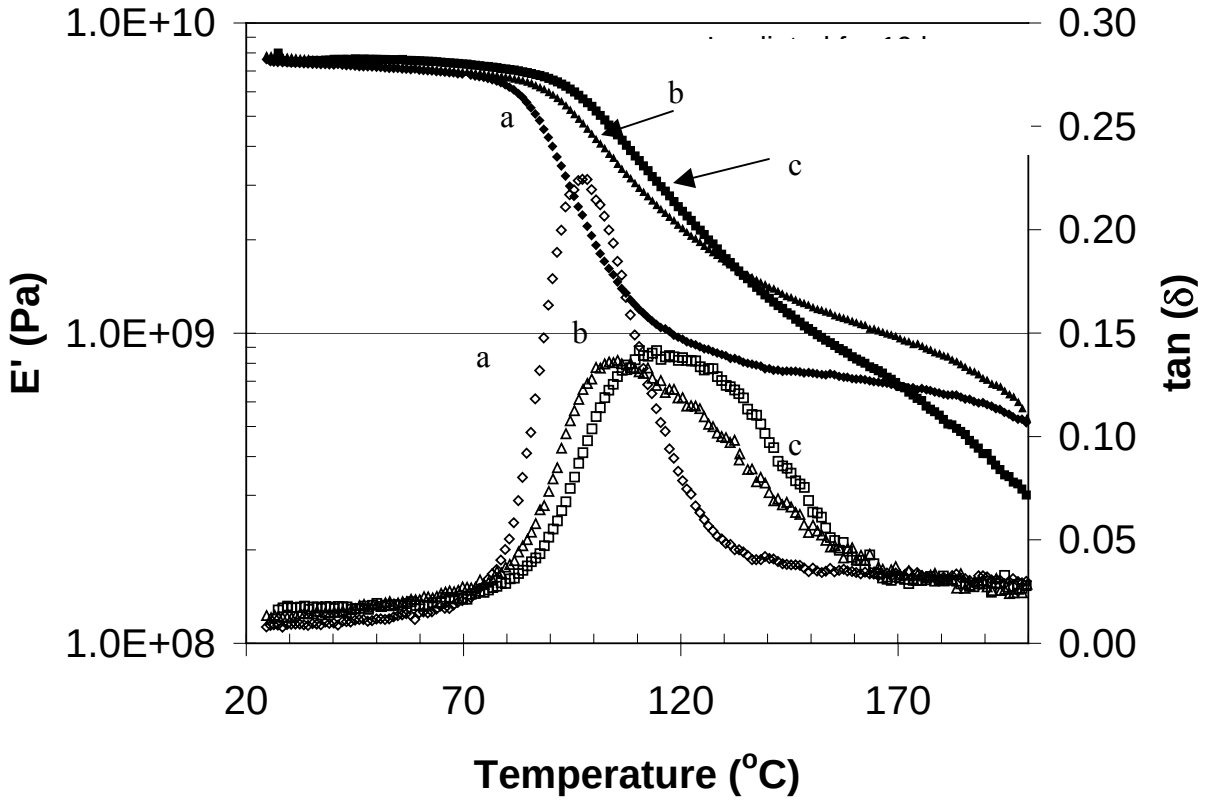

Figure 5.3. DMA of PETPBA15 fibers (a) unirradiated, (b) irradiated for 5 hours, (c) irradiated for 10 hours.

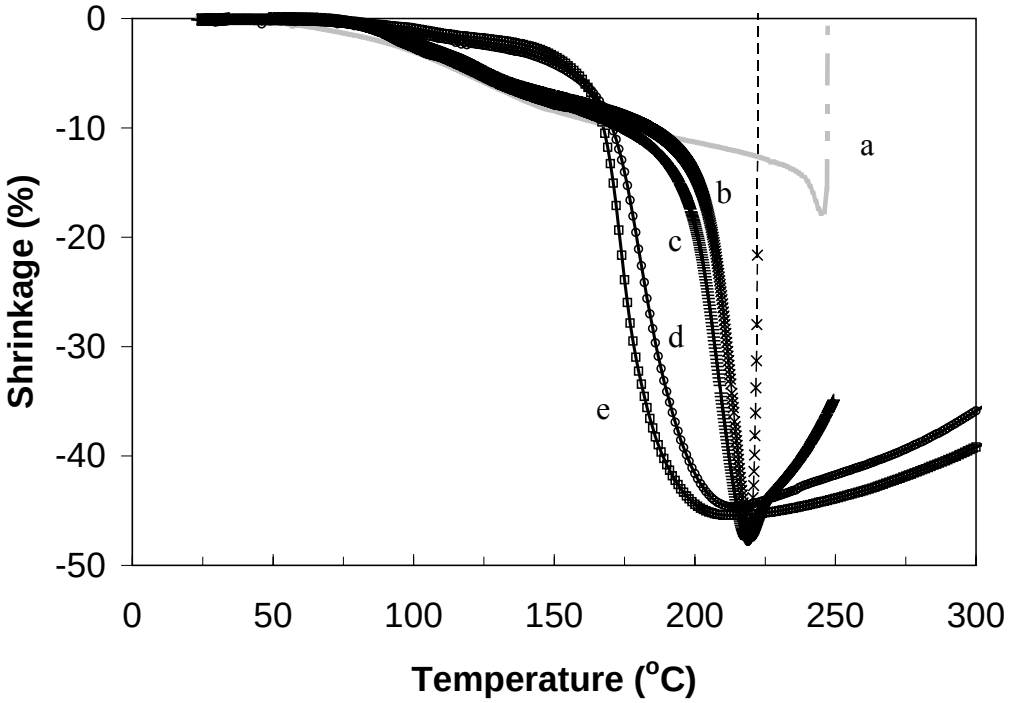

Figure 5.4. Effect of crosslinking of thermal shrinkage. (a) PET irradiated for 5 hours, (b) unirradiated PETPBA15, (c) PETPBA15 irradiated for 1 hour, (d) PETPBA15 irradiated for 5 hours, and (e) PETPBA15 irradiated for 10 hours.

5.5. References

[1] Kosar, J. *Light-Sensitive Systems*; John Wiley & Sons: New York, 1965.

[2] Macdonald, W. *J Kunststoffe-German Plastics* **1993**, *83*, 29.

[3] Clauss, J.; Mitchell, K. *Kunststoffe Plast Europe* **1996** *86*, 29.

[4] Inata, H.; Morinaga, T.; Matsumura, S. *J. Appl. Polym. Sci.* **1998**, *35*, 1705.

[5] Vargas M.; Collard, D. M.; Liotta, C. L.; Schiraldi, D. A. *J. Polym. Sci., Part A: Polym. Chem.* **2000**, 38, 2167.

[6] Suzuki, F.; Suzuki, Y.; Nakanishi, H.; Hasegawa, M. *J. Polym.Sci., Part A-1* **1969**, *7*, 2319.

[7] Nakanishi, H.; Ueno, K.; Sasada, Y. *J. Polym. Sci., Polym. Phys. Ed.* **1978**, *16*, 767.

[8] Nakanishi, H.; Ueno, K., Sasada, Y. *Acta Crystallogr., Sect. B* **1978**, *34*, 2209.

[9] Davidson, R. S. Lowe, C. *Eur. Polym. J.* **1989**, *25*, 173.

[10] Schmidt, G. M. *J. Photochemistry in the Solid State, Schmidt*, G.M. J, Ed.; John Wiley & Sons: New York, 1967, pp350.

[11] Egerton, P.L.; Trigg, J.; Hyde, E. M.; Reiser, A. *Macromolecules* **1981**, *14*, 104.

[12] Egerton, P.L.; Hyde, E. M.; Trigg, J.; Payne, A.; Beynon, P.; Mijovic, M.V.; Reiser, *J. Am. Chem. Soc.* **1981**, *103*, 3859.

[13] Egerton, P.L.; Trigg, J.; Hyde, E. M.; Reiser, A. *Macromolecules* **1981**, *14*, 100.

[14] Murase, S.; Kinsshita, K.; Horise, K.; and Morino, S. *Macromolecules* **1997**, *30*, 8088.

[15] Hu, Y.; Gamble, V.; Painter, P.C.; Coleman, M. M. *Macromolecules* **2002**, *35*, 1289.

[16] Ikeda, T.; Itakura, H.; Lee, C.; Winnik, F. M.; Tazuke, S. *Macromolecules* **1988**, *21*, 3536.

[17] Li, C-H.; Hsu, K-Y.; Chang, T-C. *J. Polym. Sci.: Polym. Chem.* **1993**, *31*, 1119.

[18] Li, C-H.; Cheng, H-P.; Chang, T-C. Chu, T-Y. *J. Polym. Sci.Part A: Polym. Chem.* **1993**, *31*, 1125.

[19] Sapich, B.; Stumpe, J. Kricheldorf, H.R.; Fritz, A.; Schönhals, A. *Macromolecules* **2001**, *34*, 5694.

[20] Jones, R.J.; Liotta, C.L.; Collard, D.M.; Schiraldi, D.A. *Macromolecules* **2000**, *33*, 1640.

[21] Skloss, T. W.; Haw, J. F. *Macromolecules*, **1994**, *27*, 6998.

[22] Lewis, F.D.; Quillen, S. L.; Hale, D. P.; Oxman, J. D. *J. Am. Chem. Soc.* **1988**, *110*, 1261.

CHAPTER VI

PROCESSING, STRUCTURE, AND PROPERTIES OF FIBERS FROM POLYESTER/ CARBON NANOFIBER COMPOSITES

6.1. Abstract

Poly(ethylene terephthalate) (PET) resin has been compounded with carbon nanofibers. The amount of carbon nanofibers utilized in each case was 5 wt %. Compounding methods included ball-milling, high shear mixing in the melt, as well as extrusion using a twin-screw extruder. PET/CNF composite resins were melt-spun into fibers using the conventional PET fiber spinning conditions. Morphology and mechanical properties of these composite fibers have been studied. The results show that CNFs can be incorporated into PET matrix with good dispersion. Compressive strength and torsional moduli of PET/CNF composite fibers were considerably higher than that for the control PET fiber.

6.2. Introduction

Single[1,2,3]and multiwall carbon nanotubes[4,5,6,7,8] as well as vapor-grown carbon nano fibers[9] are promising candidates for reinforcing various polymer matrices. Vapor grown carbon nano fibers which typically have diameters in the 50 to 200 nm range are also referred to as multiwall carbon nanotubes. By comparison, diameter of single wall

carbon nanotubes (SWNTs) are of the order of 1 nm and multiwall carbon nanotube (MWNT) diameter can be upwards of a few nanometers. Carbon nanotubes as well as nanofibers exhibithave good thermal[10] and electrical conductivity[11] and possess excellent mechanical properties.[12] Thermoplastics such as polypropylene[13, 14, 15, , 16, 17] polycarbonate[18, 19, 20, 21] nylon,[15, 22] poly(ether sulfone) ,[23] poly(phenylene sulfide),[24] thermosets such as epoxy,[24,25] acrylonitrile-butadiene-styrene[23], as well as thermoplastic elastomers such as butadiene-styrene diblock copolymer[26] have been reinforced with carbon nano fibers (CNFs). Carbon nano fibers have been blended into polymer matrices using conventional mixing methods such as use of twin-screw extruder [13, 20-22] high shear mixer,[6,24] as well as two-roll mill.[26] To improve CNF dispersion and nanofiber/polymer interfacial strength, carbon nano fibers have been purified,[16] ball milled,[15,26,24] functionalized,[16] and surface treated with plasma.[24, 15,26]

Ball-milled CNF/nylon [15] composites have slightly improved tensile strength and double the modulus of unreinforced material, while ball milled CNF/PP [15] composites have double the tensile strength and quadruple the modulus of unreinforced material. CNF/PP composites made by air-etched fiber, CO_2-etched fibers, and fibers covered with low concentrations of aromatics possessed significantly better mechanical properties than did fibers whose surface was heavily coated with aromatics.[15] In studying ball milled and plasma treated carbon nano fibers in epoxy and poly(phenylene sulfide) (PPS) matrices, Patton *et al* [26] found flexural strength to increase by up to 68 % over neat resin at 19.2 % reinforcement.

Along with the efforts towards on improvementing of matrix polymer the mechanical properties, research on preparation of multifunctional materials has was also

been carried out. [14,17,26,27,28,29] Lozano *et al.*[17] prepared CNF/PP composites and observed a percolation threshold for electrical conduction of 9-18 wt % CNF. With addition of 1 and 5 wt % HDPE, Wu *et al* [31] found the percolation threshold of PMMA/CNF (CNF from Showa Denko Co.) composites was reduced from 8.0 to 4.0 phr (parts per hundred parts) and that it could an be further reduced to 1.5 phr after annealing. The drastic decrease in percolation threshold was attributed to the selective adsorption of HDPE in PMMA/CNF composites.

The rheological,[17,22,23] crystallization,[16] and thermal degradation behavior [16] of polymer/CNF composites have also been studied. Lozano *et al* showed that the incorporation of 30 wt % CNF into PP raised the working temperature of the resin by 100 ºC [16]. They also showed that addition of CNF increased the rate of PP crystallization [16]. Increased polypropylene crystallization rates haves also been reported with addition of single wall carbon nanotubes (SWNT) [30].

In this study, different grades of CNFs have been melt blended into poly(ethylene terephthalate). Melt blended PET/CNF composites have been spun into fibers. Processing, properties, and morphology results of these studies are reported herein. presented in this paper.

6.3. Experimental

Various garades of carbon nanofibers (CNFs) used in this study are listed in Table 1 and were obtained from Applied Sciences Inc., Cedarville, Ohio. Elemental analyseis of the carbon nano fibers wereas carried out byat Atlantic Microlab, Inc. Surface

composition of carbon nanofibers was determined by X-ray photoelectron spectroscopy (XPS) using a Surface Sciences SSX-100 ESCA spectrometer employing Al Kα X-rays. The structure of the CNFs wasas also studied by Raman and FTIR spectroscopies. The Raman spectra were taken at room temperature using a Holoprobe Research 785 Raman Microscope made by Kaiser Optical System, Inc. using T785 nm excitation wavelength. FTIR spectra of CNFs were collected on Spectrum One FTIR spectrometer made by Perkin-Elmer Instruments. Samples for FTIR measurement were prepared by grinding dry carbon nano fibers with potassium bromide, then pressing into pellet of 1 cm diameter. The final spectra were average of 16 scans with a resolution of 4 cm^{-1}. The thermal stability of CNFs in air was studied using TA Instrument TGA 2950 in the dynamic heating rate mode. In this mode, to maximize weight change resolution, heating rate wasis continuously adjusted automatically in response to the changes in the sample's decomposition rate.[31] The heating rate was set as 50 ºC/min with a resolution of 4 ºC and sensitivity as 1 ºC.

Poly(ethylene terephthalate) (PET) of intrinsic viscosity 0.9 dl/g was obtained from KoSa (Spartanburg, SC) and was cryogenically grounded in powder form of particle size in the 0.7 to 1 mm range. This PET powder was dry-mixed with 5 wt % as received CNFs either by ball milling or by hand mixing, and the mixture was vacuum dried at 150 ºC for over 24 hours. Melt compounding was carried out on a Haake Rheocord 90 either using the twin-screw extruder (TW100) or the Rheomix 600 mixer with roller type rotors. The twin screw extruder has four heating zones. The temperatures from the feeding zone to die zone were set as 250, 270, 275, and 280 ^{o}C, respectively. The screw speed was 30 rpm, and a circular die of 3 mm diameter was used. The temperature in the Rheomix

600 mixer was 280 ^{o}C, rotor speed 50 rpm, and the compounding time was 5 minutes. During extrusion and melt mixing, a cloud of dry nitrogen gas was maintained over the polymer to minimize degradation. The extruded material was quenched in a room temperature water bath, before being fed to the pelletizer. The PET/CNF from the mixer was cryogenically grounded using Alpine Augsburg R010/6 grinder from the Alpine American Corp. Various compounding approaches used in this study are listed in Table 2.

For fiber spinning, PET/CNF composites wereas vacuum dried at 150 ºC for at least over 48 hours and the fibers were spun at 290 ^{o}C using a small-scale fiber spinning system (manufacturer Bradford Research Ltd.) using a single hole spinneret of 250 μm diameter and were taken up at 54 m/min take up speed. As spun fibers were drawn at 120 ºC to their maximum draw ratios (which was about four in most cases) and heat-treated in an oven at 150 ^{o}C for 10 minutes at constant length.

As received carbon nanofibers were observed in StereoScan 430 scanning electron microscope (from Leica Cambridge Ltd) without any conducting coating. For scanning electron microscopy, PET/CNF composite samples (from twin-screw extruder or rheomix mixer) and composite fibers were fractured in liquid nitrogen and coated with gold using a sSputter cCoater (from Edwards High Vacuum International). Selected as spun PET/CNF composite fibers were dissolved in trifluoroacetic acid at room temperature and carbon nano fibers filtered using a 1 μm size filter (Gelman Laboratory TF-1000 PTFE Membrane Filter). Carbon nano fibers removed from this process were again observed in the SEM.

Single filament tensile tests were carried out at 2.54 cm gauge length on an Instron tensile tester (model 5567) at a 100% per minute strain rate. At least 20 samples were tested in each case. Fiber diameters were measured using laser diffraction.[32] Dynamic mechanical analysis was carried out on a Seiko DMS (Model 220) at approximate 1.75 MPa static stress and 0.1 % dynamic strain at 1 Hz at a heating rate of 5 °C/min. Initial sample lengths used for testing wereas 20 mm. Fiber compressive strengths wereas measured using by the loop test [33,34] assuming compressive modulus values to be equal to those of the same as tensile modulis. Torsional modulis wereas measured using a pendulum test.[35] Melting temperatures and enthalpiesy of melting on drawn and heat-treated fibers wereas determined using a differential scanning calorimeter Q100 (TA Instruments, Inc.). X-ray diffraction was carried out using the synchrotron source at Brookhaven National Laboratory (X-ray wavelength 0.1542 nm). Rheological behavior of CNF/PET composites was investigated using a Haake Rheostress RS150 rheometer with 20 mm parallel plates and 1 mm gap at 290 ^{o}C.

6.4. Results and Discussion

Various grades of carbon nano fibers along with their bulk and as well as surface elemental compositions are listed Table 1. The Vvarious fiber designations used below are have been explained in the Table footnote. PR-21 hais a larger fiber diameter (about 200 nm) fiber than does the PR-24 (about 100 nm). The bulk oxygen analyses of content in PR-24-AG, PR-24-PPO, and PR-24-ISO show is comparable contents, while the surface oxygen content in PR-24-PPO and PR-24-ISO areis higher than the other fibers tested. The sulfur content in PR-24-ISO was higher than the other nanofibers. Bulk

oxygen content of the pyrolytically stripped (PS grade) fibers are is lower than thoseat for the as grown fibers (PR-24-AG), while the surface oxygen content of the two wereas comparable. High temperature heat-treated fibers showed the lowest oxygen content (PR-24-HT in Table 1).

The ratio (I_D/I_G) of the Raman intensities of the disordered band (D-band) at approximately 1355 cm^{-1} to that of the graphitic band (G-band) at approximately 1590 cm^{-1}, can be taken as a measure of the crystalline order in graphitic systems. The sSmaller I_D/I_G ratios suggests fewerless defects, lessand amorphous carbon, and higher graphitic order.[36,37] Figure 1 shows Raman spectra of the various carbon nano fibers employed in this study. The PR-21-PS is Tthe largest diameter (200 nm) carbon nano fiber, PR-21-PS, and has the highest I_D/I_G ratio of all the fibers listed in Table 1, suggesting that this fiber is most disordered. The lowest value (for PR-24-HT) observed is obviously the result of the high temperature heat-treatment process used in the manufacture of that product. Pyrolytic stripping (PR-24-PS) as well as *in-situ* (PR-24-ISO) or post oxidation processes (PR-24-PPO) do not seem to affect the order significantly, as the I_D/I_G ratios for these fibers are approximately equal to is about the same as that for the PR-24-AG.

FTIR spectra of nano fibers show three peaks at ca. 3430, 1575, and 1230 cm^{-1} (Figure 2). The latter two peaks may be assigned to the carbon skeleton[38] while the 3430 cm^{-1} peak suggests that these CNFs contain hydroxyl functional group on their surfaces.[39] Although the peaks between ca. 3000 cm^{-1} andto 2000 cm^{-1} cannot't be clearly assigned for PR-24-AG, one can deduce that after various treatment applied to of as-grown fibers (PR-24-AG), can remove some functional groups may be removed, (as PR-24-PS, PR-24-

PPO, and PR-24-HT show a relatively flat curve in that wavenumber range). Thermogravimetric analysis shows that nanofibers, with high oxygen content (PR-24-AG, PR-24-PPO and PR-24-ISO), begin to lose weight just above 300 ºC, while for fibers containing lower oxygen levels (PR-24-PS and PR-21-PS), the onset of degradation is above 500 ºC (Figure 3). The onset of degradation for PR-24-HT, which has the least amount of oxygen, is close to 700 ºC.

A high resolution transmission electron micrograph of the type of carbon nano fibers used in this study is given in Figure 4. Light part of the image on the right is the hollow core, in the middle are the nearly parallel graphitic planes, and on the left is the disordered CVD carbon. In these carbon nano fibers, nearly parallel tube walls appear to make a small angle to the fiber axis. make an angle Scanning electron micrographs (Figure 5) show that all as received nano fibers have large aspect ratios (as large as 100 or higher). The diameters of these nanofibers vary from several tens of nanometers to few hundred nanometers. Some catalystic impurity and amorphous carbon may also be present in these samples.[17] The About 2- to 5 % residual weight seen in TGA curves may be the result of the presence of the catalystic impurity. The entangled or clumped carbon nanofibers could be expected to retard the rate of matrix slow down the polymer penetration by a considerable amount. Calculations have shown that the rate of polymer melt permeability in clumps of 100 nm diameter carbon nano fibers is expected to be lower 10^{-4} times slower than that for the 10 μm diameter conventional carbon fibers by a factor of 10,000.[15]

When the dry PET/CNF mixtures wereas poured in the mixer, the torque (at 50 rpm) was initially as high as 100 Nm. However wWithin 2 minutes, however, the torque

decreased to below 20 Nm and remained at this level for remainder of the processing time. The intrinsic viscosity of the control PET drops from 0.91 to 0.62 dl/g after either extrusion or mixing, which may be a result of hydrolytic degradation, while the fiber spinning process only decreased the intrinsic viscosity of PET from 0.62 to 0.61 dl/g. Figure 6 shows a scanning electron micrograph of a PET/CNF composites before fiber spinning, showing good carbon nanofiber dispersion. N in all cases.

Both the control PET, as well as samples 1, 2, 3 and 9 (Table 2) spun quite well. The spinneret was frequently clogged during the spinning of samples 4, 5, and 7. Sample 6 initially exhibited good spinning behavior but as spinning progressed, it exhibited increasing resulted in frequency of t melt fracture. The viscosity of sample 8 at 290 ºC was very low, and yet the spinneret was being clogged frequently during spinning of this composite. Due to these spinning difficulties, no further work was carried out on samples 4 to 8. Three of these four unsatisfactory samples contained carbon nano fibers with greater than more that 2 wt% oxygen and exhibited had onsets of thermal degradation at approximatelyabout 300 ºC.

Ball milling or hand mixing followed by extrusion (samples 1 and 2) showed no obvious differences in spinnability. However, hand mixing followed by extrusion (sample 2) produced samples which exhibited better spinnability over those prepared by hand mixing followed by melt mixing (sample 5). As spun control fibers, as well as fibers of composites 1, 2, 3, and 9 were drawn at 120 ^{o}C to their maximum draw ratios, followed by heat-treatment at 150 ^{o}C for 10 minutes at constant length. A draw ratio of approximately 4six was achieved in each case. Figure 7 shows a scanning electron

micrograph of the tensile fracture of PET/NCF as-spun fiber (sample 1). Significant fiber pullout can be observed in the photograph., showing that

The typical stress-strain curves for the drawn and heat-treated fibers are given in Figure 8, and their average mechanical properties are listed in Table 3. Tensile moduli of composite fibers are slightly higher than that offor the control PET, and tensile strengths of these composite fibers are is either only comparable (sample 9) or lower (samples 2, and 3) than that measured for unfilled fibers. The reinforcement efficiency of nano fibers will depend on their intrinsic mechanical properties, aspect ratio, volume fraction, as well as on the fiber/matrix interfacial strength. A modified Cox [40] model can be used to calculate the Young's modulus of the PET/CNF composite fiber[15]. This model estimates stress transfer to nanofibers of length *l*, diameter *d*, axial tensile modulus E_f and volume fraction *V* in a matrix of modulus E_m with the factor

$$\beta = \frac{l}{d}\sqrt{\frac{E_m}{(1+\nu)E_f \times \ln(\pi/4V)}} \quad (1)$$

where ν is the matrix Poisson ratio. Combining this with the rule of mixtures, modified Cox model gives the following equation for E_c:

$$E_c = (1-V)E_m + q\left(1-\frac{\tanh\beta}{\beta}\right)VE_f \quad (2)$$

Where *q* is the orientation factor of the reinforcement, which in our case is nanofiber. For one oriented nanofibers, *q* is 1. Volume fraction of carbon nanofibers in our case is 3.6% (based on 5 wt% CNF and using densities of 2.0 and 1.40 g/cm^3 for CNF and PET, respectively), matrix modulus is 10 GPa (Control PET in Table 2), and Poisson's ratio ν

for PET is 0.37 [41]. Figure 9, assuming ideal orientation (q = 1) for the nano fiber, shows the predicted modulus for the PET/CNF composite fiber based on equation 2 as a function of CNF aspect ratio at various nano fiber modulus values. This figure shows that for the ideally oriented nano fibers, significant reinforcement is expected to be obtained when CNF aspect ratios greater than 50 and preferablye 100 are used in nanocpomposites.

To determine the carbon nanofiber aspect ratio in the composite fibers, as spun composite fibers were dissolved in trifluoroacetic acid, and nano fibers were removed by filtrationered using a 1 μm size sieve filter. The filtered solutions wereis black in color, which suggests that some carbon nano fibers of smaller length passed through the filter. Scanning electron micrographs of carbon nano fibers recovered from the composite fiber shows significantly reduced nano fiber lengths (Figure 10) as compared to the as received nano fibers. The process of This represents length reduction during mixing, melt blending, and fiber processing clearly lead to attrition of the nano fibers. Decreasing carbon nano fiber lengths while detrimental to tensile properties, would be beneficial to is good for processing, consistent with as suggested by the good spinnability of samples 1 and 9. There may be an optimum nanofiber length which provides for it to be an effective reinforcement, yet still facilitating easy processing. Therefore, controlled ball milling for a short period may be optimal, helpful, which does not degradinge nanofiber length significantly, but providing adequate at the same time disentanglement es them, thusto facilitateing melt processing. Though adequate nano fiber disentanglement can also be achieved by hand-mixing, it may be less practical than ball milling in industrial practice.compounding.

Dynamic mechanical properties (Figure 11) show that the storage modulis for the composite fibers areis somewhat higher than that for the control PET. This is consistent with the tensile test results. Variation in tan(δ) behavior as a function of temperature between the control and the composite fibers was not considered significant. While there is only moderate improvement in tensile modulus, compressive and torsional properties of the composite fibers are increased up to 50% higher as compared to the control fiber (Table 3). Compressive failure in polymeric fibers occurs by yielding which results in the formation and propagation of kinks.[36] Nano fibers may act as barrier for kink propagation, thus resulting in improved compressive strength. Carbon nano fibers have high torsional modulus,[42] which may be responsible for the increase in torsional modulus in the composite fiber. Tensile modulus is affected by fiber aspect ratio and orientation. We have already discussed the issue of aspect ratio. As discussed later, graphitic planes in carbon nano fiber exhibit much lower orientation than the PET fiber. These factors serve to explain why tensile modulus is not improved significantly.

Studies on PP/CNF[17] and PMMA/CNF composite fibers[43] showed that carbon nano fibers can be well dispersed into PP and PMMA though conventional mixing process. With the addition of CNF, the compressive strengths of PP and PMMA composite fibers could be improved significantly. Not Unlike PET/CNF composite fibers, the moduli of PP/CNF and PMMA/CNF fibers were also increased significantly compared to their parent fibers.

Differential scanning calorimetry results (Figure 14) show that both PET as well as PET/CNF composite fibers fully drawn and heat-treated melt at 255 ºC and exhibited 36% crystallinity. This was calculated based on the enthalpy of 100% crystalline PET as

138 J/g.[44] However, although the melting point and crystallinity of two samples (C2 and sample 9) are very comparable, their melting behavior does show some difference. Fibers containing nano fibers have a narrower melting peak as compared to the control PET fiber. This difference may suggest that composite fibers possess more perfect crystals or a narrower distribution of crystal size than the control PET fiber. Wide angle X-ray diffraction (WAXD) pattern (Figure 13) of the composite fiber shows (002) graphitic spacing at two-theta angle of about 26.2. From this X-ray diffraction pattern, Herman's orientation factor for the graphitic plane in carbon nanotube was estimated to be 0.22 while for the c-axis orientation in PET the Herman's orientation factor was estimated to be 0.94. Atomic force microscope images (Figure 14) showed that carbon nano fibers exhibit good orientation with respect to the fiber axis. The significant orientation difference between PET and carbon nano fibers obtained from WAXS at least in part is due to the fact that graphitic planes in the nano fibers are not aligned parallel to the nano fiber axis. However The low graphitic plane orientation further explains the relatively low modulus of the PET/CNF composite fiber. TEM studies on CNF found the average misorientaion of graphtic layer to that of the fiber axis is around 15^{o}, which implies a much lower tensile modulus of the CNF (50 GPa) than previous reported.[45]

Figure 15 shows the shear viscosity of control PET, and composite samples 2 and 9. At low shear rates (below 10 s^{-1}), composite samples have higher viscosity than the control PET, while at high shear rates (100 s^{-1}) viscosity of all three samples was the same. The composite samples exhibited pseudo-plastic behavior throughout the entire range of shear rates used in this study, while the control PET exhibited Newtonian plateau. Similar viscosity behavior has also been reported on polypropylene composites

filled with vapor grown carbon fiber VGCF[46], and on polycarbonate filled with multiwall carbon nanotubes. [47]

6.5. Conclusions

Poly(ethylene terephthalate) (PET) resin was compounded with several grades of carbon nanofibers, each at 5 wt % filler loading. Compounding methods included ball-milling, high shear mixing in the melt, as well as extrusion using a twin-screw extruder. PET/CNF composite resins were then melt-spun into fibers using conventional PET fiber spinning conditions. Morphology and mechanical properties of these composite fibers have been studied and show that CNFs can be incorporated into PET matrix with good dispersion. While tensile strength and modulus were not increased significantly by the addition of nanofibers, compressive strength and torsional moduli of PET/CNF composite fibers were considerably higher than that for the control PET fiber.

Table 6.1. Characterization of various carbon nanofibers (CNFs) used in this study[a]

CNF	Processing method	I_D/I_G[b]	Surface Composition (wt%)[c]			Composition (wt%) by element analysis[d]					
			C	O	S	C	O	H	N	S	Other
PR-24-HT	Fiber graphitized at 3000 °C	0.7	99.2	0.8		99.1	0.3	0.4	0	0	0.2
PR-24-PS[e]	Surface cleaned of all PAHs[f]	1.6	97.9	2.1		96.3	0.6	0.6	0.6	0.4	1.4
PR-21-PS[g]	High surface area version of standard fiber	3.1	95.0	5.0		96.5	1.2	0.4	0.4	0.3	1.2
PR-24-AG[h]	Slight surface contamination by PAHs	1.5	95.5	4.5		94.1	2.2	0.7	0.6	0.5	1.8
PR-24-PPO	Post production chemically oxidized version of PR-24-AG	1.6	92.9	7.1		94.5	2.1	0.4	0.6	0.4	2.0
PR-24-ISO	In situ oxidized version of PR-24-AG	1.8	90.6	7.6	1.8	95.0	2.2	0.7	0.7	1.1	0.3

a. Designation and post processing method were obtained from Applied Science, Inc.
b. I_D and I_G are the relative intensities of the D and G bands of Raman spectra, respectively (details in text).
c. Based on the results of XPS, H and N are not considered.
d. Element analysis was performed by Atlantic Microlab, Inc.
e. PS indicates pyrolytically stripped.
f. Polynuclear Aromatics Hydrocarbons.
g. Grade 21 is reported to be a larger diameter fiber than 24.
h. AG stands for as grown.

Table 6.2 Processing of PET/CNF (5 wt%) composite

Sample[1] code	CNF used	Compounding	
		Dry mixing[2]	Melt mixing[5]
C1	None		E
C2	None		M
1	PR-24-PS	BM[3]	E
2	PR-24-PS	HM	E
3	PR-21-PS	HM	E
4	PR-24-AG	HM	E
5	PR-24-PS	HM	M
6	PR-24-PPO	HM	E
7	PR-24-PPO	HM	M
8	PR-24-ISO	HM	E
9	PR-24-HT	BM[4]	M

1. C1 and C2 are control PET samples
2. BM: ball milling; HM: hand mixing PET powder with CNF for about 10 min before melt mixing
3. Ball milling for 24 h
4. Ball milling for 1 h
5. E: twin-screw extruder; M: Rheomix 600 mixer

Table 6.3. Mechanical properties of PET/CNF (5 wt%) composite fibers

Sample code	Fiber diameter (μm)	Tensile modulus (GPa)	Tensile strength (GPa)	Elongation at break (%)	Compressive strength (GPa)	Torsional modulus (GPa)
C2*	24 ± 3	10 ± 3	0.43 ± 0.08	26 ± 2	0.08	0.7
2	27 ± 6	11 ± 2	0.33 ± 0.06	18 ± 7	0.12	1.0
3	27 ± 5	11 ± 3	0.25 ± 0.10	13 ± 8	0.10	0.9
9	25 ± 2	11 ± 2	0.42 ± 0.06	20 ± 4	0.09	1.1

*C1 has similar mechanical properties as C2.

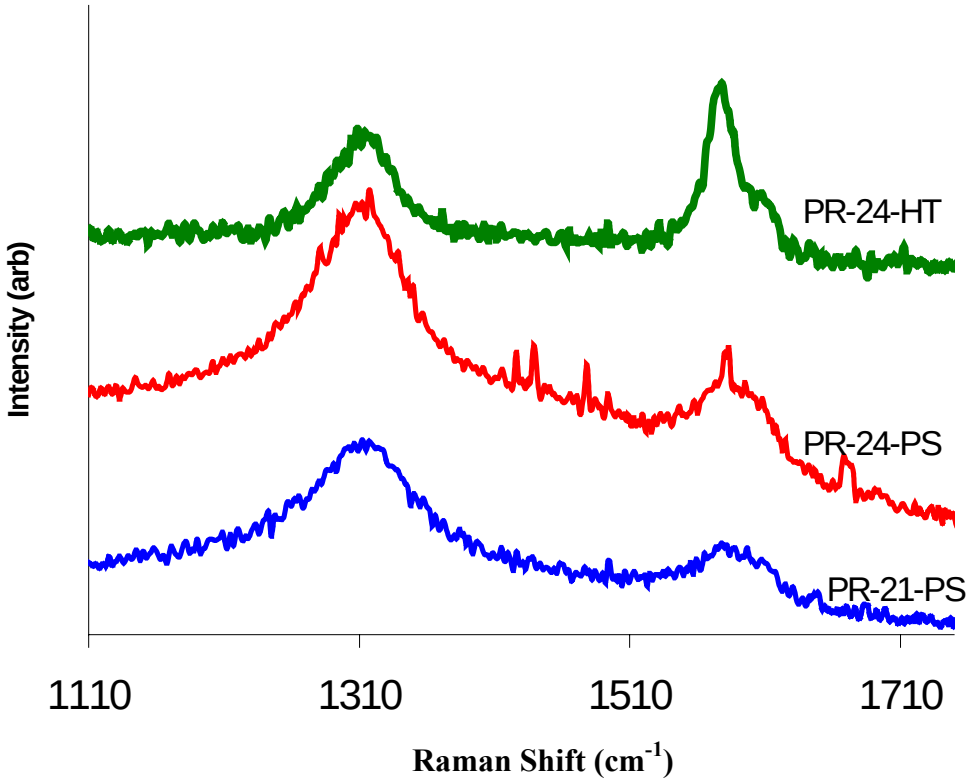

Figure 6.1. Raman spectra of various carbon nano fibers.

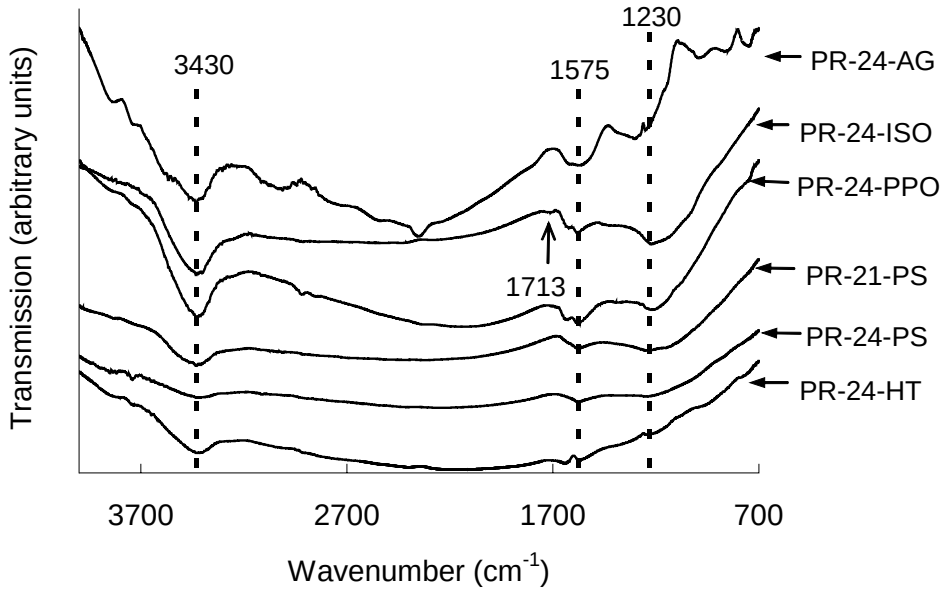

Figure 6.2. FTIR spectra of various carbon nano fibers

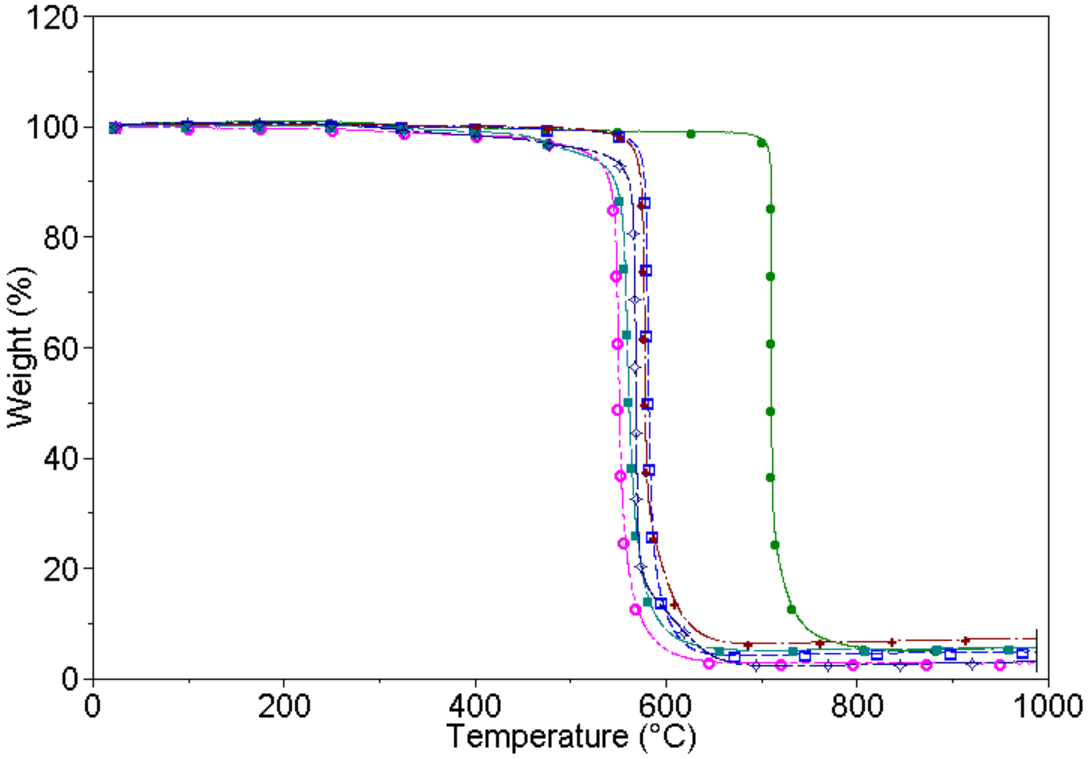

Figure 6.3. Weight loss in air as a function of temperature in various carbon nano fibers**.**

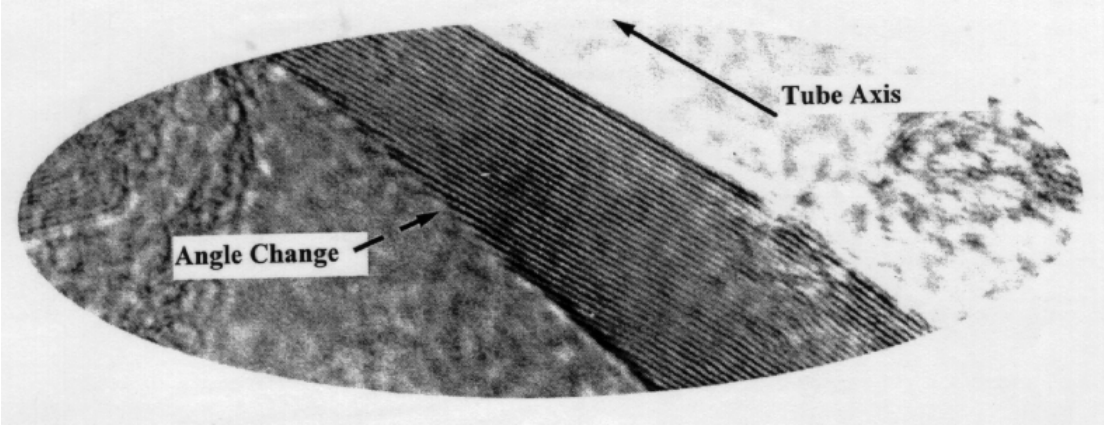

Figure 6.4. TEM image of the wall of a carbon nano fiber (from Applied Sciences Inc.). Distance between graphitic planes is 0.334 nm.

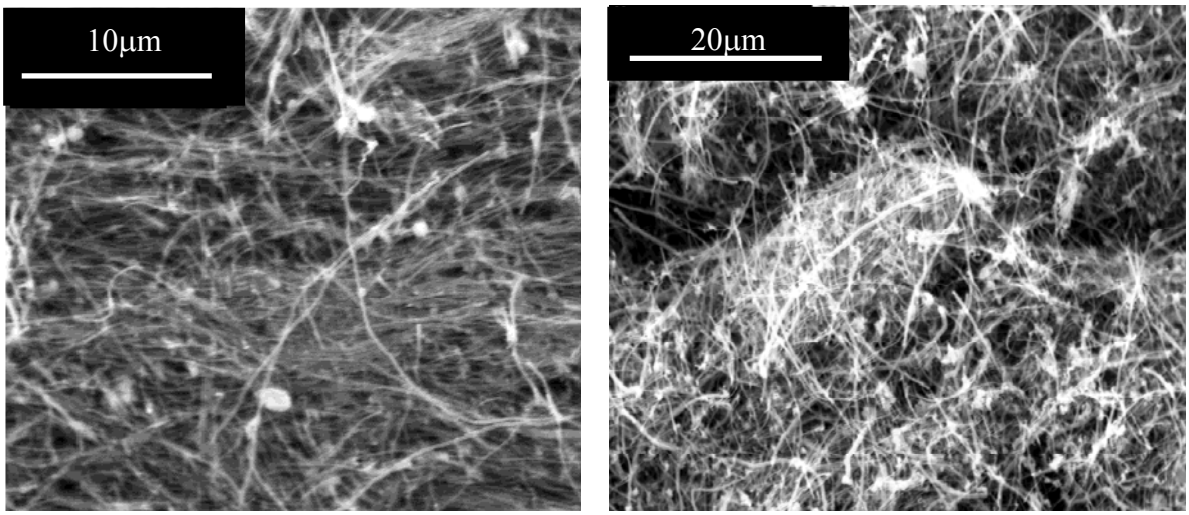

Figure 6.5. Scanning electron micrograph of as received carbon nano fibers: (a)PR-24-PS; (b) PR-21-PS.

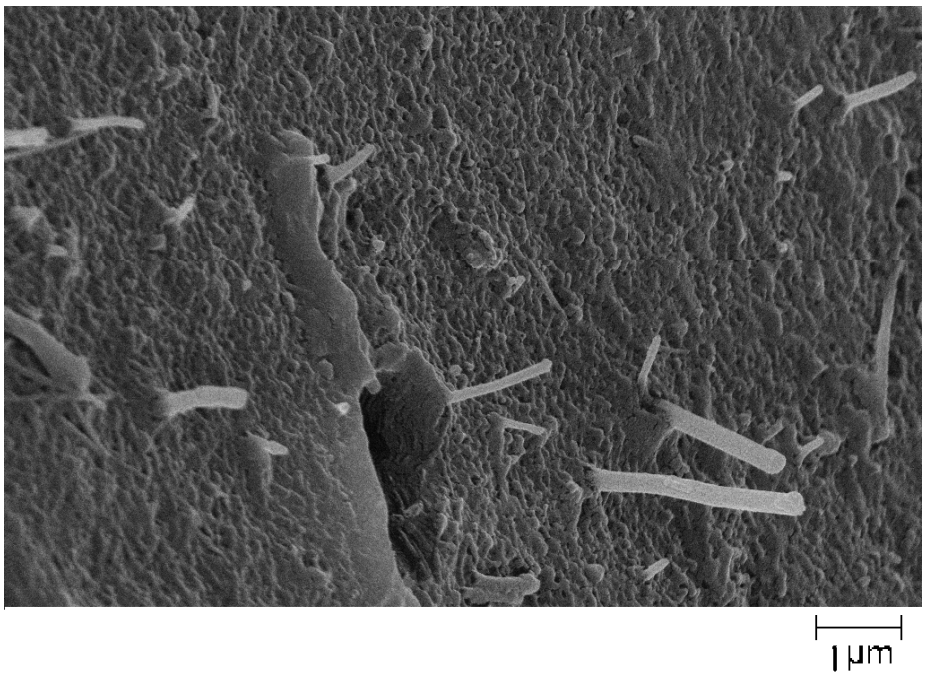

Figure 6.6. Scanning electron micrograph of PET/CNF(PET/PR-24-HT) composite (sample 9 in Table 2).

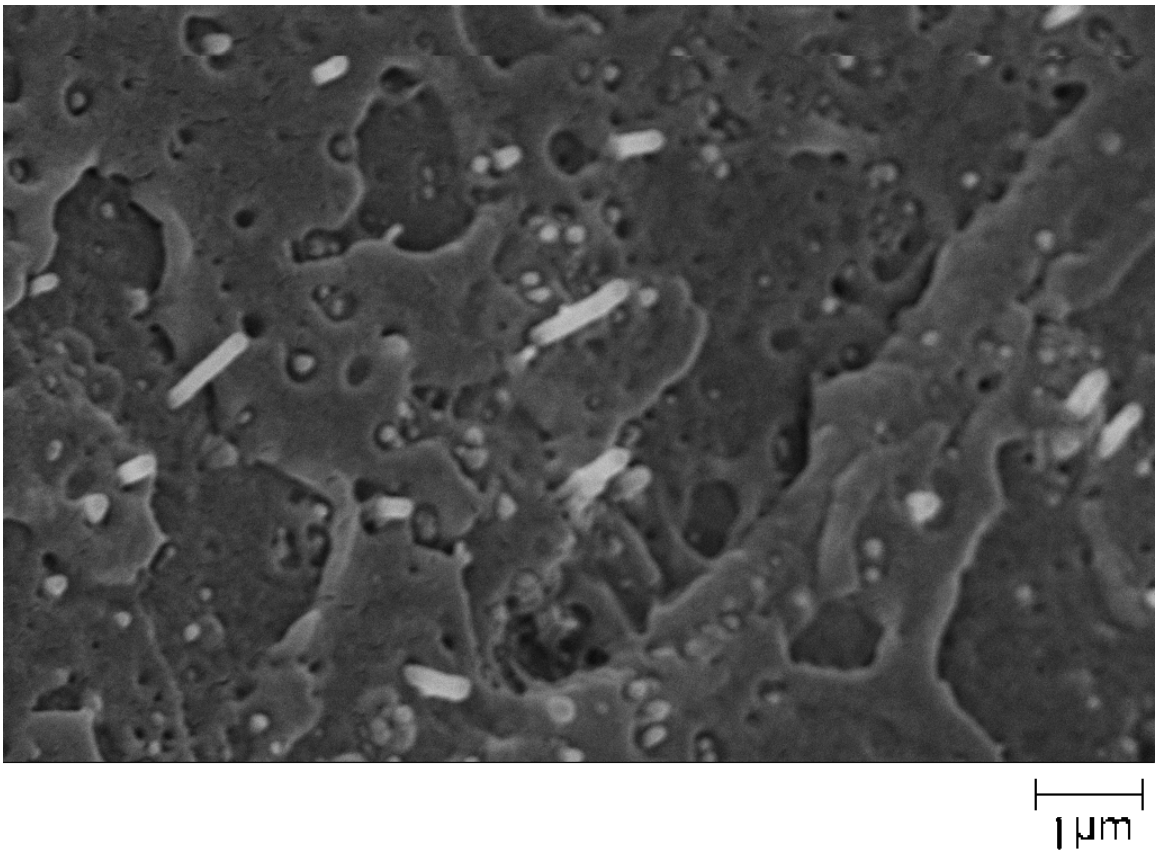

Figure 6.7. Scanning electron micrograph of PET/PR-24-PS as spun fiber (sample 1 in Table 2).

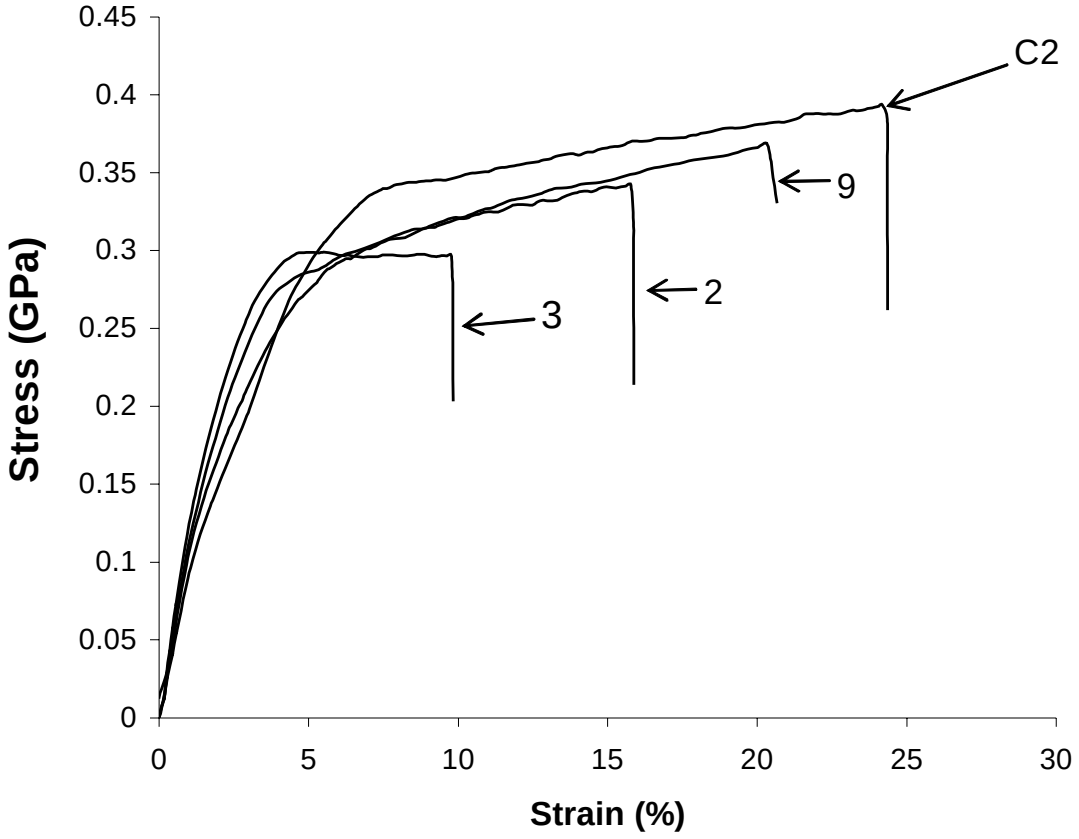

Figure 6.8. Typical stress-strain curves for drawn and heat-treated PET/CNF composite fibers.

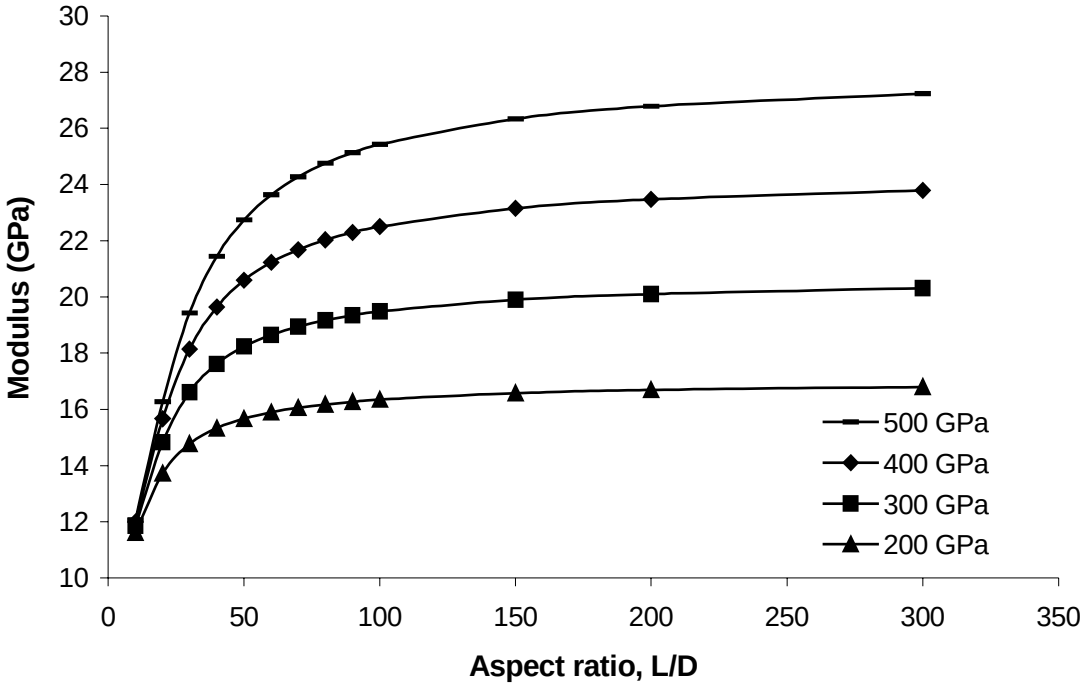

Figure 6.9. Cox model estimation for PET/CNF composite fiber tensile modulus assuming ideal CNF orientation**.**

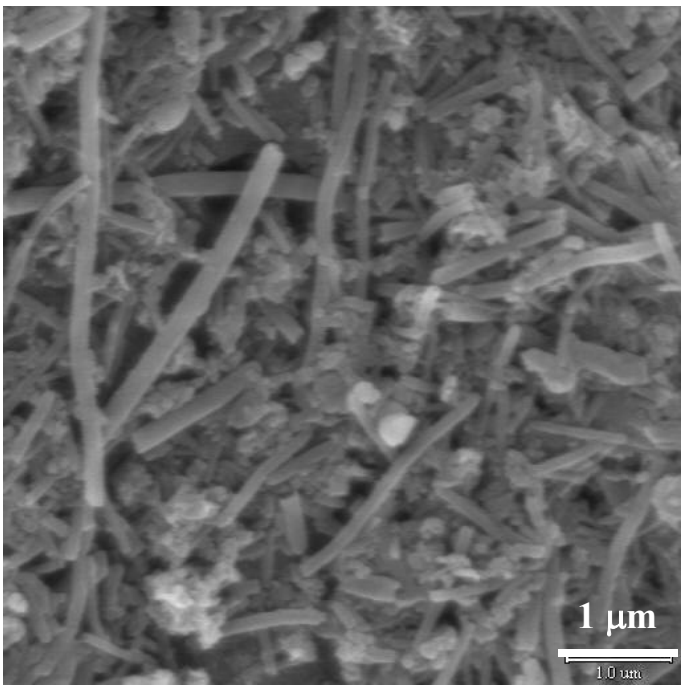

Figure 6.10. Scanning electron micrograph of carbon nano fibers extracted from PET/PR-24-PS as spun fiber.

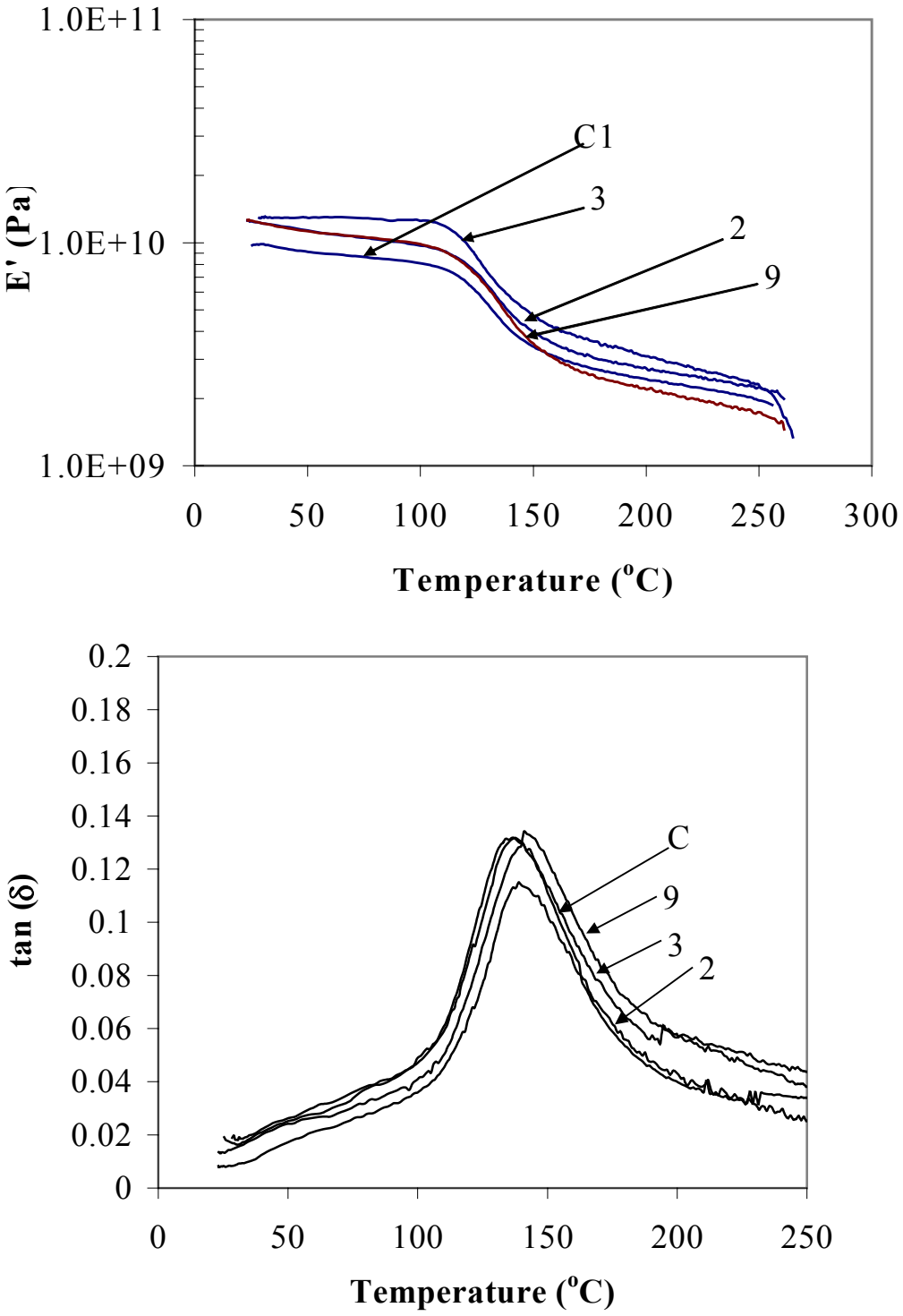

Figure 6.11. Dynamic mechanical properties for drawn and heat treated PET/CNF composite fibers (sample numbers refer to Table 2).

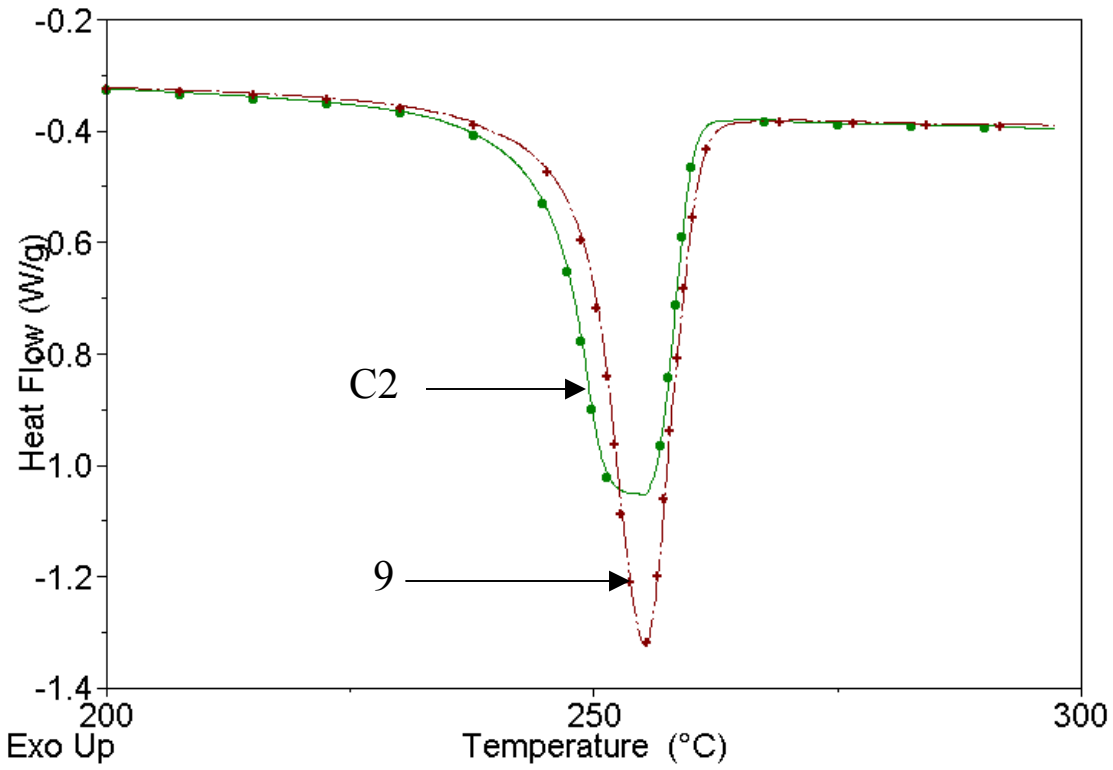

Figure 6.12. Differential scanning calorimetry scans of drawn and heat-treated PET (C2) and PET/CNF (9) fibers. Sample numbers refer to Table 2.

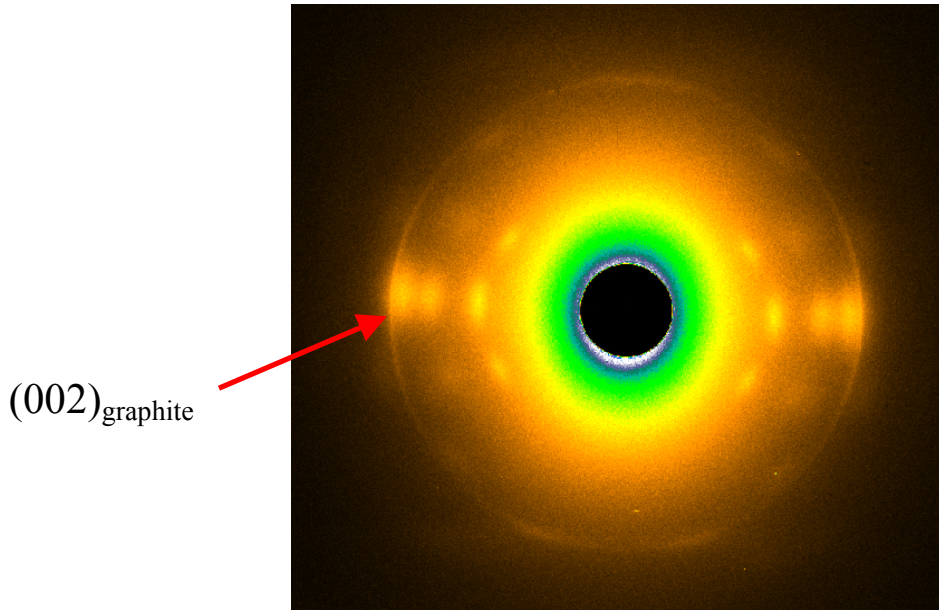

Figure 6.13. WAXD pattern of PET/CNF composite fiber.

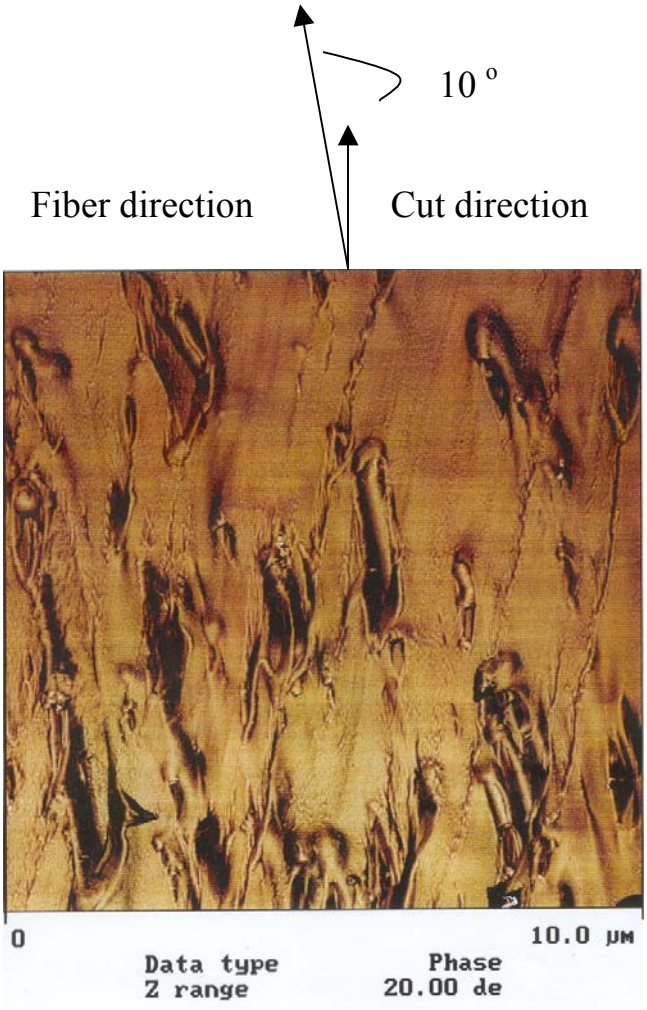

Figure. 6.14. Atomic force microscope image of PET/CNF composite fibers.

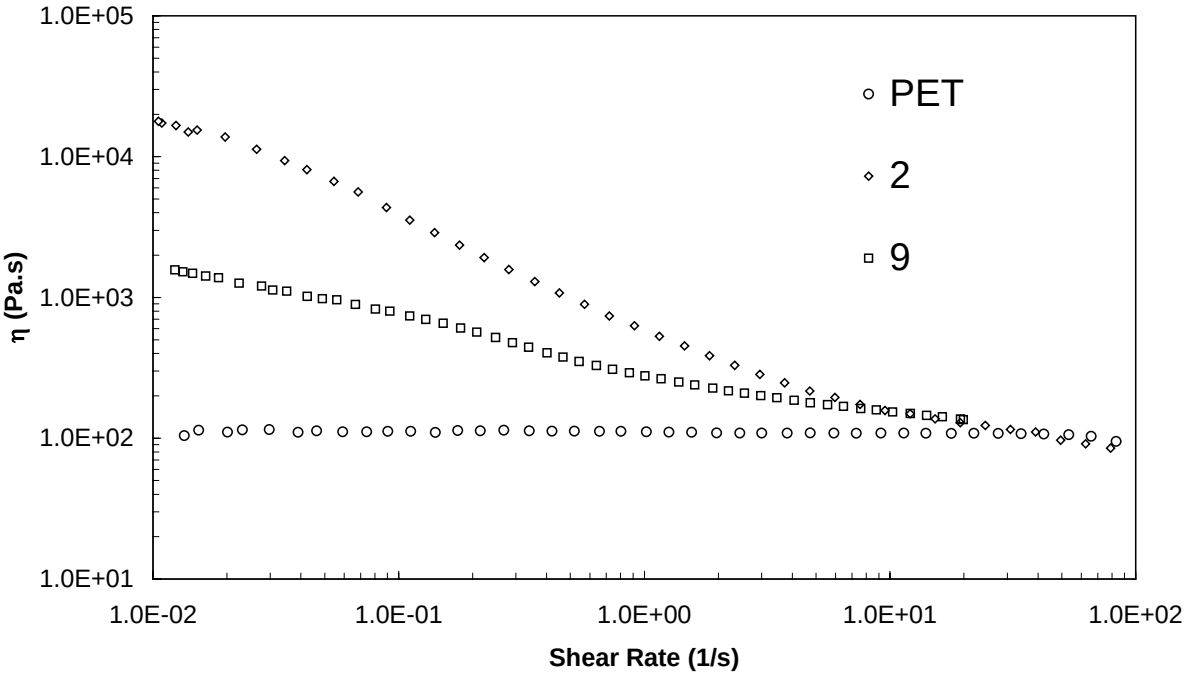

Figure 6.15. Shear viscosity for CNF/PET composite

6.6. References

[1] Andrews, R.; Jacques, D.; Rao, A.M.; Rantell, T.; Derbyshire, F.; Chen, Y.; Chen, J. Haddon, R.C. *Appl. Phys. Lett.* **1999**, *75*, 1329.

[2] Haggenmueller, R.; Gommans, H.H.; Rinzler, A.G.; Fischer, J.E.; Winey, K.I. *Chem Phys Lett* **2000**, *330*, 219.

[3] Yakobson, B.I.; Smalley, R.E. *Ameri. Sci.* **1997**, *85* 324.

[4] Qian, D.; Dickey, E.C.; Andrews, R.; Rantell, T. *Appl. Phys. Lett*. **2000**, *76*, 2868.

[5] Shaffer, M.S.P.; Windle, A.H. *Adv. Mater.* **1999**,11, 937.

[6] Jin, L.; Bower, C.; Zhou, O. *Appl. Phys. Lett.* **1998**, *73*,1197.

[7] Dupire, M.; Michel, J. European Patent 1, 054, 036 A1. November 22, (2000).

[8] Schadler, L.S.; Giannaris, S.C. Ajayan, P.M. *Appl. Phys. Lett.* **1998**, *73*, 3842.

[9] Tibbetts, G.G.; Devour, MG. U.S. Patent 4, 565, 684. January 21, (1986).

[10] Heremans, J.; Beetz, Jr. C.P. *Phys. Rev. B: Condens. Matter.* **1985**, *32*, 1981.

[11] Heremans, J. *Carbon* **1985**, *23*, 431.

[12] Endo ,M.; Kim, Y.A.; Hayashi, T.; Nishmura, K.; Matusita, T.; Miyashita, K.; Dresselhaus, M.S. *Carbon* **2001**, *39*,1287.

[13] Van Hattum, F.W.J.; Bernardo, C.A.; Finegan, J.C.; Tibbetts, G.G.; Alig, R.L.; Lake, M.L. *Polym. Comp*. **1999**, **20**, 683.

[14] Gordeyev, S.A.; Macedo, F.J.; Van Hattum, F.W.J.; Bernardo,C.A. *Phys. Rev. B: Condens. Matter.* **2000**, *279*, 33.

[15] Tibbetts, G.G.; McHugh, J.J. *J. Mater. Res.* **1999**,*14*, 2871.

[16] Lozano, K. Bonilla-Rios J.; Barrera, E.V. *J. Appl. Polym. Sci.* **2001**, *80*, 1162.

[17] Kumar, S.; Doshi, H.; Srinivasarao, M.; Park, J.O.; Schiraldi, D.A. *Polymer* **2002**, *43*, 1701.

[18] Dasch, C.J.; Baxter, W.J.; Tibbetts, G.G. 21st Bienn. Conf. Carbon. Buffalo, NY 1993, 82.

[19] Carneiro, O.S.; Covas, J.A.; Bernardo, C.A.; Caldiera, G.; Van Hattum, F.W.J.; Ting,

J.M.; Alig, R.L.; Lake, M.L. *Comp. Sci. Tech.* **1998**, 58,401.

[20] Caldeira, G.; Maia, J.M.; Carneiro, O.S.; Covas, J.A.; Bernardo, C.A. *Polym. Comp*. **1998**, *19*,147.

[21] Caldeira, G.; Maia, J.M. *Polym. Comp.* **2000**, 21, 970.

[22] Pogue, R.T.; Ye, J.; Klosterman, D.A.; Glass, A.S.; Chartoff, R.P. *Composites, Part A: Appl. Sci. Manu.* **1998**, 29,1273.

[23] Shui, X.; Chung, D.D.L. Proc 38th Inter SAMPE Symp. 1993,1869.

[24] Patton, R.D.; Pittman, C.U. Jr; Wang, L.; Hill, J.R. *Composites, Part A: Appl. Sci. Manu.* **1999**, *30*,1081.

[25] Ciminelli, D.L.; Kearns, K.M.; Ragland, W.R. Proc 41st Inter. SAMPE Symp. 1996, 496.

[26] Chellappa, V.; Chiou, Z.W.; Jang, B.Z. Proc 26th SAMPE Tech. Conf. 1994, 12.

[27] Macedo, F.J.; Ferreira, J.A.; Van Hattum, F.W.J.; Bernardo, C.A. *J. Mater. Proc Technol.* **1999**, *92*, 151.

[28] Zhang, C. Yi, X.S.; Yui, H. Asai, A. Sumita, M. *Mater. Lett* **1998**, *36*,186.

[29] Wu, G.; Asai, S.; Sumita, M. *Macromolecules* **1999**, *32*, 3534.

[30]Bhattacharyya, A.R.; Sreekumar, T.V.; Kumar, S.; Ericson, L.M.; Smalley, R.E. to be published.

[31] TA Instruments Literature: High resolution thermogravimetric analysis-a new technique for obtaining superior analytical results TA-023.

[32] Perry, A.J.; Ineichen, B.; Eliasson, B. *J. Mater. Sci.* **1974**, 9, 376.

[33] Sinclair, D. A. *J. Appl. Phys.* **1950**, *21*, 380.

[34] Kozey, V.V.; Jiang, H.; Mehta, V.R.; Kumar, S. *J. Mater. Res.* **1995**, *10*, 1044.

[35] Mehta, V.R.;, Kumar S. *J. Mater. Sci.* **1994**, *29*, 3658.

[36] Darmstadt, H.; Summchen, L.; Ting, J.M.; Roland, U.; Kaliaguine, S.; Roy, C. *Carbon* **1997**, *35*, 1581.

[37] Endo, M. Kim, Y.A.; Takeda, T.; Hong, S.H.; Matusita, T.; Hayashi, T.; Dresselhaus,

M.S. *Carbon* **2001**, *39*, 2003.

[38] Shaffer, M.S.; Fan, X.; Windle, A.H. *Carbon* **1998**,*36*, 1603.

[39] Li, Y.H.; Xu, C.; Wei, B.; Zhang, X.; Zheng, M.; Wu, D.; Ajayan, P.M. *Chem. Mater.* **2002**;*14*, 483.

[40] Cox, H.L.; *Brit. J. Appl. Phys.* **1952**, *3*, 72.

[41] Ward, I.M. J. Macromol. Sci., Phys. **1967**;*1*, 667.

[42] Chen, J.; Lu, Y.; Church, D.B.; Patel, D. *Appl. Phys. Lett.* **1992**, *60*, 2347.

[43] Zeng, J.; Kumar, S.; Schiraldi, D.A. To be submitted.

[44]Wang Z.G.; Hsiao, B.S.; Sauer, B.B.; Kampert, W.G. *Polymer* **1999**; *40*, 4615.

[45] Uchida, T.; Kumar, S. To be published.

[46] Carneiro, O.S.; Maia, J.M. *Polym. Comp.* **2000**; *21*, 970.

[47] Pötschke, P.; Fornes, T.D.; Paul, D.R. *Polymer* **2002**; *43*, 3247.

CHAPTER VII

CONCLUSIONS AND RECOMMENDATIONS

7.1. Conclusions

PET fiber is a highly structured material, in the sense that the fiber properties strongly depend on fiber morphology, i.e. crystallinity, crystal structure, as well as the orientation of amorphous and crystalline regions. The amorphous regions of the fiber play significant role in determining the thermomechanical properties and dimensional stability. The density of physical crosslinks in the amorphous region either by chain entanglements or by crystallites, the effective chain length between crosslinking points, chain segmental orientation and mobility are important factors to consider when attempting to modify the structure of PET fiber by either changing the fiber processing conditions or by modification of its chemical structure.

In this thesis, it has been shown that in the case of PETBB copolymer , addition of more than 45 mole percent bibenzoate units has brought profound changes in fiber structure and properties. Crystal structure changed from PET type crystal to PEBB type crystal structure at 35 mol% of BB. In 45 to 65 BB composition range, the copolymers are able to crystallize with considerable degree of crystallinity. The crystals thus formed are relatively large in lateral direction but the thickness along the polymer chain is limited due to random distribution of the two comonomer units. These thin plate crystals are

distributed randomly along the fiber direction with extremely high orientation. Amorphous region of drawn PET fiber has low orientation f_a ~0.4, however in the case of high BB containing fibers the orientation factor of the amorphous regions is ~0.8. While the amorphous regions of PET fiber consists of less rigid PET chain segments, the amorphous regions of high BB containing fibers consists of more rigid PET/BB chains. These differences contribute to the much improved tensile and thermomechainical properties of PET/BB 45, 55 and 65 fibers.

In the second part of this thesis, PET/PBA fibers were UV crosslinked after prolonged irradiation. Crosslinked structures were identified by solid state NMR spectroscopy. Crosslinking results in improved tensile and thermomechainical properties as well as improved solvent resistivity. However, the property improvements were less than desired and the crosslinking time was too long to be practically meaningful. This was attribute to the following reasons. First, the probability for phenyl bisacrylate group encountering at 15 mole percent of PBA concentration in the copolymer is considered low to give a high enough crosslinking density that is significant to compared as the density of physical entanglement in PET fiber. Second, the effective penetration depth of UV irradiation was found to be relatively low. Unreacted phenyl bisacrylate groups act as strong UV absorber, thus forming a screening effect, resulting in reduced UV intensity. The steric requirements of the reaction are also stringent for cycloaddition to occur between units in amorphous regions, especially under the glass transition temperature of PET.

For the PET/CNF composites, no significant improvement in fiber tensile properties was observed in this study by the addition of carbon nanofibers. This was

particularly attribute to carbon fiber breakage during melting spinning and fiber processing. CNF recovered from composite fibers were found to have significantly reduced length. While the orientation of CNF in PET fiber were found out to be generally good, X-ray diffraction indicated the misorientaion of the graphite layers in CNF. TEM studies on CNF found the average misorientaion of graphtic layer to that of the fiber axis is around 15^{o}, which implies a much lower tensile modulus of the CNF (50 GPa) than previous reported. However, the compression and torsional properties of the composite fibers were significantly higher than the control PET fiber. Presence of nanoscale objects within the fiber prevent kinking and kink propagation causing compression failure.

7.2. Recommendations for future work.

7.2.1. PET/BB

Further annealing of high BB containing fiber at suitable temperatures has the potential to further crystallize the fiber, as the amorphous chains are highly aligned. Keeping the polymer in the melt state for longer time during melt spinning may help the development of more stable liquid crystalline phase. Use of specially designed spinneret can result in further improvement in chain orientation. In terms of chemical structure, it would be worth making blocky structure of PEBB if transesterfication during melt can be limited. One may also try to use longer linear aromatic monomer fragment.

7.2.2 Crosslinking

Further increase in PBA concentration may incur situation similar to PET/BB copolymer system. Addition of more PBA unit will increase the chain rigidity and help

orientation. Then crosslinking may be more likely due to higher functional group concentration as well as better orientation. Above certain PBA concentration, the crystal structure is expected to be changed to PBA type. It will be interesting to see crosslinking happen in the crystalline regions.

Crosslinking groups be incorporated as short side chains, which may be more mobile and thus yield higher crosslinking efficiency. It may also be desirable to allow functional groups come off from the branch, free to move and crosslink with in the matrix. A simpler version of that would be to use both blend type and copolymer type crosslinking agent at the same time.

7.2.3 Carbon nanotube reinforcement

Mutiwall and single wall nanotubes of appropriate diameter and well aligned graphite layers along the tube axis are likely to be the best candidates for mechanical property reinforcement. However MWNT and SWNTs are more difficult to disperse. There will always be balance between interaction and processability. The interface area and the interaction between polymer chain and the nanotube will increase with the tube length and its aspect ratio, which is also likely to increase the melt viscosity.